Automated Microreactor System for Reaction Development and Online Optimization of Chemical Processes

by

Jonathan Patrick McMullen

B.S. Chemical Engineering, Lehigh University (2004)
B.S. Integrated Business and Engineering, Lehigh University (2005)
M.S. Chemical Engineering Practice, Massachusetts Institute of Technology (2006)

Submitted to the Department of Chemical Engineering
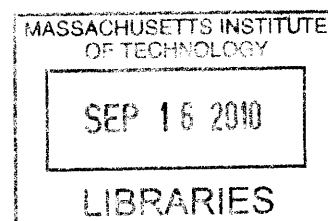in partial fulfillment of the requirements for the degree of

Doctor of Philosophy in Chemical Engineering
at the

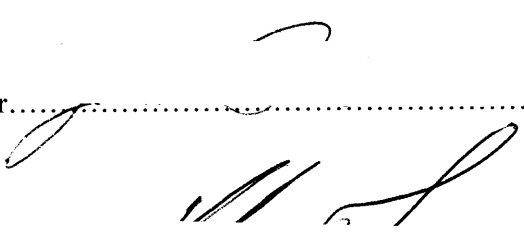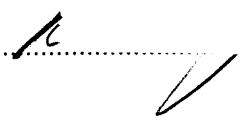MASSACHUSETTS INSTITUTE OF TECHNOLOGY

July 2010

[S~p~~~~r /010]
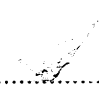
Author..
Jonathan Patrick McMullen
Department of Chemical Engineering
July 15, 2010

Certified by...
Klavs F. Jensen
Department Head, Chemical Engineering
Warren K. Lewis Professor of Chemical Engineering
Professor of Materials Science and Engineering
Thesis Supervisor

Accepted by..
William M. Deen
Carbon P. Dubbs Professor of Chemical Engineering
Chairman, Committee for Graduate Students

Automated Microreactor System for Reaction Development and Online Optimization of Chemical Processes

by

Jonathan Patrick McMullen

Submitted to the Department of Chemical Engineering on July 15, 2010
in partial fulfillment of the requirements for the degree of
Doctor of Philosophy in Chemical Engineering

Abstract

Developing the optimal conditions for chemical reactions that are common in fine chemical and pharmaceutics is a difficult and expensive task. Because syntheses in these fields have multiple reaction pathways, a significant number of experiments are required to determine the conditions that maximize the yield of the desired product. With few exceptions, these experiments have been performed in flask reactors. The goal of this thesis research was to improve the efficiency and the accuracy of these reaction optimization investigations through the use of an automated microreactor system.

Previous studies have illustrated the benefits of silicon microreactors for the study of chemical reactions. Such advantages include the small reactor volume and the continuous flow operations that enable microreactors to achieve a high throughput rate of experiments while using minute amounts of expensive material. Heat and mass transfer rates in microreactors are orders of magnitude larger than those in traditional laboratory equipment, thus rendering microreactors ideal tools for accurate reaction optimization and kinetic investigations. Moreover, the integration of chemical and physical sensors with microreactors permits accurate monitoring of the reaction progress. Combining these measurements with appropriate feedback algorithms offers a means to automate experiments and to perform real-time optimization and kinetic modeling of chemical reactions.

Several automated microreactor systems were developed in this thesis research to improve reaction development. One such system was used in the multidimensional screening investigation of densely functionalized heterocycles. As demonstrated in this example, the use of an automated microreactor system greatly improved the speed and efficiency involved in reaction library development. Incorporating a feedback algorithm into the system operations provided a method for rapid reaction optimization. With throughputs as high as one experiment performed and analyzed per 10 minutes, rapid multi-variable reaction optimization was demonstrated for several chemistries. It was also possible to quickly and accurately extract the kinetics of a reaction by incorporating model-based optimization approaches. The results from these optimization studies were used to scale up reaction production by factors as large as 500 in a mesoflow reaction system. Future extensions for automated microflow systems were identified, and the technology developed in this thesis research was used to optimize a two-step synthesis and to more efficiently study reactions that produce solid by-products.

3

To my parents,

Bernadette and Timothy,

and in memory of my grandfather,
John

Acknowledgements

Contents

11

List of Figures

13

List of Tables

15

List of Schemes

Chapter 1
Introduction and Motivation[†]

1.1 State of Reaction Development in Pharmaceutics

Success in pharmaceutical research is directly related to the speed at which it can discover and manufacture novel active pharmaceutical ingredients (API). The process of moving from the initial discovery experiments performed in the research laboratory to the commercial manufacturing, however, is long and consumes a significant amount of research resources. After identifying and validating the biochemical target of a disease or illness, thousands of reactions are screened on the milligram scale to determine potential drug candidates. The most promising reactions, those that afford product in acceptable yields, are optimized and synthesized on the kilogram scale for toxicology, dosing, and animal studies. Only a few of the molecules that enter this so-called "lead optimization stage" will advance to the clinical stages, where tons of API are produced for the required regulatory assessments.

With few exceptions, these reaction development stages are performed in batch reactors. Synthetic chemists screen reactions in test-tubes or 96-well plates, and process chemists and engineers scale up these reactions using the optimal conditions that were determined in the lab. While this approach has been employed for decades, it can be ineffective or inefficient. The disparate mass and heat transfer rates of the batch reactors in the laboratory and in thepilot plant, combined with the complicated catalytic cycles and reaction pathways of the multi-functional compounds common to pharmaceutics, result in undesirable product yields in the larger reactors.

---

† Themes from this chapter were used in McMullen, J.P.; Jensen, K.F., *Annu. Rev. Anal. Chem.*, 2010, (3) 1

This method of reaction development for API continues despite these inherent limitations because of the flexibility and the versatility of batch reactors.[1] A single vessel can be used for myriad reactions, both homogeneous and multi-phase, and subsequent separation stages such as extraction, distillation, and crystallization. To gain adoption, the benefits of using microreactors and other continuous-flow reactors for reaction development must be clear and substantial.

The use of continuous-flow methods for the manufacturing of pharmaceutical compounds, or intermediates, instead of using conventional batch methods offers the industry several advantages. These benefits include the ability to perform reactions at high temperatures and pressures, safer handling of reactive intermediates, efficient heat transfer, and more flexible scale of production.[2] Well-designed continuous processes are expected to use less capital, have a smaller equipment footprint, require less labor, and generate less waste than batch systems.[3] Because not all reactions improve under continuous-flow processing conditions, a combination of batch and flow reactors can be used to remove bottlenecks in a synthetic process.[4] By using microreactors to understand the effects of the various parameters on the performance of a reaction and using the results to predict operating conditions on the manufacturing scale, the pharmaceutical industry can capitalize on the aforementioned benefits and bring drug candidates to market sooner.

1.2 Microreactors – Powerful Tools for Laboratory Research

Applications for microfluidics have significantly advanced from its roots in microanalytical chemistry to include high throughput screening,[5] biological analysis of cells,[6] and proteins,[7, 8] portable energy devices,[9] and reaction kinetics and mechanisms studies.[10, 11] Enhanced heat and mass transfer rates, continuous-flow operations, and the potential inline

analysis inherent to microsystems for chemistry have enabled chemical researchers to investigate myriad reactions under experimental conditions not easily achieved using conventional laboratory batch equipment, such as glass flasks and test tubes.[12] As a result, microreactor systems are gaining attention in pharmaceutical and fine chemical industries as a platform technology that is to be used for discovery and reaction development in the research laboratories and scales to satisfy production throughput requirements.[13, 14] Reported economic advantages and improved safety metrics from microreactors for production purposes have further encouraged the adoption of microreactors for these industries.[1, 4, 15]

For reaction screening and optimization investigations of pharmaceutics, there are numerous advantages of using microreactors over flask reactors. With reactor volumes on the order of 100 µL, numerous reactions can be screened sequentially for library development.[16, 17] The minimal handling of reagents and the small length scales of microreactors render these microdevices ideal tools for screening particularly hazardous reactions, such as direct fluorination[18] and phosgene generation.[19] The small length scale of microreactors, typically on the order of 100 µm, results in reactors with large surface-to-volume ratios and significantly increases mass and heat transfer rates. Consequently, more accurate optimization and kinetic studies can be performed in microreactors than in flask reactors. The enhanced transport phenomenon is especially important for reactions with multiple reaction pathways, such as lithium-halogen exchange reactions,[20] selective oxidations,[21] and nitrations.[22] Furthermore, the well-understood transport rates in microreactors and the ability to observe the intrinsic kinetics ensures more facile scale up of the reactor systems.

Micromixers, separators, and analysis units have been developed to address the assortment of reaction steps involved in the synthesis of API. The integration of these devices to

form a microchemical system extends the benefits of microscale processing to the entire synthesis route as presented in several case studies.[23-26] Additionally, physical and chemical sensors are easily incorporated with these devices to provide continuous monitoring of reaction conditions and the extent of reaction. The following sections focus on microfabrication and microfluidic devices, with an emphasis on integration techniques for online measurement and automation, to demonstrate the wide range of operations that are relevant to the pharmaceutical industry and achievable in microfluidics.

1.2.1 Microfabrication Techniques and Microfluidic Devices

Microreactors are fabricated in a range of materials, including ceramics, polymers, stainless steel, and silicon. Common fabrication techniques, advantages, and disadvantages of these different materials are listed in Table 1.1 and discussed in further detail by Madou.[27] Polymer based microfluidic systems, especially systems based on poly(dimethyl siloxane),[28] are frequently used for biological application because of the reduced cost and the potential for one-time use to avoid cross contamination. However, most polymers swell or dissolve in common solvents used in chemical synthesis. Ceramic systems are often difficult to microfabricate and are typically limited to high temperature applications. Consequently, organic chemical synthesis is typically performed in metal, glass, and silicon microreactors. Stainless steel microreactor networks range from simple systems comprising of T-shaped micromixers and narrow tubing[29] to commercial systems with microfabricated components.[30-33] Glass microreactors offer the benefit of visualizing the reaction progress, but are limited in reactor designs by the difficulty in creating high aspect ratio structures. Alternatively, a glassy, inert reaction environment with high thermal conductivity can be produced by oxidizing the channel walls of silicon

microreactors. Additional benefits from these reactors include the ability to operate at elevated temperature and pressure.[12]

Table 1.1: Fabrication and highlighted features of various microreactors.

Material	Fabrication techniques	Advantages	Disadvantages	Ref.
Ceramic	Stereolithography μpowder molding, electro discharge machining, laser machining	Stable at high temperatures with low heat loss, chemically resistant	High development costs, shrinkage after sintering	34, 35
Glass	Photolitography, powder-blasting wet etch ultrasonic machining	High chemical resistance, direct visualization of reaction	Deep, anisotropic etch is difficult, incompatible with strong aqueous bases at moderate temperature	36, 37
Plastic	Soft lithography, injection molding, hot embossing	Fast fabrication, inexpensive development costs	Incompatible with organic solvents, not suitable for high temperatures and pressures	38, 39
Silicon	Photolithography, wet and dry etching	Operate at high pressure and temperature, superior heat conductivity, high aspect ratio designs	Incompatible with strong aqueous bases at moderate temperature	40, 41
Stainless Steel	LIGA, stamping micromaching	Operate at high pressure and temperature,	Incompatible with acidic media except for expensive, specialized steels	42, 43

Novel microfabrication techniques and reactor peripherals are continuously being developed as microreactor applications expand. Micromixers are designed to use interdigitated multi-lamellae,[44, 45] chaotic advection,[46, 47] segmented flow of immiscible fluids,[48, 49] or active micromixing techniques.[50, 51] Separation of homogenous mixtures on the microscale is achieved

by distillation[52, 53] or crystallization,[54] while multi-phase mixtures are separated by taking advantage of the dominating surface forces.[55-57] Microchemical systems are established by integrating microdevices with the appropriate fluidic interfacing scheme.[58-60] The advantages of using these miniaturized reaction networks for multi-step chemical synthesis have been demonstrated in several case studies.[23-26] Selected examples of current microfluidic devices for reaction and separation are shown in Figure 1-1.
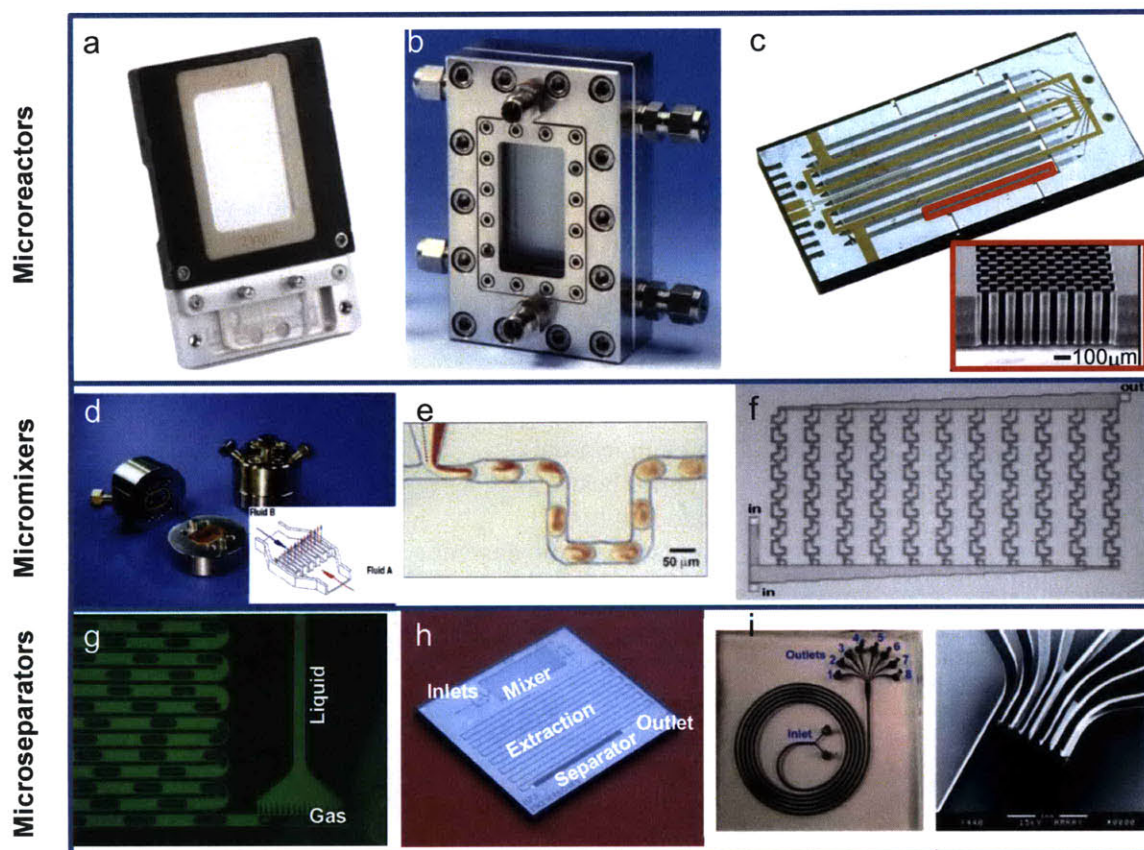
Figure 1-1: Selected examples of microfluidic devices.
a) Glass microreactor used in Syrris' Africa Flow Chemistry System (Reproduced with permission by Syrris Ltd.), b) stainless steel reactor fabricated by IMM (Reproduced with permission by IMM-Mainz GmbH), c) multi-channel silicon microreactor, highlighting in-channel, platinum catalyst coated pillars,[61] d.) interdigtial micromixer by IMM with flow patterns inset (Copyright 2009 American Chemical Society),[62] e) example of chaotic advection with liquid-liquid segmented flow (Image reproduced, with permission from Ref. 46), f) split-and-recombine mixer (Copyright Wiley-VCH Verlag GmbH & Co. K GaA. Reproduced with permission),[63] g) microseparator for gas-liquid slug flow,[55] h) integrated liquid-liquid extractor and separator,[56] i) size-based particle separator (reproduced by permission of The Royal Society of Chemistry).[64]

1.2.2 Integration of Physical and Chemical Sensors with Microfluidics

Incorporation of chemical and physical sensors with a microreactor leads to "integrated microreactors" or "instrumented microreactors," and enables online monitoring of the reaction conditions and the extent of reaction.[65] Consequently, process lead times are accelerated and associated developmental costs are reduced by gathering a wealth of reaction knowledge with integrated microreactors in the research laboratory and translating the results to production systems.[66] The ability to rapidly identify a reaction path, optimize the reaction conditions, and scale up and/or scale out the results for manufacturing will engender a shift from reaction development in glass flasks to continuous flow operations in microreactors.

Reaction temperature, residence time, and stoichiometry can be measured through integrated sensors and controlled with on-chip or modular components. Thin layers of platinum are deposited on microreactors to record and adjust reactor temperatures (Figure 1-2a).[67] Resistive electrical heaters[61] and heat exchangers[11] are also used to control temperatures. Additionally, temperature gradients created by exotherms from mixing or reaction are closely monitored by fabricating thin film calorimeters (Figure 1-2b),[68] or by monitoring hot spots thermographically with an IR camera.

Flow rates are measured with micropressure sensors,[69] microflow anemometers,[70] or optical fiber cantilevers (Figure 1-2c)[71] and adjusted in several manners. Electroosmotic flow (EOF) is used in glass microreactors to generate precise, plug flow,[72] but is typically only applicable for aqueous systems, low flow rates, and small channel dimensions.[73] Alternative flow control methods include commercial syringe pumps or pneumatic,[74, 75] peristaltic,[76] and passive pumping[77] systems. Gas-liquid segmented flow in microreactors is characterized by integrating microfluidics with an inverted fluorescence microscope and a CCD camera.[78] This

approach is also used to measure gas-liquid slug velocity and uniformity in multi-channel, scaled out microreactors by including a waveguide that uses internal reflection (Figure 1-2d), as demonstrated by de Mas.[79] Fluorescent measurements are used to characterize mixing (Figure 1-2e)[80] and dispersion[81] in transparent microreactors. Recently, Andrew Chan et al. characterized mixing profiles of H_2O and D_2O throughout an entire PDMS microreactor with ATR-FTIR spectroscopy by placing the device above an ATR crystal and using a focal plane array for spatial imaging (Figure 1-2f).[82] Advancements in this technology will lead to faster methods for determining reaction kinetics and optimal conditions.

A variety of spectroscopic methods have also been integrated with microreactors. Advances in fiber optics and flow cell technology offers continuous monitoring of the reaction stream with UV/Vis/NIR,[83] Raman,[84] ATR-IR,[11] XAS,[85] and NMR.[86] The potential to monitor the entire reaction progress in a microreactor is exemplified in Damean et al.[87] In this work, the authors used diffraction grating and array of microlenses to disperse light from a bright-field microscope through a PDMS microreactor. Absorbance spectra of components at multiple locations in a microarray or microchannel are obtained by collecting and resolving the diffracted light images with a charge-coupled device (CCD) camera.

Microfluidic devices for the separation of analytes are coupled with microreactors to improve chemical detection on the miniaturized scale. Separation of proteins, metabolites, and other biological macromolecules are quickly performed in devices that use a form of electrophoresis.[88, 89] A common technique to separate smaller molecules is liquid chromatography. Basic designs for this technique involve packing the microfluidic channel with HPLC beads,[90] coating the channel walls with adsorbent material,[91] or creating a functionalized
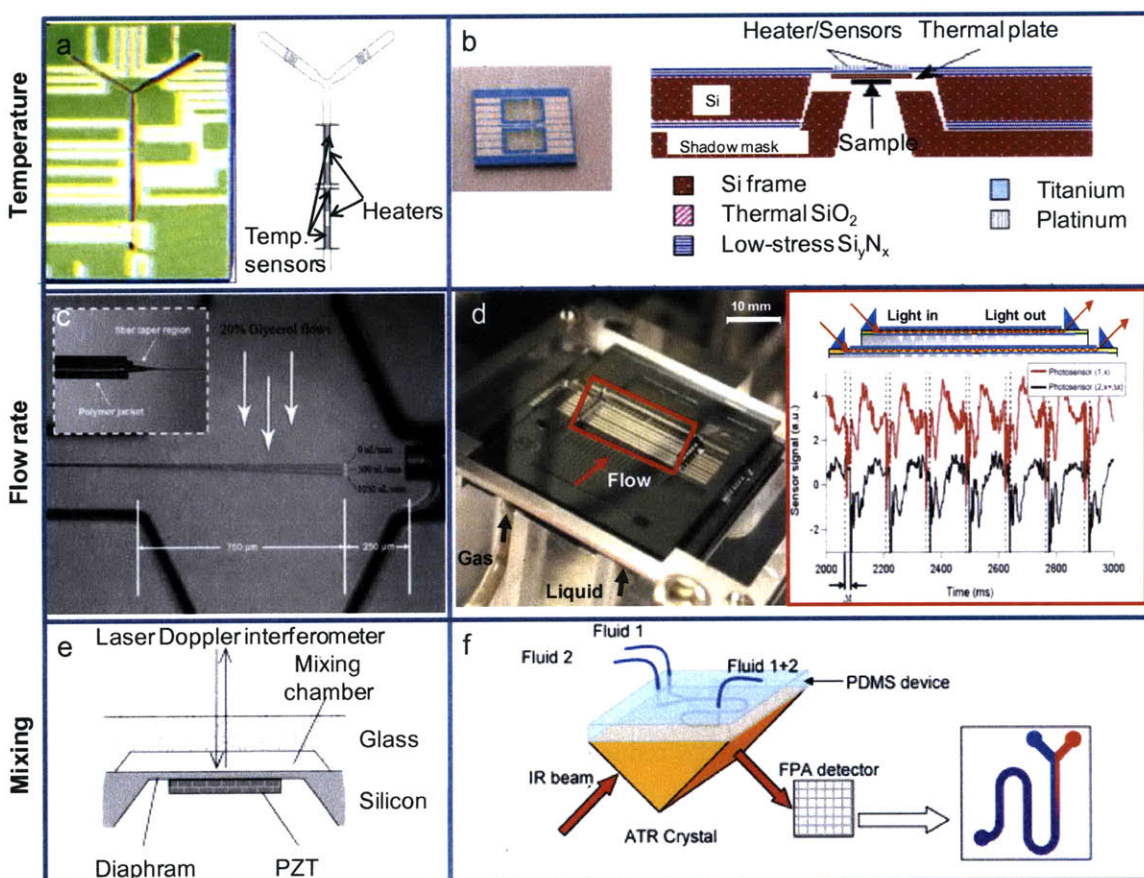
Figure 1-2: Selected examples of microfluidics integrated with sensors for measuring physical properties.
a) Microreactor integrated with Pt deposited temperature sensors and heaters (left) and schematic of device (right),[67] b) microcalorimeter capable of measuring exotherms,[68] c) micro-opto-fluidic flow measurement with optical position marked at 0, 500, and 1050 µL/min (reproduced by permission of The Royal Society of Chemistry),[71] d) gas-liquid flow sensor using ATR-FTIR spectroscopy and waveguides,[79] e) ultrasonic micromixer schematic with fluorescent imaging of mixing for water and uranine (reprinted from ref. [80] Copyright 2001, with permission from Elsevier), f) schematic microfluidic device capable of monitoring mixing throughout microfluidic device with ATR-IR spectroscopy (reproduced by permission of The Royal Society of Chemistry).[92]

monolith as the separation column.[93] Chiral separation is achieved in EOF microfluidics by adding a chiral selector to the mixture.[94] Common problems associated with gradient methods in reversed-phase chromatography, such as long equilibration times, can be avoided on the micro-scale by using an isocratic method and temperature gradient interaction chromatography (TGIC) as shown by Shih et al.[90] In this work, the authors fabricated an integrated column separator

from silicon and parylene that was 8 mm long, 100 μm wide, 25 μm deep and packed with 5 μm

C18 silica beads. Platinum was deposited on the silicon to create a resistive heater, a

temperature sensor, and an electromchemical analyte sensor. Using a variable power source, a

constant temperature gradient across the column allowed separation and detection of five

derivatized amino acids.

1.3 Motivation: Integrated Microreactor System for Reaction Automation as a Means to Improve Reaction Development

Incorporating feedback control with instrumented microreactors leads to full automation

of continuous-flow experiments, thereby reducing the time and the material costs associated with

reaction discovery and development. Benefits from automation and microreactors for reaction

screening have been demonstrated for the synthesis of cycloadducts,[95] pyrazoles,[96] and

Ciprofloxacin analogues.[97] Heterogeneous reactions can also be screened in a continuous flow

manner, as presented by Griffiths-Jones and coworkers, who developed an automated multi-step,

continuous flow system with immobilized reagents to generate a 48-member sulfonamide

reaction library.[98] In this platform, monoalkylation of a Boc-protected primary sulfonamide was

performed in a glass reactor column packed with PS-TBD, followed by deprotection in a second

column packed with polystyrene-supported sulfonic acid Amberylst H-15. By integrating these

columns with a liquid handler/fraction collector, syringe pumps, 4-way valves, and necessary

computer logic, the authors demonstrated the ability to automate the loading of the Boc-protected

primary sulfonamide on the PS-TBD column, the loading of the monomer on the PS-TBD

column for reaction, the detection and collection the final product following deprotection, and

the regeneration of the PS-TBD column. Although some manual intervention was required to

remove the spent H-15 and eventually deactivated PS-TBD column, this application exemplifies the numerous experimental steps that can be automated with a continuous flow system.

After identifying the successful "hits" involved in reaction screening, the next step in reaction development is profiling the parameter space to evaluate the reaction rate, to determine the optimal operating, and to calculate the kinetic parameters. This information-driven approach for characterizing reaction influences has recently received more attention with the Quality by Design (QbD) initiative by the Food and Drug Administration (FDA).[99] Automation of microfluidic platforms adheres to the principles of this program and gathers the required reaction information without requiring significant amounts of time or resources.

An automated microreactor system to quickly profile the parameter space of a Sonogashira reaction was designed by Sugimoto and coworkers.[100] This PC-controlled system consisted of two HPLC pumps for fluid handling, temperature control, a 500 x 1000 μm micromixer followed by a 1000 μm i.d. x 10 m residence time unit, and a fraction collector. After inputting the desired experimental matrix, i.e. the set of reaction temperatures and residence times of interest, the system performed the specified reactions and collected samples in an automated fashion. Fractions were then analyzed offline by HPLC, and the results were used to determine the optimal yield of 96% at 20 minutes, 1.25 equivalents of p-tolyacetylene, 3.0 equivalents of base and a reaction temperature 120 °C. These optimal conditions were then translated to a larger system that consisted of a stainless steel, 200 μm i.d. micromixer and a 2mm i.d. x 20 m residence time unit. This scaled-up system was operated for 6 hours at the previously determined optimal conditions to provide 113 g of product after recrystallization.

Additionally, Koch et al. demonstrated the ability to use an automated microfluidic platform to profile the removal of a p-methoxyphenyl protecting group.[101] The microfluidic

system consisted of syringe pumps for control over residence time and reagent stoichiometry, a 7.02 µL glass microreactor, a thermoelectric module for temperature control, and a fraction collector for sampling. Offline analysis was used to quantify the reaction yield. The authors applied an optimal design of experiment to investigate reaction temperatures between 60 and 90°C, residence times between 0.5 and 4 min, and 1 to 4 equivalents of acid.

Based upon the design approach of the authors, the platform performed 51 experiments in an automated fashion. It is interesting to note that the required material for these automated experiments was minimal – each sample required just 0.2 mg. Furthermore, the total time sampling for this profiling investigation was only 5.6 hours. A polynomial response surface was fitted to these experiments and indicated that a conversion greater than 99% combined with the shortest reaction time occurred at 1.3 minutes, 3.2 equivalents of acid, and a reaction temperature of 90 °C. These optimal results were repeated on a larger stainless steel reactor with a volume of 950 µL. However, on this larger system, the authors noted that the solvent boiled at 90 °C and lowered the reaction temperature to 80 °C and increased the reaction time to 4 minutes to obtain 100%, as specified by their profiling experiments in the microreactor. Under these conditions, the system produced approximately 213 mg/h of the deprotected product.

The addition of an optimization feedback to an integrated microreactor system enables a means for rapid reaction optimization.[102] An automated system that is capable of performing a reaction, analyzing the results, and incorporating the data into an optimization algorithm to select sequential experiments would promise faster and more efficient reaction optimization than that of batch experimentation. Depending on the objective of the experiments, automated microreactor systems could be used to optimize a reaction for a specific metric, such as yield or

selectivity, or for information, such as determining the global reaction kinetics. These experiments provide valuable information during the scale up stages of reaction development.

1.4 Thesis Objective and Overview

To become a potential instrument in pharmaceutical research and development, automated microreactor systems must accommodate a wide range of chemistries, and convincingly demonstrate benefits in multiple stages of reaction development. As discussed in Chapter 2, automated microreactor systems can be used in the discovery stages for fast screening of hundreds to thousands of reactions to identify potential candidates. The developed system, which was used to study transformations of densely functionalized scaffolds, required careful consideration to flow patterns in the microreactor to increase throughput rates and eliminate cross-contamination of reaction screens. Advantages from this technology include the ability to rapidly investigate how the discrete variables, such as the base or a reaction partner, and the continuous variables, such as temperature and residence time, affect the reaction pathway.

Integration of an inline analytical chemistry tool and a feedback algorithm leads to automated reaction optimization in microreactor systems. Selection of the appropriate experimental optimization algorithm requires consideration to the number of experiments that are likely to be required for convergence, and the ability of the algorithm to work effectively with experimental error and noise in data. Algorithms that were considered for this thesis research are discussed in Chapter 3, and the applications of several of these algorithms are presented in Chapter 4. Reactions examples include a Knoevenagel condensation, a series oxidation, and a Heck reaction.

Although obtaining optimal conditions is a vital component of reaction development, knowledge of the kinetics may be more desirable when designing the reactor configuration and

the optimal process control strategy. As discussed in Chapter 5, implementing a model-based optimization framework with an automated microreactor system provides a method for rapidly determining the kinetics. Using a Diels-Alder reaction as an example, an approach that uses Information Theory and Bayesian statistics was used to determine the global reaction rate law, followed by a D-optimal experimental strategy to determine the pre-exponential and the activation energy of the rate constant. As described in Chapter 6, results from the automated optimization studies of Chapter 4 and the kinetic investigation of Chapter 5 are used to develop a roadmap for continuous-flow reaction scale up. Highlights from Chapter 6 include the ability to scale the Diels-Alder reaction by a factor of 500.

Chapter 7 describes extensions to the automated microreactor systems to handle reaction applications involved in pharmaceutical research. Because syntheses of API typically require more than one reaction step, an automated system was established to profile reaction conditions for multi-step syntheses. This system consisted of two packed-bed reactors and was used to investigate a palladium catalyzed amination and subsequent Suzuki reaction. Because many pharmaceutical reactions generate salt by-products that precipitate, designing reactor systems that avoid clogging is essential. To this end, an automated flushing system was designed and constructed to remove salt build-up before clogging the reactor.

Milestones of this thesis research and the future outlook for research related to the further developments and applications of automated microreactor systems are discussed in Chapter 8.

Chapter 2
Automated Reaction Screening for Library Development[†]

Combinatorial chemistry and high throughput screening have become research staples in the pharmaceutical industry to reduce the time and the costs associated with exploring potential drug candidates. Screens have typically been performed in 96-well plates to provide a high degree of parallelization to improve the speed of this process. For homogenous systems where the reaction time scale is less than the mixing and heat transfer time scales of the 96-well plate reactors, more insightful results are achieved by performing reaction screens in a microreactor. Obtaining a high throughput of screens while eliminating contamination is a significant challenge involved in screening reactions in single continuous-flow device. Unlike the 96-well plate reactor, screens are not physically isolated from one another by the reactor walls in a microreactor. The introduction of an inert, immiscible fluid, such as a fluorous phase, to create slug-flow can be used to improve throughput and remove contamination concerns.[103, 104] This approach is limited, however, to exploring reaction conditions at temperatures where the second fluid remains insoluble in the reaction droplet. Alternatively, integrating sensors and feedback to control and monitor the reactions offers a more robust method for fast reaction screening.

To demonstrate the wealth of reaction screening information that can be rapidly obtained with an automated silicon microreactor system, the transformations of densely functionalized bicyclo[3.2.1]octanoid scaffolds were investigated.[105] In addition to exploring how these

---

†This chapter describes work that was done in close collaboration with Dr. J. R. Goodell, Dr. A. B. Beeler, and Prof. J. A. Porco, Jr. of the CMLD-BU.

substrates reacted with different nucleophiles, electrophiles, bases, and solvents, this microreactor system also investigated the effects of temperature and residence times. Although not commonly explored in reaction screening applications, including these latter variables enables observation of reaction pathways that may not be otherwise observed. Furthermore, the high thermal conductivity and strength of silicon extends the potential reaction design space of this system to higher temperature and pressures than those explored in common 96-well plate reactors. Approximately 850 automated reaction screens were performed in the investigation of the example scaffold transformation to illustrate the high throughput capabilities of an automated microreactor system and the ease in generating reaction libraries while using minimal material.

2.1 Motivation

Historically, major pharmaceutical breakthroughs have been enabled by complex chemical structures – often complex natural products – with unique biological mechanisms.[106] Recently, there have been numerous efforts to discover new complex chemical scaffolds through organic synthesis.[107-109] A chemical reaction discovery approach coined "multi-dimensional reaction screening" by the CMLD-BU has been formulated to synthesize novel chemotypes and structural frameworks.[110] In this approach, chemical reactions are evaluated using integer variables, such as different substrates, and continuous variables, such as temperature, in an array format. This method addresses an ongoing challenge in drug discovery: the decreasing availability of new chemical entities for biological screening and discovery of new synthetic methodologies to access novel compounds of interest.[111, 112]

Miniaturization and automation of biological screens have enabled an unprecedented level of throughput.[112] However, such developments have been slower in the area of chemical reaction discovery.[113-115] To demonstrate the ability to use microfluidics to rapidly screen

chemical reactions, an automated microreactor system was developed for a series of multi-dimensional reaction screens involving bicyclo[3.2.1]octanoid scaffolds.[116] The general form of these multifunctional chemotypes is shown in Figure 2-1, with the reactive moieties highlighted.[117-119]
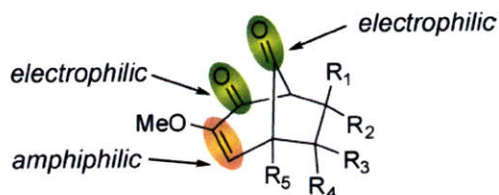
Figure 2-1: Diverse functionality of bicyclo[3.2.1]ocatonoid scaffold used in automated microreactor system for multi-dimensional screening.

2.2 Automated Microchemical System Design and Components

The successful integrated microreactor system for discovery applications performs reaction screens at a high throughput rate to quickly provide researchers with accurate information, without compromising the following design criteria:

- Screens require a minimal, yet detectable, amount of material.

- Screens remain uncontaminated throughout the procedure.

- Screens can be isolated for analysis and subsequent work-up.

- Reagents for reaction screening do not lose reactivity during storage.

The automated microreactor system that was designed and constructed to satisfy these goals and constraints is shown in Figure 2-2. A liquid handler was used to select various screening compounds. The residence time was controlled by manipulating the flow rate of a carrier fluid that was loaded onto a multi-head syringe pump. A thermoresistor and a thermoelectric module were used to measure and control reaction temperature, respectively. Reaction samples were

detected by inline UV spectroscopy, and collected with a fraction collector. The following subsections describe the various components and operations in more detail, as well as the considerations that were involved in developing an automated screening microreactor system.

2.2.1 Fluid Delivery System for Controllable Reaction Screening

The total experimental time involved for reaction screening in a continuous-flow manner ranges from hours to days, depending on the residence time and number of screens. Minimizing the preparation time of the reagents for screens increases the efficiency of the process. However, the level of reactivity of these compounds must remain intact when in storage, which can be a difficult task for air, moisture, and light sensitive reagents. To accomplish this task, an aluminum storage block was designed and machined at Boston University. This multi-layered chamber consisted of a 96-well bottom plate that accommodated commercially available HPLC glass vials (Waters Inc.), and an argon gas chamber to ensure reagent long-term reagent stability. A positive argon pressure was continuously provided to the gas chamber, and rubber septa were inserted between each plate layer to provide long-term reagent stability.

Selection of chemical reagents for screens was controlled with a Gilson Quad-Z 215 liquid handler equipped with three independently controlled syringes. The selection of components for screens was programmed in Trilution® software (Gilson). The integrity of the reagents was maintained during handling by programming the liquid handler to withdraw a segment of dry wash solvent, followed by a segment of argon from the gas chamber, followed by the reagent, and then an additional argon segment from the gas chamber (Figure 2-3). Each reagent was injected into the microreactor system via a 6-way actuated valve.

34
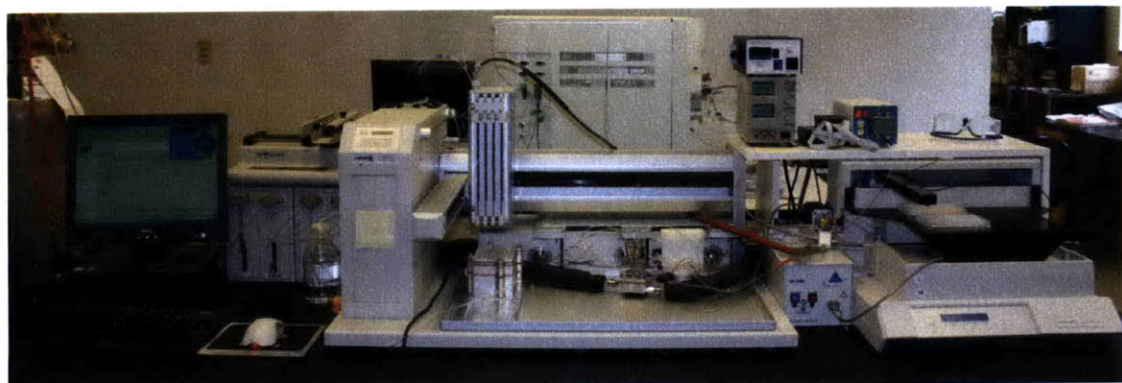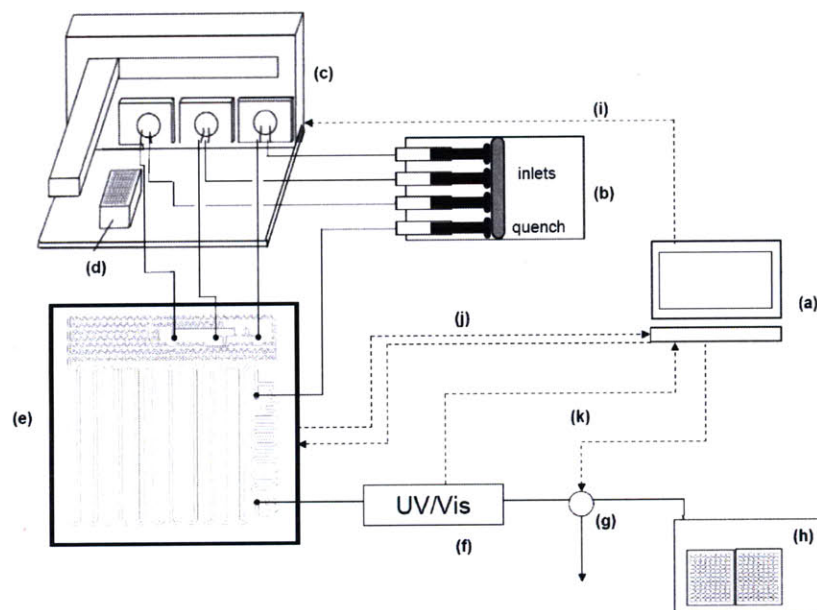
Figure 2-2: Automated microreactor system for reaction screening applications.
Top) Components include (a) computer with operating software, (b) multi-head syringe pump, (c) liquid handler, (d) 96-well reagent block, (e) compression packaging which houses microreactor and thermoelectric module, (f) UV detection for optical triggering, (g) sampling valve, (h) 96-well plate fraction collector, and feedback control loops (i – k) for reagent injection, temperature control, and sample collection, respectively and the experimental system that was used for investigating bicyclo[3.2.1]octanoid transformations. Bottom) Experimental system that was constructed in the CMLD-BU.
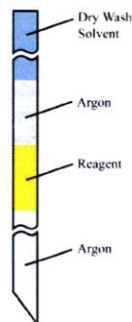
Figure 2-3: Schematic of programmed withdraw procedure for reagent handling.

2.2.2 Flow Patterns to Increase Throughput and Eliminate Contamination

A high throughput of screens can be realized by having multiple reactions occur simultaneously at various positions in the microreactor. As previously mentioned, the use of an immiscible liquid increases the number of reaction slugs present in a microreactor but limits the range of reaction temperatures. The use of argon as a separation phase between reaction slugs was attempted, but several complications were observed. Because the liquid phase wets the reactor walls, there is a liquid meniscus that connects sequential liquid slugs.[120] Inserting a solvent wash slug between reaction plugs could minimize, but not eliminate, this cross-communication.

An irresolvable problem with gas-liquid flow for sequential reaction screening was the lack of control for appropriate insertion of gas plugs between the reactions plugs. In preliminary experiments, a large pressure drop was incorporated by inserting a capillary tube (75 μm i.d.) between an argon gas tank and the microreactor. This design principle was based on recommendations from pervious gas-liquid slug flow applications.[48, 49] Steady gas-liquid slug flow, however, was never experimentally observed. This instable flow was attributed to two

36

features: 1) the size of the reactor and tubing for downstream processing was large and resulted in an unacceptably long time scale for achieving stable flow, and 2) the continual disturbances to the flow from reagent injections and sample collections created pressure waves that destabilized the slug-flow. Figure 2-4 illustrates the typical gas-liquid flow behavior that was present in the microreactor system. Therefore, to ensure a comprehensive range of reaction conditions and to eliminate cross contamination, reactions plugs were injected into a continuous stream of solvent to create a "pulse flow."

Figure 2-4: Difficulty in robustly controlling gas-liquid plug resulted in reaction plugs (yellow) to be undesirably separated.

This pulse flow technique is similar to the injection method used to characterize the residence time distribution of a reactor. In the same manner, a disadvantage of applying this homogenous flow style is the axial dispersion of the reaction pulses associated with laminar flow (Figure 2-5). Dispersion causes a dilution of reaction material near the tails of the reaction segment, but the effects can be reduced by minimizing dead volumes and using minimal lengths of PTFE tubing upstream and downstream of the reactor. Because the central portion of this reaction segment contains the most relevant information, it was collected for analysis; whereas the tail ends were discarded to waste. An optically triggered collection system (components f, g, and k of Figure 2-2) was established to collect the central section of these pulses, while the tail

37

ends were discarded (Figure 2-5b). Furthermore, programmed delays between the pulses were incorporated to prevent cross-contamination of the reaction screens.
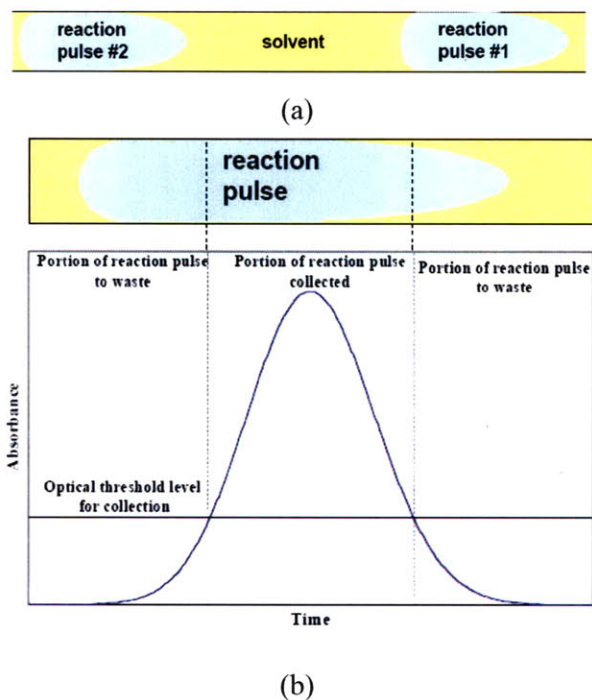
Figure 2-5: Injection and collection method used in screening applications.
a) Illustration of sequential plugs and the dispersion caused as a result of laminar flow and surface wetting.
b) Example of sample collection via optical triggering. Collection begins and terminates once concentration of reaction pulse crosses a specified threshold, thereby enabling collection of the central portion of the slug

2.2.3 Microreactor Design

The microreactor used in this investigation was fabricated from silicon for several reasons. The reactor channel walls, typically silicon dioxide or silicon nitride,[27] ensure that the reactor will be chemically compatible with a broad range of solvents and reagents. The high thermal conductivity of silicon also ensures that the reactor can quickly reach thermal equilibrium, guaranteeing a minimal lag-time between experiments. The reactor design used in

this work was a modified version of a design previously used for the optimization of glycosylations,[121] and a schematic of the reactor design is shown in Figure 2-6. The fabrication process for this device is given in Appendix A.
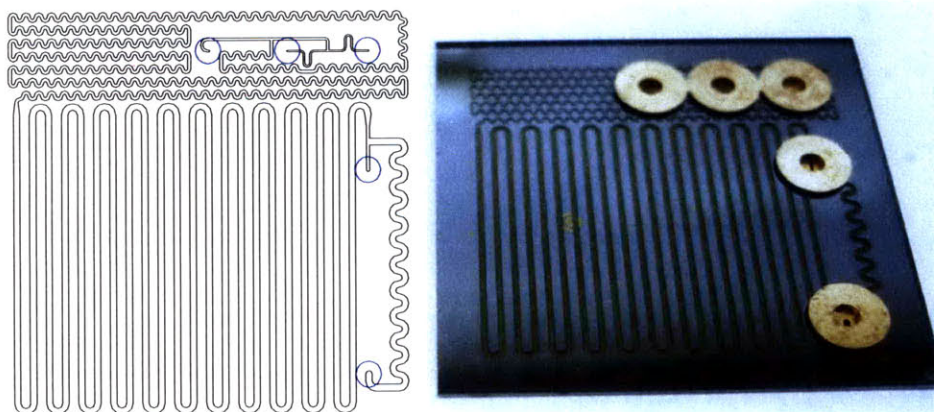
Figure 2-6: Microreactor design for reaction screening applications.
Schematic (left) of integrated microreactor design with mixing, reaction, and quench zones. Blue circles denote port holes. Fabricated chip used for screening experiments (right).

The microreactor framework consisted of 3 fluid inlets, followed by an 18 μL mixing zone and a 69 μL reaction zone. A small quench zone is used to ensure that the reaction is terminated before exiting the chip. The reactor was designed to be a versatile, multi-purpose fluidic device, usable for continuous-flow and slug-injection-flow applications. The design was intended to maximize mixing, minimize pressure drop, allow for flow visualization, and be chemically robust. T-mixers at the inlet zone are used to control and promote mixing of the reagents. The quench also includes a T-mixer and serpentine path to ensure good mixing and termination of the reaction. The first design generation of these devices used a solder packaging scheme to make fluidic connections between macroscopic fluid handling equipment and the microreactor.[58] However, later designs used a compression packaging scheme for fluidic connections due to the inability to consistently deposit chrome and copper onto the Pyrex for soldering.
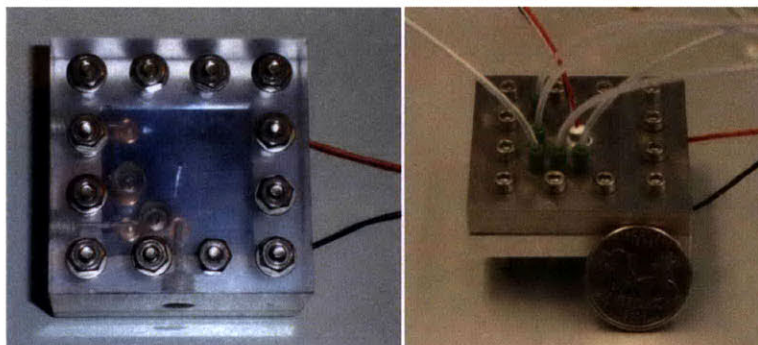
Figure 2-7: Compression packaging schemes designed for reaction screening applications.
A polycarbonate design (left) is used to visualize aqueous reactions and uses common 1/4-28 fluidic connections. A stainless steel design (right) with M6-40 connections minimizes dead volume and is applicable for organic reaction screens. Both designs also housed the thermoelectric module that was used for heating and cooling the microreactor.

The compression packaging scheme shown on the right-hand side of Figure 2-7 was used for the screening investigations of bicyclo[3.2.1]octanoids. This compression chuck houses the microreactor and a thermoelectric (TE) element. This TE device is capable of heating or cooling the microreactor by adjusting the electric current.[88] The wetted material of the compression piece (top half) is made from stainless steel to ensure compatibility with a broad range of reagents, while the bottom portion is constructed from aluminum to create a sufficient heat sink for the thermoelectric device. The reaction temperature is monitored with a thermoresistor that is in direct contact with the microreactor and is inserted into the top plate. The assembly of this packaging scheme is given by Figure 2-8.
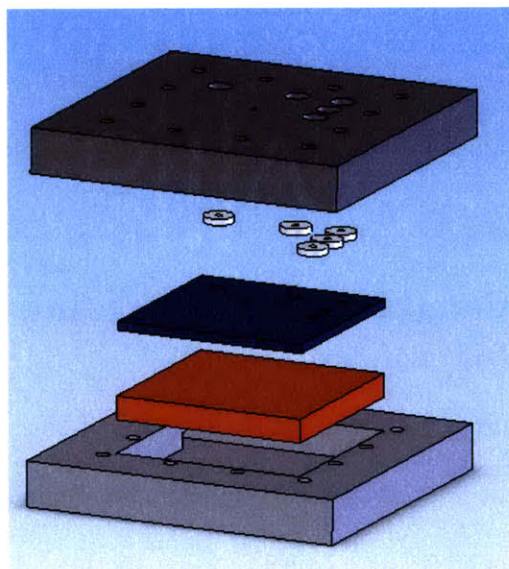
Figure 2-8: Assembly of compression packaging scheme for microreactor used in reaction screening investigation.

Introducing reagents into the microreactor system as injections required balanced pressure drops between the liquid hander and the T-mixing junctions of the inlet zone for each reagent. The Hagen-Poiseuille Equation (Eq. 2.1) was used to calculate the pressure drops for a given set of reactor channel dimesions. Then, the necessary channel widths and lengths for the three inlet channels were calculated, such that the first two reagents enter the first T-mixer simultaneously, and the resultant stream enters the second T-mixer at the same time as the third reagent. The channel widths were then 118 µm wide for the first two inlets, 150 µm wide for the third inlet and the stream from the first T-mixer, 200 µm wide in the mixing zone, and the reaction zone channels were 400 µm wide. The time scale for mixing by diffusion (t_D), given by Eq. 2.2, is 10 seconds; therefore mixing was not a concern for screens that have reaction time scales on the order of a minute.

$$\Delta P = \frac{8\mu QL}{\pi R^4}$$ 2.1

41

$$t_D \sim \frac{R^2}{D}$$ 2.2

2.3 Multi-dimensional Reaction Screening of Bicyclo[3.2.1]octanoids

The dense functionality of bicyclo[3.2.1]octanoid scaffolds such as **1** and **2** is highly desirable for reaction discovery. A set of 23 heteroatom nucleophiles, 16 carbon/dipole nucleophiles, and 16 electrophiles were screened using the microfluidic system. Due to the presence of multiple electrophilic centers on the substrate, reaction partners capable of tandem nucleophilic additions were also included. Two non-nucleophilic bases offering a range of basicity, 1,5,7-triazabicyclo[4.4.0]dec-5-ene (TBD) and 1,8-diaza-bicyclo[5.4.0]-undec-7-ene (DBU), were utilized in the multi-dimensional screen. A complete representation of the screening dimensions is shown in Figure 2-9.

2.3.1 Experimental Procedure

Each reaction was performed using 1 µmol of substrate (typically 0.25 mg), with 2.0 to 3.0 equiv of reaction partner and 1.2 equiv of base with a total reaction volume of 24 µL. This reaction volume was achieved by delivering 8 µL of each reaction component from stock solutions in the reagent storage block to the reactor simultaneously. The required stock solutions were prepared in both DMSO and CH_3CN in oven-dried glass sleeves with minimal exposure to air as 0.125 M solutions of the bicyclo[3.2.1] substrates, 0.250 M solutions of the reaction partners, and 0.150 M solutions of the bases.

Reaction times of 5 min and 20 min were achieved by utilizing set flow rates of 4.5 µL/min and 1.2 µL/min respectively (multi-head syringe pump with 4 - 10 mL syringes). Reactions were quenched in the reactor with 10 % v/v acetic anhydride, and collected into 96-

well plates using UV- triggered fraction collection. The diluted reactions (final concentration =

1 mg/mL) were analyzed using UPLC/MS/ELSD without further preparation.
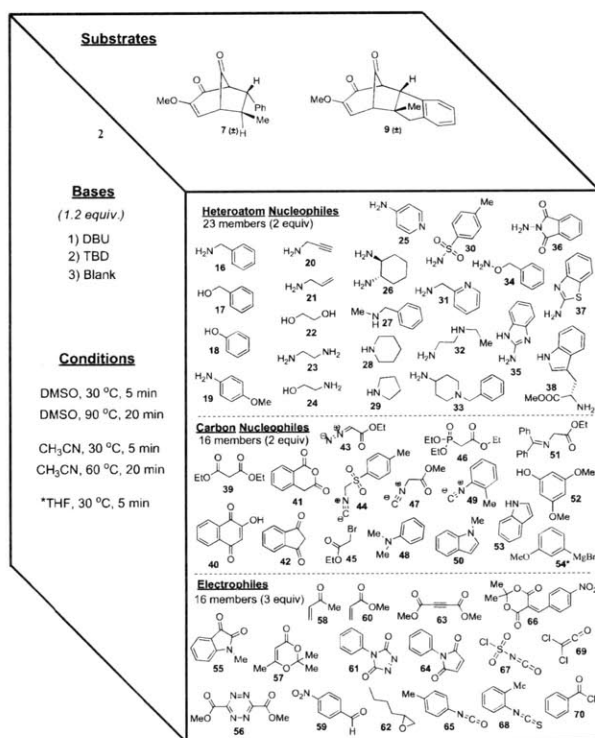
Figure 2-9: Range of multi-dimensional reaction screening parameters.
Parameters included substrates (1 and 2), different reaction partners (16 -70), solvents (DMSO and acetonitrile), bases (DBU and TBD), as well as three different reaction temperatures and two different residence times.

2.3.2 **Results**

The automated microreactor screening system investigated reactions of two substrates with 55 reaction partners (23 heteroatom nucleophiles, 16 carbon/dipole nucleophies, 16 electrophiles) and two bases (DBU and TBD) in two different solvents (acetonitrile and DMSO) at two different residence times (5 and 20 minutes) and two temperatures (30° and 60° C in acetonitrile and 30° and 90° C in DMSO). These combinations lead to 880 automated

experiments performed by the microreactor system. To demonstrate the wealth of reaction information that can be extracted from this system, a summary of the results are highlighted below. A more detailed discussion of the reaction results is provided elsewhere.[105]

Analysis of UPLC/MS/ELSD data for the reaction screen indicated positive outcomes for 11 out of 23 heteroatom nucleophiles investigated. All of the primary amine nucleophiles afforded retro-Dieckmann-type ring-opened products. Positive results utilizing substrate **1** were observed when either DBU or TBD were used; whereas positive results utilizing substrate **2** were only observed when TBD was used as base. Neither heteroatom nucleophiles without an alkyl primary amine nor secondary amines, with exception to pyrrolidine, reacted under any of the conditions examined in the screen. Reaction partners with the potential for tandem nucleophilic additions also afforded retro-Dieckmann-type ring-opened products, but did not undergo a second, intramolecular addition.

2.4 Conclusions

This thesis research demonstrated the ability to use automated microreactor systems to screen hundreds of reactions on the analytical scale. Chemical libraries of reaction data are rapidly compiled with this technology to allow researchers to hypothesize what reaction pathways are likely to afford the desired target molecule. For example, the library developed for the model retro-Dieckmann reaction indicated that primary amine nuclueophiles were the most reactive molecules of the different compounds investigated. Because this insight narrows the design space to the most likely candidate reactions, the speed at which candidates move from the discovery to the developmental stages is greatly accelerated. In comparison to the current 96-well plate, screening reactions in an automated microreactor system is valuable when

investigating fast reactions, where the outcome will be highly dependent on the mixing quality, and when exploring reactions at high temperatures and pressures.

Chapter 3
Experimental Optimization Algorithms

Due to the high value of raw materials, intermediates, and API in pharmaceutics, determining the reaction conditions that maximize product yield is a critical and a time consuming task. Numerous factors, such as temperature, concentrations of reagents and catalyst, residence time, pH, ionic strength, and solvent composition, impact the success of a reaction. Univariable search techniques, where a single variable is adjusted at a time, are commonly applied in academic research labs to determine the optimal reaction conditions. Although this approach can effectively describe the relationship between the reaction outcome and a single variable, it can be inefficient at finding the optimal conditions and it is incapable of evaluating the interaction between variables.[122] Statistical methods, such as Design of Experiment (DoE),[123] can capture these interactions and are used to model the reaction response surface over a broad range of conditions. Classical response surface modeling techniques, however, are limited to describing this response surface through linear and quadratic models.[124] Caution should be exercised when using these models to locate the optimal conditions for complex chemical systems, such as those with multiple reaction pathways, because these systems are likely to have nonlinear, nonconvex response surfaces.

These uni- and multi-variable searches are common laboratory practices in reaction optimization, despite the disadvantages and limitations, because the approaches are conducive for batch experimentation. The set of experiments are pre-determined, and multiple flask reactors can be operated in parallel to quickly obtain the reaction results. The ability to

incorporate inline analytics and perform sequential experiments in continuous-flow reactors grants the opportunity to consider alternative approaches. Such an approach could incorporate previous reaction results with a feedback mechanism to select experiments aimed at more efficient reaction optimization. While this strategy is straightforward, selecting the most appropriate experimental optimization algorithm warrants consideration.

Developing the methodology that guarantees a global solution to nonconvex Chemical Engineering problems and subsequent demonstration through computational simulations are a focus of many research investigations.[125-128] While these studies are critical to ensure that a process does not operate at suboptimal conditions, they require an explicit expression for the objective function. Applying these approaches to reaction optimization requires knowledge of the reaction pathways over the feasible space, a rate law model for each pathway, and precise kinetic estimates for each rate law. Because this knowledge is seldom available or is prohibitively difficult to experimentally to ascertain, black-box optimizations were initially implemented into the automated microreactor system. The following sections briefly describe some of the salient features of several algorithms that were considered. When selecting an algorithm for experimental optimization, a method that locates the area of optimality in relatively few experiments is often preferable to a method that pinpoints the optimum.

3.1 Description of Considered Optimization Algorithms

Selecting the most appropriate optimization algorithm with limited reaction information is difficult because the objective function can be simple and monotonic or highly corrugated, depending upon the complexity of reaction scheme. If the objective function was a plane over a convex set, then a linear programming method would be most suitable. Alternatively, if the objective function was nonlinear and convex over a convex set, then it would be advantageous to

use a gradient-based algorithm. However, deciding upon the search direction and the step size that minimizes the number of experiments required to find the optimum is also a challenging task for gradient-based methods. Finally, a nonlinear, nonconvex objective function may be associated with systems that have multiple reaction pathways. Sophisticated methods and heuristics exist to solve this class of problems, but can require numerous iterations for convergence. These methods would be unattractive in experimental optimization, where approaches with many iterations are translated as exceedingly many experiments.

The following sections describe the concepts and details of algorithms that were considered for implementation in the automated microreactor system.

3.1.1 Black-Box Optimization

Black-box optimization approaches are ideal when obtaining the objection function values are expensive, prone to error, or noisy. This scenario can exist in experimental optimization when performing a reaction is difficult due to limited research resources, and when there is adequate variance in experimental measurements.

3.1.1.1 Nelder-Mead Simplex

The Nelder-Mead Simplex is a direct search method which forms a polyhedron on the reaction parameter with $k+1$ equidistant vertices, where k is the number of independent optimization variables (i.e., temperature, time).[129] Coded variables are commonly used to center and to normalize the "main effect" of each reaction variable. For any reaction variable, ξ, the coded variable, x, is computed by Eq. 3.1, where ξ^o is a reference value, and $\Delta\xi$ is the step-size of the variable.

48

$$x = \frac{\xi - \xi^o}{\Delta \xi} \hspace{5cm} 3.1$$

The conditions for each experiment corresponds to a vector, **x**, with elements of x_i, where i is an index used to denote the reaction variable. The size of **x** is determined by the number of variables involved in the optimization procedure, k. Using **x**=**0** as the base point of the simplex, the remaining k vertices of the initial simplex are computed by Eq. 3.2, where n is the index denoting the experiment number (i.e., 2 for the 2nd experiment,..., N for the Nth experiment) and α is a step size metric.

$$x_{n,i} = \begin{cases} \dfrac{\alpha\sqrt{k+1}+k-1}{k\sqrt{2}} & \text{for } i = n \\[4mm] \dfrac{\alpha\sqrt{k+1}-1}{k\sqrt{2}} & \text{for } i \neq n \end{cases} \hspace{3cm} 3.2$$

After evaluating the objective function for each point of the simplex, the point with the worst objective function is selected, x_w, and the center point of the remaining vertices, x_c, is calculated. The conditions for the next experiment, x_{new}, are calculated by reflecting x_w about x_c, as defined in Eq. 3.3.

$$x_{new} = 2x_c - x_w \hspace{5cm} 3.3$$

The experiment at x_{new} replaces x_w in the simplex if the objective function at x_{new} is better than the objective function at x_w. Otherwise, x_{new} is excluded from the simplex, and a new sequential experiment is calculated based upon the point in the simplex with the next lowest objective function value. This procedure is repeated until no further reflections improve the objective function. Depending on the termination criteria, this procedure would continue with a contracted

simplex for a finer search of the reaction space, or report the observed optimal conditions and terminate.[130] This procedure is illustrated in Figure 3-1.
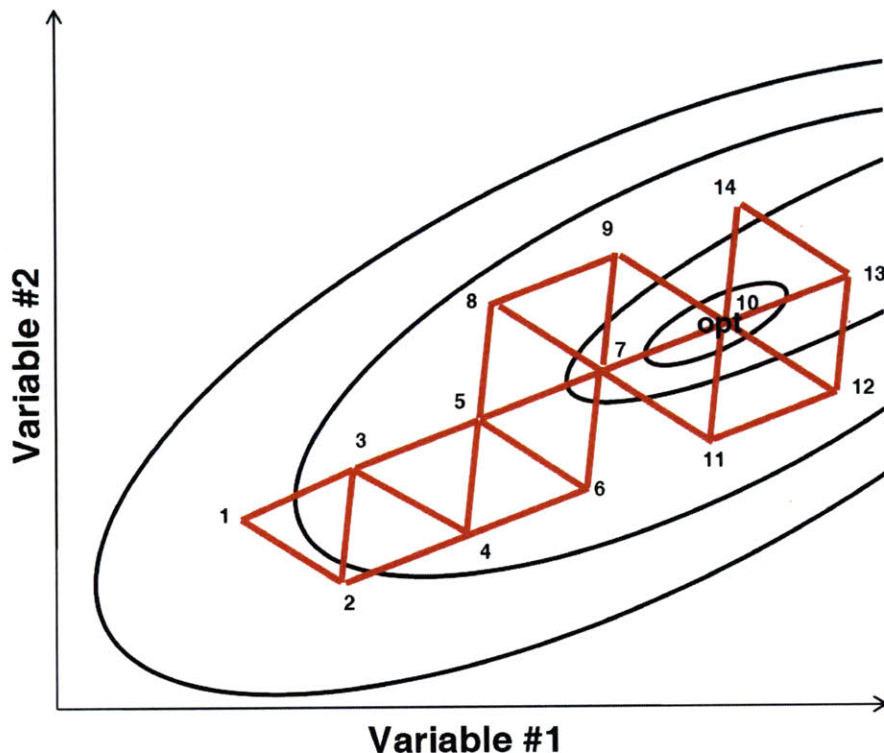
Figure 3-1: Illustration of Nelder-Mead Simplex Method.
Numbers denote sequence of iterations (experiments) used to find optimum (opt).

This approach requires no knowledge of first or second derivatives of the response surface, it is straightforward to implement, and monitoring of the optimization procedure is simple. Moreover, the algorithm is even effective when there is error in the experiment or in the measurement of the objective function because it acts on the worst point rather than the best.[131] The Nelder-Mead Simplex is not ideal for optimization searches where the optimum is near the border of the parameter space due to the slow convergence. To prevent this issue, a penalty function can be used to bias the search away from the bounds of the feasible space until the simplex has contracted to a specified length.

3.1.1.2 Stable Noisy Optimization by Branch and Fit (SNOBFIT)

SNOBFIT, originally developed by Huyer and Neumaier,[132] combines local and global search methods to optimize an objective function over a feasible space defined by lower and upper bounds on each design variable. Rather than selecting a single sequential experiment, each call to the SNOBFIT program outputs a set of sequential experiments. The tuneable parameters for this algorithm include 1) the set size of sequential experiments performed between calls to the SNOBFIT function, and 2) the fraction of sequential experiments that are performed in unexplored regions of the parameter space, denoted as p. After the initial set of space-filling experiments, the set of sequential experiments belong to one of the following classes:

- Class 1: The experimental point of class 1, x_1, that minimizes a quadratic model around the nearest neighbors of the best point, x_{best}. The coefficients $\mathbf{g}$ and $\mathbf{G}$ of Eq. 3.4 are determined through an error minimizing technique, as discussed by Huyer and Neumaier.[132]

$$\mathbf{x}_1 = \arg\min f\left(\mathbf{x}_{best}\right) + \mathbf{g}^T\left(\mathbf{x}_1 - \mathbf{x}_{best}\right) + \frac{1}{2}\left(\mathbf{x}_1 - \mathbf{x}_{best}\right)^T \mathbf{G}\left(\mathbf{x}_1 - \mathbf{x}_{best}\right) \qquad 3.4$$

- Class 2: Experimental points of class 2, x_2, are local solutions to Eq. 3.5, where D is related to the expected errors of the experimental measurements, and $d(\mathbf{x})$ is a trust region size vector. A local solution to Eq 3.5. is one where the expected value, $f(x_2)$, falls within a specified range of objective function values of the nearest neighbors of $\mathbf{x}$.

$$p = \arg\min \mathbf{g}^T p + \sigma p^T Dp$$
$$s.t. p \in [-d(\mathbf{x}), d(\mathbf{x})] \qquad 3.5$$

$$\mathbf{x}_2 = p^* + \mathbf{x} \qquad 3.6$$

- Class 3: Solutions to Eq. 3.5 that are not local.

- Class 4: The fraction of experimental points, defined by input parameter p, that are performed in unexplored regions of the feasible space.

Experiments associated with Class 1 − 3 are local search methods, aimed at quickly locating local optima; whereas Class 4 points represent the global search component of this algorithm. For the design space size common in most chemical syntheses, this algorithm is likely to locate a local optimum after the first or second iteration. The subsequent iterations provide more confidence that the reported local optimum is a global solution, or present a better opportunity of finding the global solution in comparison to other common experimental optimization algorithms.

3.1.2 Gradient-Based Methods

Algorithms that use gradient information are more efficient because the gradient points in steepest direction towards a local optimum. Gradients can be experimentally estimated using response surface modeling techniques and DoE. The full factorial designs are used to model 1st order main effects and interaction terms; whereas central composite designs are the most popular choice when trying to capture quadratic characteristics.[124]

3.1.2.1 Full Factorial Designs

For reaction systems with k number of design variables, the full factorial design also known as the 2^k factorial design, is a popular DoE technique for evaluating main effects and interaction terms of a response surface. The 2^k factorial involves n_F points located at "high" and "low" levels for each variable, and can include n_C repeat experiments at the center of the design. Responses from 2^k designs are used to fit the a first-order response surface model given by Eq. 3.7 via a sum of squared errors method.[133] The presence of quadratic curvature effects can be

statistically evaluated through an F-test (Eq. 3.8), by calculating the single-degree-of-freedom sum of squares, $SS_{Pure\ Quadratic}$ (3.9), and the error estimate, $\hat{\sigma}$ (3.10).[124] The null hypothesis, quadratic curvature effects are not present in the response surface, is accepted if $F < F_{\alpha, n_F - p, n_C - 1}$, where α is the significance level and p is the number of fitted parameters in the linear regression. Alternatively, if $F > F_{\alpha, n_F - p, n_C - 1}$, pure quadratic effects may be present and a second order response surface model is required.

$$f = \beta_0 + \sum_{i=1}^{2^k + n_C} \beta_i x_i + \sum_{i=1}^{2^k + n_C - 1} \sum_{j=i+1}^{2^k + n_C} \beta_{i,j} x_i x_j \qquad 3.7$$

$$F = \frac{SS_{Pure\ Quardratic}}{\hat{\sigma}} \qquad 3.8$$

$$SS_{Pure\ Quardratic} = \frac{n_F n_C \ \overline{f}_F - \overline{f}_C}{n_F + n_C} \qquad 3.9$$

$$\hat{\sigma} = \frac{\sum_{l=1}^{n_C} f_{C,l}}{n_C - 1} \qquad 3.10$$

Although the 2^k factorial design provides a significant amount of information regarding the response surface, it can require many experiments if k is not small. However, several methods exist to maintain high information content while reducing the number of experiments. For example, factorials can be confounded, or partially confounded, to decrease the number of experiments by a factor of two.[123] However, as a consequence, higher order interactions are aliased with the main effects.

3.1.3 Second Order Response Surface Designs

Although 2^k factorial designs may be appropriate for surfaces far from the optimum, second-order regression models are required to fit the high curvature that typically exists at the optimal conditions. The central composite design (CCD) is the most popular design method used to fit these surfaces.[133] The CCD expands upon the 2^k design with $2k$ axial points, which are a distance α away from the center point. Generally, α is selected to generate rotatable design where the variance is equal for all points $\mathbf{x}$ that are the same distance from the center point.[124] A quadratic model given by Eqs. 3.11 and 3.12 is used to characterize this response surface.

$$f = \beta_0 + \mathbf{x'b} + \mathbf{x'Bx} \qquad 3.11$$

$$\mathbf{x} = \begin{bmatrix} x_1 \\ x_2 \\ \vdots \\ x_k \end{bmatrix} \quad \mathbf{b} = \begin{bmatrix} \beta_1 \\ \beta_2 \\ \vdots \\ \beta_k \end{bmatrix} \quad \mathbf{B} = \begin{bmatrix} \beta_{11} & \beta_{12}/2 & \cdots & \beta_{1k}/2 \\ & \beta_{22} & \cdots & \beta_{2k}/2 \\ & & \ddots & \\ \text{sym.} & & & \beta_{kk} \end{bmatrix} \qquad 3.12$$

Similar to the 2^k factorial design, there are methods to reduce the number of experiments while maintaining the sufficient information required for establishing a second-order model. The Box-Behnken Design uses 2^k factorials with incomplete block designs, resulting in a rotatable, or nearly rotatable, design.[133] When $k=2$, further reduction of experiments can be accomplished with a small composite design, which uses a fractional factorial where the main effects are aliased with two-factor interactions.[124]

3.1.3.1 Steepest Descent (Cauchy's) Method

Although numerous gradient methods exist, the simplest technique to implement is Cauchy's method, also known as the Steepest Descent Method. The application of the Steepest

Descent Method to find a local optimum point is based on a first-order Taylor's expansion of the function's gradient about a given point, x_i. The gradient can be estimated using the response surface modeling techniques discussed in the previous sections. The sequential point, x_{i+1}, is selected according to Eq. 3.13, where $\nabla f(x_i)$ is the gradient evaluated at x_i and λ_i is the step-size.

$$x_{i+1} = x_i - \lambda_i \nabla f\left(x_i\right) \qquad 3.13$$

Progression of experiments continues in this fashion until the objective function increases. At this point, a new gradient is calculated and the Steepest Descent Method continues until the gradient is approximately zero, corresponding to a local optimum. For most optimization applications, the gradient is updated after every iteration. For experimental optimizations, however, this update requires a 2^k factorial design or CCD and can result in a prohibitively large number of experiments.

The step size, λ_i, is a tunable parameter in this algorithm that can be adjusted to minimize the number of iterations required to reach the optimum. In the original Steepest Descent Method, the value of λ that satisfies Eq. 3.14 is selected at each iteration. However, this step-size criterion is difficult to employ in experimental optimization applications, because reasonable objective functions can only be approximated near the experimental design. Objective function values extrapolated beyond this design space are likely to be inaccurate and hinder the speed of the optimization process.[134] Heuristic step sizes have been proposed for convergance,[135] but must follow the criteria set by Eqs. 3.15 and 3.16 to achieve convergence.[136]

$$\lambda_i = \arg\min_{\lambda} f\left(x_i + \lambda \nabla f\left(x_i\right)\right) \qquad 3.14$$

$$\lim_{i \to \infty} \lambda_i = 0 \qquad 3.15$$

$$\sum_{i=1}^{\infty} \lambda_i = \infty \qquad\qquad\qquad 3.16$$

For experimental optimization, where the response surface is not known *a priori*, the Steepest Descent Method can lead to slow convergence due to zig-zag trajectories when traveling down steep valleys. Furthermore, convergence can be relatively slow around the optimum where the gradient is approximately zero. Analogues and modifications to the Steepest Descent Method exist to avoid these disadvantages. The conjugate gradient method can avoid the oscillatory behavior of the Steepest Descent Method by incorporating the previous gradient information in the calculation of the new search direction.[137] Newton's Method evaluates the curvature in the objective function by computing the Hessian, and uses this information to take a more direct route to the optimum. Quasi-Newton methods approximate the Hessian using a variety of techniques, such as the Broyden-Fletcher-GoldFarb-Shanno (BFGS) method or David-Fletcher-Powell (DFP) formula.[138]

3.2 Conclusions

The algorithms discussed in this Chapter were used in the automated microreactor system for online reaction optimization. These algorithms represent a fraction of the techniques that could be used as a feedback mechanism for experimental optimization. Selection of an appropriate algorithm is dependent upon the number of experiments that can be performed, as well as the desired precision in the optimization results in comparison to the experimental variance.

The Nelder-Mead Simplex Method was applied to various reaction optimization investigations because of its robustness, ability to handle experimental error, and the small number of experiments required to follow the gradient. The Steepest Descent Method is ideal

when the objective function is linear, or when the experiments involved in the initial DoE characterize the gradient over a large portion of the feasible region. For reactions that require multiple gradient computations, the number of experiments performed to characterize the response surface ranges from 2^k to 2^k+2k. These experiments, while necessary to accurately find the optimum, may not be ideal when research resources are limited. The progression of the Simplex Method implies that at most $2k$-1 experiments will be necessary to determine a subgradient direction. The SNOBFIT Method was also incorporated into the automated microreactor system because it is a direct search method that is more likely to find the global solution than the Simplex Method or Steepest Descent Method, but also requires more experiments.

Chapter 4
Automated Optimization in Microreactor Systems

The small length scales inherent to silicon microreactors permits reactions to be explored without transport limitations and provides more precise control over operating conditions. These attributes make microreactors an ideal technology for reaction optimization and kinetic investigations. However, the specialized equipment required for microreactor systems also increases the difficulty of screening reaction conditions in parallel as is commonly performed in batch. Therefore, the development of efficient strategies to optimize reaction conditions in a series of consecutive experiments is particularly valuable for microreactors. Towards this end, a self-optimizing microreactor system that uses previous reaction data to efficiently select future experiments was developed in this thesis research.

To become a viable research instrument for pharmaceutical research and development, the automated microreactor system must be chemically compatible with a broad scope of reactions, and the automated experimental protocol must be efficient. The latter requirement involves consideration to the amount of material that is lost during transient times between experiments and during reaction analysis. For example, after changing operating conditions of a flow reactor, the system is flushed before steady-state data is collected. Flushing the system with more material increases the likelihood of collecting accurate steady-state data, but also results in a larger loss of expensive reagents. Developing procedures that would consume the least amount of material and provide reproducible data was a priority in this thesis research. Further design concepts and system components are discussed in the following sections. General features of the

developed software programs are discussed where appropriate, and more specific details are provided in the Appendices.

4.1 Automated Microreactor System

A general schematic of the automated microreactor system developed in this thesis research is shown in Figure 4-1.
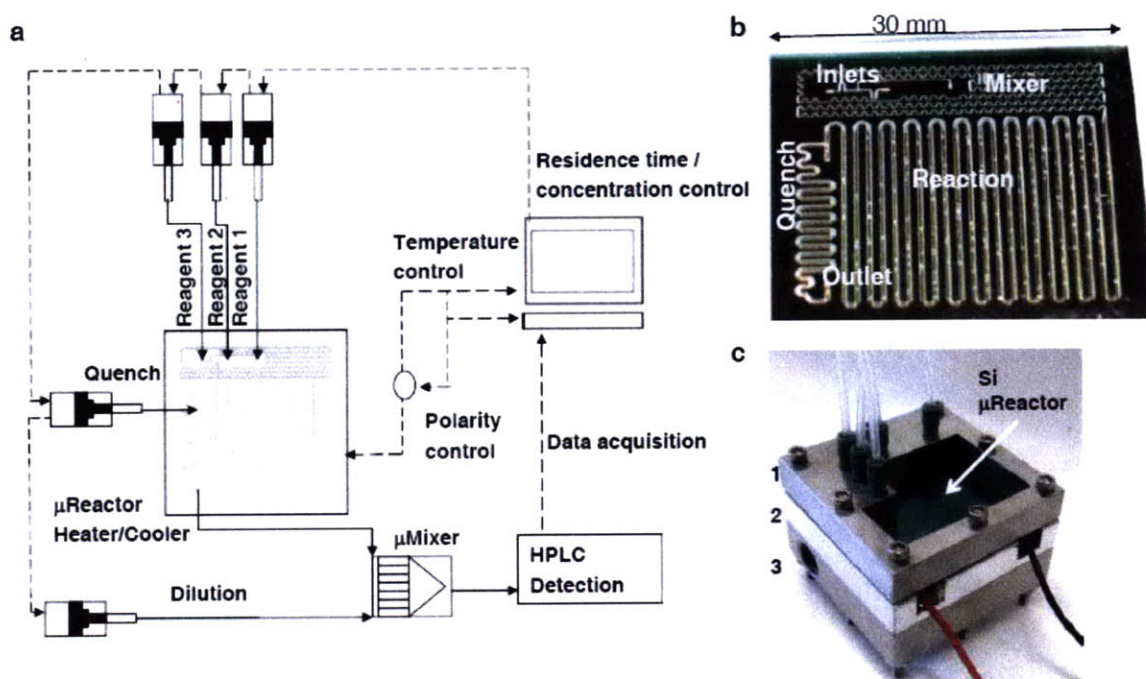
Figure 4-1: Microreactor system for automated reaction optimization.
(a) Schematic of automated microfluidic system consisting of syringe pumps, microreactor, micromixer, HPLC, and process computer with associated LabVIEW interface hardware. (b) Microreactor used in optimization study with mixing, reaction, and quench zones (c) Packaging scheme for the microreactor including fluidic connection in the top plate (1), a recessed plate (2) to house the microreactor and TE device, and baffled heat exchanger (3) for sufficient heat removal and additional temperature control.

4.1.1 Microreactor Technology and Fluidic Interfacing

The silicon reactor (Figure 4-1b) was fabricated using standard lithography and deep reactive ion etching (DRIE) techniques.[59] The channels were etched 400 μm deep and consisted of three zones – a mixing zone with 200 μm wide channels (18 μL) to promote mixing, followed

59

by a reaction zone with 400 μm wide channels (69 μL) to act as a residence time unit, followed by a 8μL quench zone to terminate the reaction on chip. The reactor was coated with silicon nitride and capped with Pyrex to create a chemically inert environment that is suitable for numerous chemistry applications.

A compression packaging scheme (Figure 4-1c) was used to interface macrofluidic instruments with the microreactor. The top plate of the compression unit was machined from stainless steel for chemical compatibility with reaction components, while the middle and lower plates were fabricated from aluminum to increase heat transfer in the compression unit. Port holes for the reagents, quench, and outlet streams were machined for PEEK 6-40 connections (IDEX, M-644-03, M-650) on the front side of the top plate. Recesses for PTFE O-rings (McMaster-Carr, AS568A Dash No. 003) were drilled on the back side of these ports to establish a fluidic seal when compressed. The middle plate was recessed to house the microreactor and thermoelectric element (TE) device (TE Technology, HP-127-1.0-1.3-71), which acted as the heating and cooling source for the reactor. The bottom plate of the compression unit was a baffled heat exchanger used to remove heat accumulated by the TE device. All other fluidic connections were established using standard 1/4-28 flangeless fittings and 1/16" OD PFA tubing (Idex).

A time scale analysis for this device was performed to determine the most appropriate reaction design space. The time scale for mixing was calculated by modeling the transient diffusion problem given by Eq. 4.1. After properly scaling the terms and applying the boundary conditions, it can be shown that the solution follows the form of the complementary error function.[139] Therefore, the time required to achieve 95% complete mixing, is given by Eq. 4.2, where D is the diffusion coefficient and W is the width of the channel. Assuming a diffusion

coefficient of 1×10^{-9} m^2/s and using the width of the mixing zone channels (200 µm), this time scale is equal to 5 s. For accurate optimization and kinetic investigations, the upper bound on the flow rate through the microreactor was determined by requiring 95% complete mixing to occur within the mixing zone. For the mixing zone of 18 µL, this maximum flow rate corresponds to 216 µL/min. If faster flow rates were investigated, it was understood that the results may be specific to the microreactor.

$$\frac{\partial C}{\partial \tau} = D \frac{\partial^2 C}{\partial x^2}$$

4.1

$$t_D = \frac{W^2}{7.84D}$$

4.2

To ensure that the reaction occurred isothermally, the reaction stream was modeled as a Graetz problem (Eq. 4.3).[139] For simplicity, the reactor was modeled as a tube with hydrodynamic radius, R_H. After the appropriate scaling of this equation, it can be shown that the thermal entrance length, L_T, is given by Eq. 4.4. For the maximum flow rate determined above, and assuming a nominal thermal diffusivity of 1×10^{-7} m^2/s, the maximum thermal entrance was calculated as 2 mm. Because the length of the reactor is approximately 400 mm, this small thermal entrance length indicates that reactions were investigated isothermally under all flow conditions. Additionally, FemLab (Comsol, version 2.3b) simulations indicated that there was less than 1°C temperature difference between the Pyrex$^\circledR$ side that was heated and the silicon side where the temperature was measured. Therefore, it was anticipated that reactions investigated in the automated microreactor system would be isothermal and that precise reaction temperatures measurements would be recorded.

$$2U\left[1-\left(\frac{r}{R_H}\right)^2\right]\frac{\partial T}{\partial z} = \frac{\alpha}{r}\frac{\partial}{\partial r}\left(r\frac{\partial T}{\partial r}\right) \qquad\qquad 4.3$$

$$L_T = 0.0628 Pe \cdot R_H = 0.0628\frac{2UR}{\alpha}\cdot R_H \qquad\qquad 4.4$$

4.1.2 **Temperature Control for High Throughput and Wide Parameter Space**

Controlling the reaction temperature in a microreactor is commonly accomplished by immersing the device into a bath.[140] However, the large thermal mass of the bath creates a long lag-time between experiments that involve different temperatures. This dead-time is prohibitive for a system where a high throughput of experiments is required. Resistive tapes and cartridges have been used to quickly heat microreactors,[25, 141] but cooling by convection between experiments can also result in slow dynamics. Furthermore, this approach is not acceptable when the microreactor needs to be cooled below ambient temperature. Because an optimization algorithm may explore both warmer and cooler reaction temperatures, it was imperative to seek a temperature control scheme that was capable of continuous heating or cooling.

A TE module was used to heat or cool the microreactor, thus providing a temperature control scheme that broadened the parameter space during optimization investigations and decreased transient lag-times. A pulse width modulated (PWM) approach with a proportional-integral-derivative (PID) controller on the duty cycle provided reaction temperatures within 1.5 °C of the set point temperature. A separate control algorithm on a double pole, double throw switch (Potter Brumfield, KUP-11D15-24) controlled the direction of the current through the TE element, offering a means to heat or cool the reactor without discontinuity in operations. The algorithm, named "TemperatureController.vi", was set to cool the reactor if the temperature was

5°C above the set-point temperature or if the set-point temperature was below ambient temperature. More details of the temperature control program are provided in Appendix B.

When cooling, the heat removed by the TE module will return to the microreactor through conduction and natural convection if it is not dissipated correctly. The baffled heat exchanger mentioned in the preceding section was used as heat sink for the TE module. This heat sink used pipe and tube fittings (McMaster-Carr, 1/8" x 1/16" pipe adapter, 3/8" hose x 1/8" pipe adapter) to make the necessary connections to a circulating temperature bath (Fisher Scientific, Isotemp 3016D) that pumped water at 10°C through the bottom plate heat exchanger. This arrangement provided reaction temperatures from -30° to 120°C, giving the automated microreactor system a wide range of temperatures to explore during the optimization procedure. Lower temperatures could be achieved by lowering the temperature of the circulating bath and stacking multiple TE modules. Characterization experiments were performed to assess the transient time between several different temperatures for three different controller schemes (Figure 4-2). The method of active heating and cooling with a heat sink provided the most desirable results.
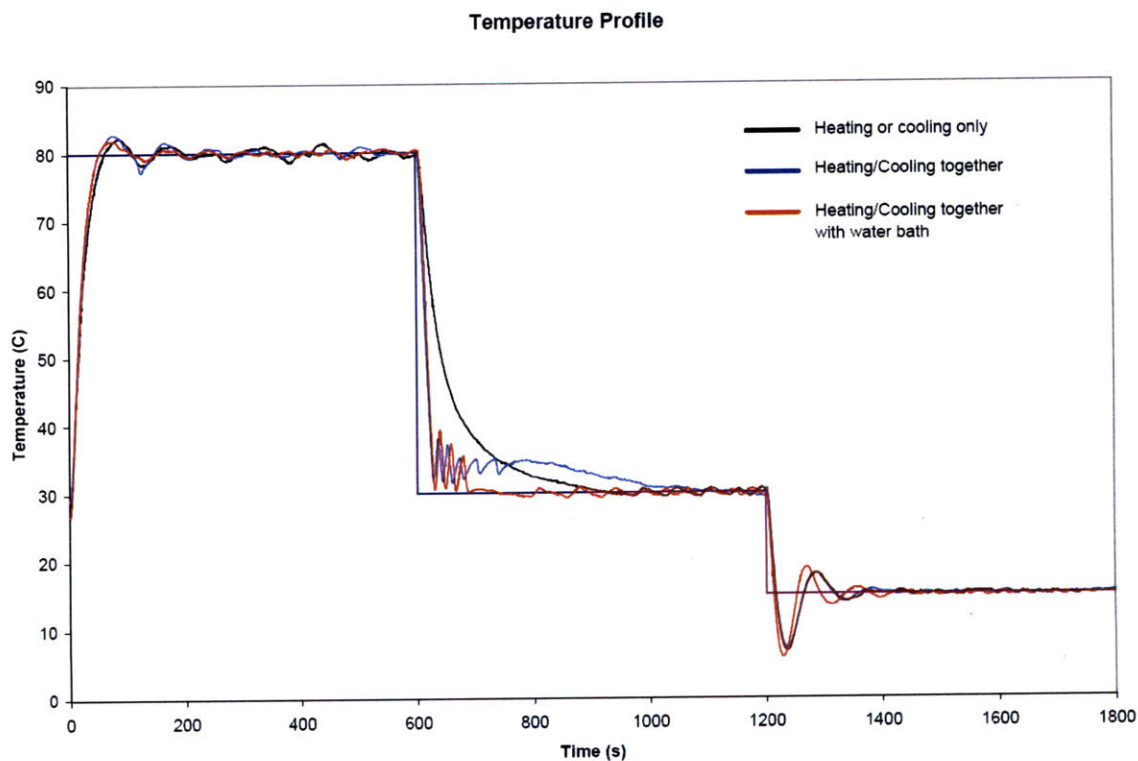
**Figure 4-2: Temperature profile for different controler configurations.
The most desirable behavior corresponded to the active heating and cooling scheme with a heat sink.**

4.1.3 Detection and Analytical Components

Previous works have relied on inline spectroscopy for monitoring of the reaction progress.[63, 83, 102, 142, 143] An ultraviolet photospectrometer and Z-path flow cell (10 cm flow path, Ocean Optics) were initially used for inline spectroscopic analysis of the reaction stream. Several problems were observed with the application of this technology. First, gas bubbles that entered the system during start-up or evolved with solvent degassing would become trapped in the flow cell and ruin detection. Additionally, the absorbance signals were variable with the pressure drop across the flow cell. A back pressure regulator could be included downstream of

the flow cell, but this additional pressure limited the flow rates that could be investigated with standard syringe pumps.

Organic synthesis typically requires a method that can distinguish between regio- and stereochemically different compounds.[144] Furthermore, slight differences between reactant and product structures can be difficult to quantify with spectroscopic measurements alone. For these reasons, a HPLC was integrated with the automated microfluidic system for online detection. Reaction samples were loaded into the HPLC system through a 6-way valve that was activated by contact closure through the relay module. Isocratic HPLC methods were created and operated using Empower software. Two analog outputs from the photodiode array, corresponding to the absorbance values at two specified wavelengths, were also configured using Empower. After specifying the retention time for each analyte, a baseline absorbance value for each wavelength was computed by averaging the absorbance signal at $10 - 30$ s before analyte elution. HPLC methods were developed to ensure that the analyte peaks were sufficiently separated at the specified wavelengths to avoid biasing this baseline measurement. Chromatograms were created by recording the absorbance signals that surpassed a threshold absorbance value around the specified retention times. Numerical integration functions in LabVIEW (Numeric Integration VI) and Matlab (trapz) were used to integrate a chromatogram, and the resulting area measurement was related to the analyte concentration through a calibration curve. An example of a chromatogram that was recorded with the automated microreactor system is given in Figure 4-3.
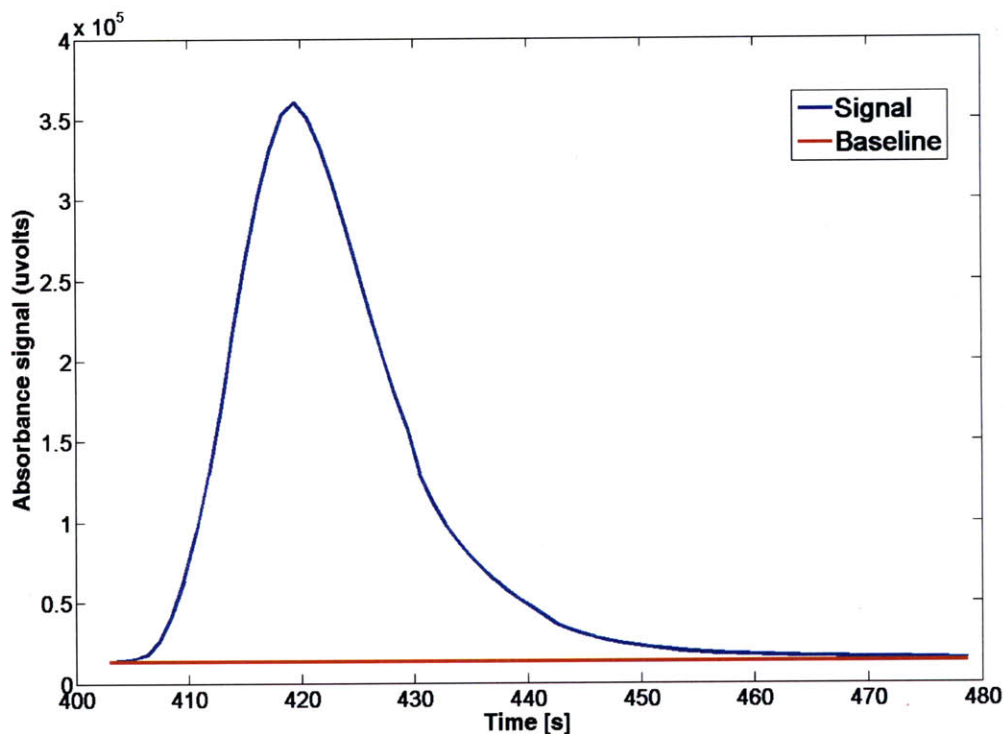
Figure 4-3: Example chromatogram recorded by automated microreactor system.
Integration functions in Matlab were used to integrate the area of the chromatogram above the baseline measurement.

4.1.4 Strategies for Efficiency, Repeatability and Reproducibility

During the development of this microreactor system, several methods to increase efficiency and reproducibility of data were identified. These inefficiencies are related to the amount of reagents that is lost during transient states of the systems or during HPLC analysis. Flushing the system several times is required to guarantee steady-state data collection, but excessive flushing results in unnecessary material loss. For the 87 µL microreactor and downstream tubing of approximately 60 µL, 600 µL of reactant material was flushed through the system before analysis. This corresponds to approximately 4 system volumes. Due to the compliance in the plastic tubing and syringes,[145, 146] some time is required for compression

before stable flow occurs. This equilibration would occur during the beginning of the flush. Reactant material was also preserved by lowering the flow rates of all syringe pumps to 2 µL/min during HPLC analysis.

It was also observed that certain flow conditions of the reaction stream and the quench stream caused poor mixing within the small volume of the quench zone, producing an unquenched reaction sample. Experiments and numerical simulations in FEMLab (COMSOL, version 2.3b) were performed to evaluate the mixing relationships and quench capabilities over a range of reaction and quench flow rates. Simulation results for a range of reaction flow rates (Q_r) and quench flow rates (Q_q) are shown in Figure 4-4. These simulations provided insight to appropriate quench techniques. For smaller flow rates $(Q_r = Q_q = 5$ µL/min, $Q_r = Q_q = 30$ µL/min), the amount of time that the fluid resides in the 8 µL quench zone is on the same order of magnitude as the time scale for mixing by diffusion (20 s). Therefore, effective reaction quenching was expected at these conditions, and confirmed experimentally. At larger equal flow rates $(Q_r = Q_q = 150$ µL/min), the fluid does not reside in the quench zone long enough for thorough mixing; therefore, the reaction stream was not anticipated to be completely quenched. This prediction was confirmed with experimental observations. Increasing the the quench flow rate $(Q_r = 150$ µL/min, $Q_q = 600$ µL/min) decreases the penetration depth required for effective quenching, but creates a concentration across the width of the microreactor channel. A 101-channel interdigitated micromixer[147] was incorporated downstream of the microreactor to create a uniform mixture before HPLC analysis. This methodology provided reproducibility equal to that of the HPLC detection, and the appropriate quench technique was considered for each reaction optimization investigation.
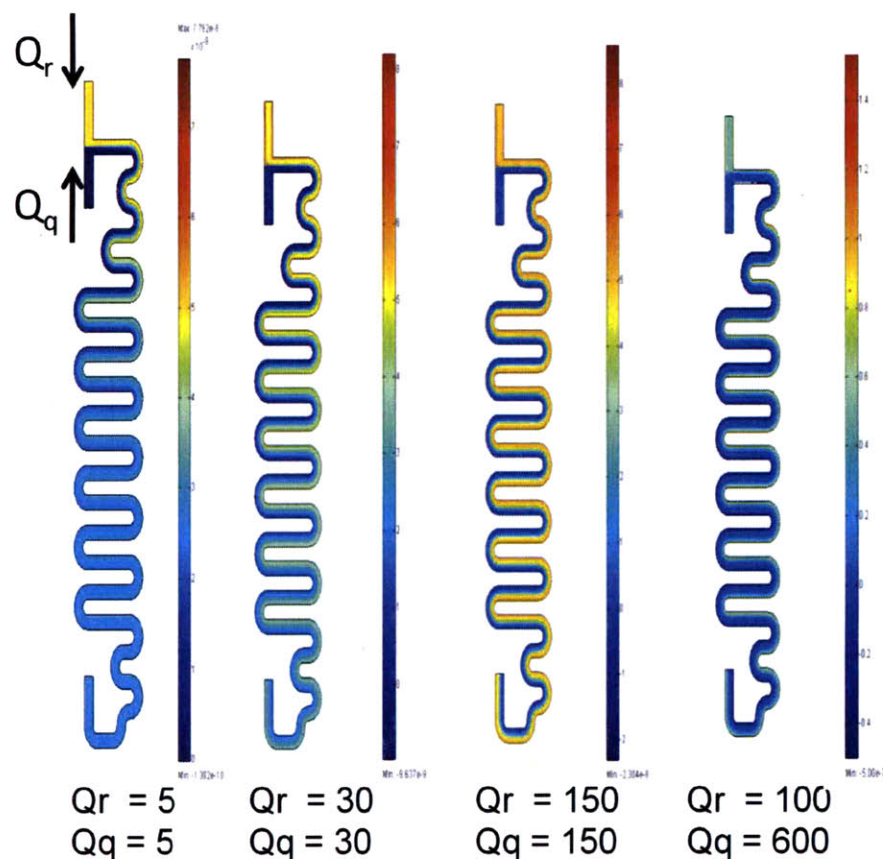
Figure 4-4: Numerical simulations that were used to determine appropriate reaction quenching technique. A uniform mixture, which implies effective quenching, is observed when there is a small color gradient across the outlet. All flow rates are in units of µL/min.

4.1.5 Experimental Protocol

The experimental procedure that was developed, validated, and implemented into the operations of the automated microreactor system is shown in Figure 4-5. First, the necessary criteria for the optimization and control methods were inputted into the program. After providing this information, the process became completely automated and user intervention was obviated. Each experiment began by thermally equilibrating the microreactor – defined as the absolute difference between the reaction temperature and the set point temperature (T_{SP}) being less than a specified tolerance, nominally 3 $^{\circ}$C. The system was then flushed adequately,

generally four system volumes (V_{sys}), to ensure steady-state conditions. A sample was then injected into the HPLC system and the chromatographic data was recorded with the LabVIEW hardware. The area of the chromatogram was computed to determine the concentration of the different components. After using these measurements to calculate the objective function, the optimization algorithm determined the next sequential experiment in the procedure, or terminated if appropriate.
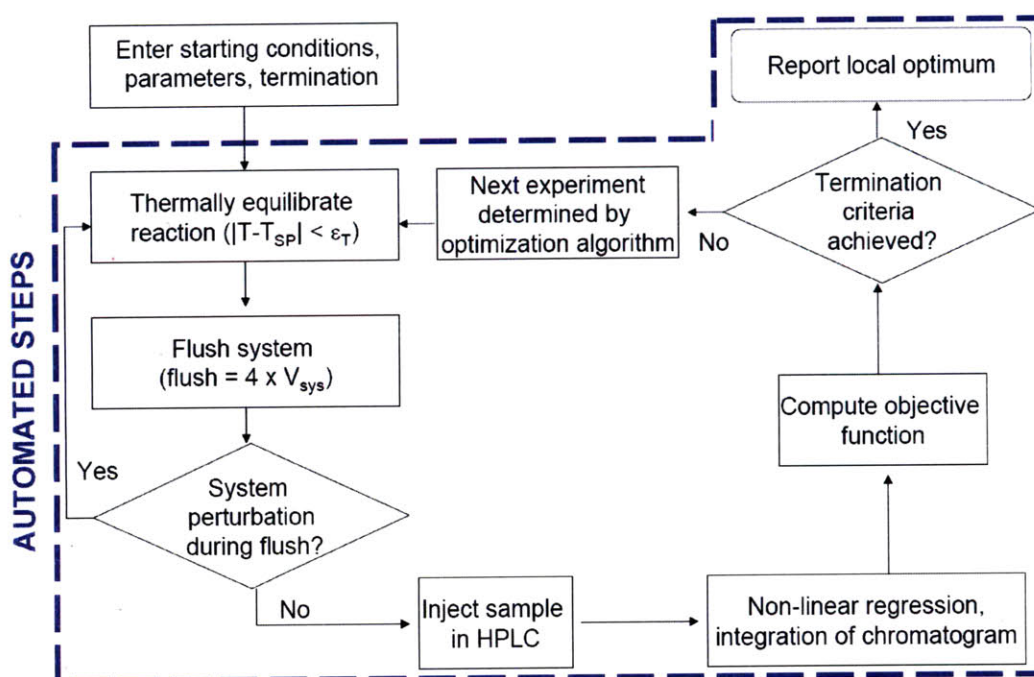
Figure 4-5: Flowsheet description of operations implemented into automated microreactor system.

4.1.6 Automated Calibration

The monotonous process of formulating a calibration curve for the reaction species of interest was automated by loading each compound onto a syringe pumps and adjusting the flow rate of each pump appropriately. For *c* chemical species of interest, *c+1* independently controlled syringe pumps were required. These *c+1* streams were combined in a micromixer to create a

uniform solution for HPLC detection. In this manner, precise calibration curves were quickly created

4.2 Automated Optimization

The automated microreactor system was used to perform various reaction optimizations. The experimental details and results are provided in the following sections.

4.2.1 Case Study I: Knoevenagel Condensation

The reversible, condensation reaction involving 4-methoxybenzaldehyde **1** and malononitrile **2** catalyzed by 1,8-diazabicycl[5.4.0]undec-7-ene (DBU) was selected as the first model reaction (Scheme 4.1).[148] Using three different feedback algorithms, the system maximized the weighted objective function, f_1 (Eqs.4.5-4.9), by varying reaction temperature and residence time within a constrained parameter space. This objective function, which is a combination of the production rate ($Q_{exp}Y_{exp}$) and the yield (Y_{exp}), biases the system to look at shorter residence times without sacrificing yield.[149] For reversible reactions, this approach searches for equilibrium conditions that can be achieved on smaller time scales. Algorithms used to optimize this reaction included the Nelder-Mead Simplex,[150] Steepest Descent Method using Design of Experiment (DoE) techniques for response surface modeling,[124] and Stable Noisy Optimization by Branch and Fit (SNOBFIT).[132] Implementing these algorithms demonstrated the robustness of the system and the ability to easily incorporate future algorithms aimed at optimizing complex reaction schemes and multi-step organic syntheses.
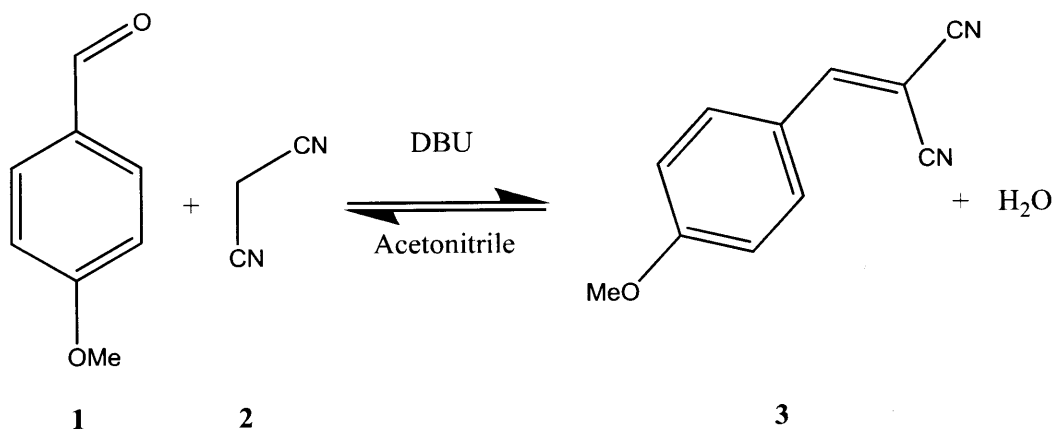
Scheme 4.1: Knoevenagel condensation of 4-methoxybenzaldehyde and malononitrile.
Knoevenagel condensation was performed in the automated microfluidc system with various optimization approaches to demonstrate the ability to implement numerous feedback methods into the system operations.

$$f_1 = \max_{T,\tau} \frac{Q_{exp} Y_{exp}}{Q_{max} Y_{max(theory)}} Y_{exp} \qquad 4.5$$

$$Q_{exp} : \text{Experimental flow rate} \qquad 4.6$$

$$Y_{exp} : \text{Experimental product yield} \qquad 4.7$$

$$Q_{max} : \text{Maximum flow rate, set by constraints on parameter space} \qquad 4.8$$

$$Y_{max} : \text{Maximum theorectical yield, 100\%} \qquad 4.9$$

4.2.1.1 Experimental procedure

<u>General method</u>   4-methoxybenzaldehyde, malononitrile, 1,8-diazobicyclo[5.4.0]undec-7-ene (DBU), naphthalene, trifluoracetic acid (TFA) and acetonitrile were purchased from the Sigma-Aldrich chemical company and used as received. The malononitrile bottle was heated to 40°C in a temperature bath to melt the reagent for solution preparation.   The product, 2-p-anisylidenemalononitrile, was produced in batch and isolated by chromatography. A calibration curve for the HPLC chromatograms was created using this isolated product.

Preparation of the substrate solution To a 10 mL flask was added 4-methoxybenzaldehdye (200 mM, 272 mg), malononitrile (200 mM, 132 mg), and the internal standard, naphthalene (100 mM, 128 mg). The solution was made up to 10 mL with acetonitrile.

Preparation of the DBU solution To a 10 mL flask was added DBU (80 mM, 122 mg). The solution was made up to 10 mL with acetonitrile.

Preparation of the TFA solution To a 10 mL flask was added 1 mL of TFA (~1000 mM). The solution was made up to 10 mL with acetonitrile.

4.2.1.2 Automated Reaction Optimization

Each reagent solution was loaded into a 10 mL SGE syringe, mounted on a single syringe pump, and connected to an inlet of the microreactor. The third microreactor inlet was plugged. By mounting both reaction solutions on the same syringe pump, the inlet concentrations of each reagent was half that of the prepared solution. Because the two-dimensional optimizations that were performed with this model reaction used only temperature and residence time as variables, these inlet concentrations remained constant throughout the experiments. The reaction was quenched with the TFA solution. This quench solution was loaded into a 10 mL SGE syringe and mounted on a syringe pump that was programmed to flow at the same rate as the DBU solution. Referring to Figure 4-1, this arrangement corresponded to the substrate solution as "Reagent 1," the DBU stream as "Reagent 2," "Reagent 3" stream was plugged, TFA was the "Quench." The "Dilution" stream and the downstream micromixer were not required.

A 6-way actuated valve with a 2 μL sample loop was used to inject reaction samples into the HPLC for analysis. Adequate and reproducible analyte separation was observed with an isocratic HPLC method using 0.7 mL//min of methanol and 0.3 mL/min of 0.1% (v:v) formic acid in water. The reaction yield was measured using a response factor and the ratio of absorbances of 4-methoxybenzaldehyde at 400 nm to naphthalene at 250 nm.

Multiple two-dimensional optimization procedures were performed using the Knoevenagel condensation example reaction to demonstrate the versatile range of operations that could be implemented into the automated system. Each optimization procedure varied the temperature (T) and residence time (τ) to maximize the objective function specified by Eq 4.5a within the specified feasible space enclosed by box constraints given by Eq 4.10a-b. For the Simplex Method and Steepest Descent Method, the optimization initiated from 70°C and 180 s, while the SNOBFIT Method required no initial condition information. Input parameters for the various algorithms are listed in Table 4.1 - Table 4.3. The programs used in these optimizations were "Simplex.vi," "SNOBFIT.vi," and "Steepest_Descent.vi." More details to the operation of these VIs are located in Appendix C - Appendix E.

$$40°C \leq T \leq 100°C \qquad\qquad 4.10$$

$$30\,s \leq \tau \leq 300\,s \qquad\qquad 4.11$$

Table 4.1: Parameters that were used in Nelder-Mead Simplex Method for Knoevenagel case study.

$T°$ (°C)	70	Initial temperature
ΔT (°C)	10	Temperature step size
$\tau°$ (s)	180	Initial residence time
$\Delta \tau$ (s)	30	Residence time step size
α	1	Simplex step size metric
N	2	Dimensionality
α'	¼α	Contraction size

Table 4.2: Parameters that were used in SNOBFIT for Knoevengal case study. Notation adopted from Huyer and Neumaier.[132]

Δf	0.03	3% error in data
N	2	Dimensionality
n_{req}	$n + 4$	Desired number of experiments generated after calling SNOBFIT function
Δn	5	Parameter used for safeguard nearest neighbors
n_{call}	6	Number of times SNOBFIT function would be called before termaination. Total number of experiments given by $n_{call} \times n_{req}$
u	[30, 40]	Vector of lower bounds, corresponding to reseidence time (s) and temperature ($^{\circ}$C), respectively
V	[300, 100]	Vector of upper bounds, corresponding to residence time (s) and temperature ($^{\circ}$C), respectively

Table 4.3: Parameters that were used in Steepest Descent Method in Knoevenagel case study.

T^{o} ($^{\circ}$C)	70	Initial center point temperature
ΔT ($^{\circ}$C)	10	Temperature step size
τ^{o} (s)	180	Initial center point residence time
$\Delta\tau$ (s)	30	Residence time step size
N	2	Dimensionality
n_C	3	Number of center point repeats
T_{min} ($^{\circ}$C)	40	Minimum temperature constraint
T_{max} ($^{\circ}$C)	100	Maximum temperature constraint
τ_{min} (s)	30	Minimum residence time constraint
τ_{max} (s)	300	Maximum residence time constraint
α	$(\frac{1}{4})^{i}$	Iterative step-size
i	[-]	Counter for gradient computations

4.2.1.3 Results and Discussion

Results from each optimization procedure are shown in Figure 4-6.
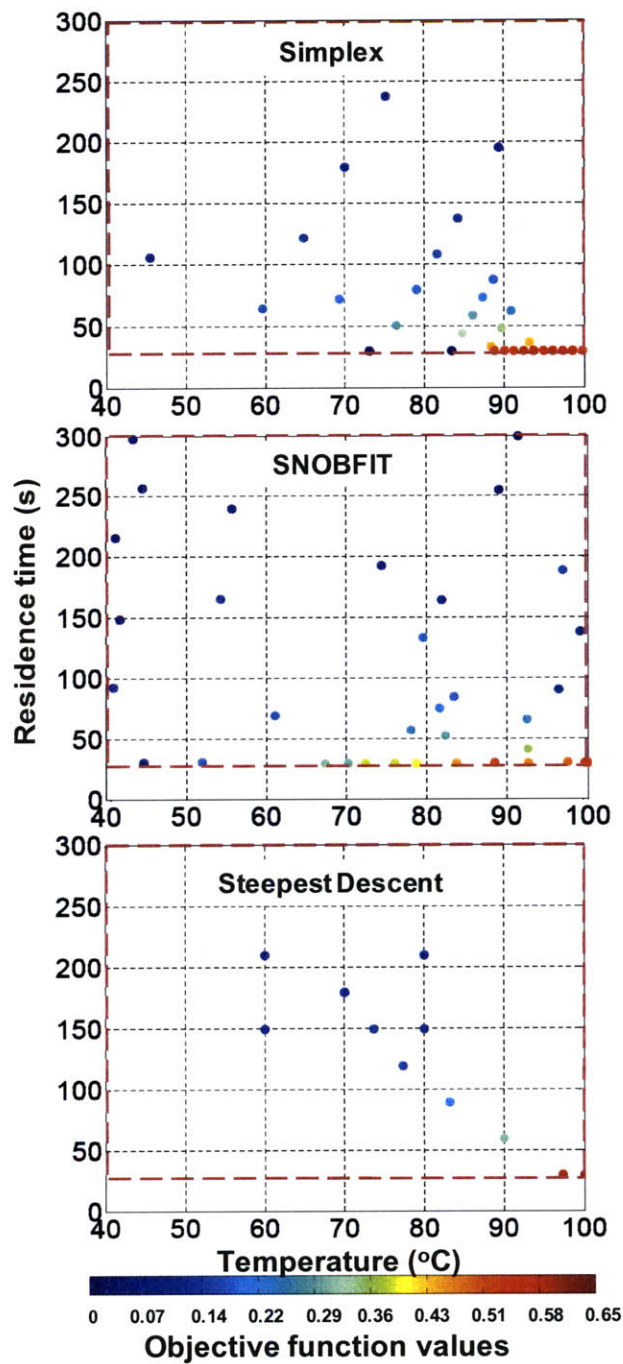
Figure 4-6: **Optimization results for Knoevenagel reaction.**
The optimization algorithms used in this investigation were Simplex Method, SNOBFIT, and Steepest Descent Method. Objective function values, as defined by Eq 4.5a, are denoted by the color bar and range from 0 (poor) to 0.65 (optimum). Boundaries on the reaction variables are denoted by red dashed lines.

From the specified starting point, the Simplex Method maximized the objective function by methodically selecting experiments at higher temperatures and lower residence times. After attempting to select experiments outside of the feasible space, the simplex contracted in order to hone in on the optimum. This contraction corresponds to the cluster of experiments between temperatures of 85 and 95 °C at residence times between 30 s and 100 s on Figure 4-6a. As the Simplex Method continued to select experiments near the minimum residence time constraint, the simplex collapsed on this value (30 s) and the method performed a one-dimensional optimization search by varying only temperature. As determined by the Simplex Method, the optimum for the objective function was located at a temperature of 99 °C and a residence time of 30 s.

As shown by Figure 4-6b, the local fitting feature of the SNOBFIT algorithm preferentially selected experiments at low residence times and higher temperatures. After performing 36 automated experiments, the SNOBFIT also located the optimum of the objective function near the vertex of the feasible space, with a temperature 99 °C and a residence time of 30 s. Additionally, because the SNOBFIT method performed experiments in unexplored regions of the parameter space, more confidence that these conditions correspond to the global maximum was gained.

For the specified objective function and inputted parameters, the optimum was located in the fewest number of required experiments using the Steepest Descent Method. As shown in Figure 4-6c, the program performed a two level factorial with three repeats at the center. Because the algorithm determined that quadratic curvature was not present in the response surface, the program calculated the gradient and progressed towards experiments at higher temperatures and lower residence times. After attempting to select an experiment outside of the

feasible region, the program selected the final experiment at the vertex of the temperature and residence time constraints. The program terminated at this point, since the objective function at the active constraints was higher than any value obtained within the interior of the parameter space. This process is similar to gradient based optimization techniques for linear problems.

4.2.2 Case Study II: Heck Reaction[†]

The Heck reaction of 4-chlorobenzotrifluoride **4** and 2,3-dihydrofuran **5** (Scheme 4.2) was selected as an example reaction because the desired product **6** readily reacts with a second equivalent of the aryl chloride.[151] Thus, the yield of the reaction is highly dependent on the number of equivalents of **5** that are employed. Moreover, developing flow conditions for the Heck reaction of aryl halides would be desirable since this transformation is commonly used in the synthesis of a variety of compounds[152, 153] including active pharmaceutical ingredients,[154] fine chemicals,[155] and natural products.[156, 157] While several continuous flow Heck reactions of aryl halides have been reported using microreactors, these works focused on the use of heterogeneous palladium catalysts under ligandless conditions and were therefore limited to aryl iodides or activated aryl bromides as substrates.[31, 158-163]

Conditions that Fu and coworkers reported to efficiently couple deactivated aryl bromides and aryl chlorides with alkenes at room temperature served as the foundation for this reaction investigation.[151] These conditions were modified to avoid generating insoluble ammonium salts and palladium black that would likely lead to clogging in a microreactor. A variety of solvents, phosphine ligands, and palladium sources were screened in order to find conditions to solubilize the ammonium salts and minimize formation of palladium black. The

---

† This work was done in close collaboration with Dr. Matthew Stone, who at the time was a post-doctorial associate in the research group of Professor Stephen Buchwald.

combination of palladium(II) acetate and the *tert*-butyl-MePhos ligand **I**, in *n*-butanol was found

to be a highly active and stable catalyst system that did not cause clogging when the reaction was

performed in a microreactor under flow conditions. The reaction reached full conversion in less

than 10 min with 1% palladium at 90°C. At higher reaction temperatures, a palladium

precipitate was observed to accumulate on the sides of the microreactor channels and

corresponded with a decrease in the yield of **6**. However, at 90°C, palladium deposition was

significantly slower and the reaction yield was demonstrated to be stable over long periods of

time.
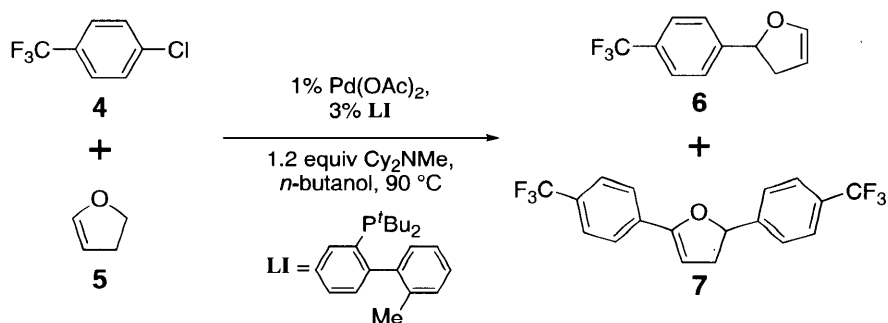
Scheme 4.2: Heck reaction of monoarylated product 6.

The automated microreactor system was used to maximize the yield of the monoarylated

product, **6**, by varying residence time and equivalents of **5**. The optimization problem

formulated for this case study corresponds to Eq. 4.12 - 4.14. The Nelder-Mead Simplex

Method was used to solve this problem.

$$f_2 = \max_{\tau, 5} Y_6 \qquad\qquad 4.12$$

$$\tau \geq 0 \qquad\qquad 4.13$$

$$5 \leq 6.0M \qquad\qquad 4.14$$

4.2.2.1 Experimental Procedure

General Method   Both n-butanol and dioxane were purchased from the Aldrich Chemical Company in Sure-Seal bottles and were used as received.   Acetonitrile and methanol that were used as diluting solvents were purchased from Mallinckrodt Chemicals and were used as received.   The aryl chloride, amine base, and naphthalene standards were purchased from Aldrich Chemical Company and TCI America and were used as received.   2-Di-tert-butylphosphino-2'-methylbiphenyl (tBu2MePhos) was either prepared according to a reported procedure164 or purchased from Strem Chemicals Inc.   Palladium(II) acetate was received as a gift from BASF.   Flash chromatography was performed by standard technique on SilicaFlash® F60 silica gel available from Silicycle.

Preparation of the aryl chloride solution   To a 10 mL volumetric flask was added palladium(II) acetate (48 mg, 0.2 mmol), 2-di-tert-butylphosphino-2'-methylbiphenyl (187mg, 0.6 mmol), and naphthalene (51 mg, 0.4 mmol, internal standard).   The flask was outfitted with a sealed cap, and then evacuated and filled with argon (2×).   Then 4-chlorobenzotrifluoride (2.66 mL, 3.60 g, 20 mmol), dioxane (1 mL), and N,N-dicyclohexylmethylamine (5.2 mL, 4.74 g, 24 mmol) were added via syringe.   The solution was made up to 10 mL with *n*-butanol and loaded into a 10 mL syringe.

Preparation of the alkene solution   To a 10 mL volumetric flask was added 2-methylnaphthalene (58 mg, 0.4 mmol, internal standard).   The flask was outfitted with a sealed cap, and then evacuated and filled with argon (2×).   The solution was made up to 10 mL with 2,3-dihydrofuran and loaded into a 10 mL syringe.

<u>Preparation of dilution solution</u>   To a 10 mL volumetric flask was added 1,5-dimethoxynaphthalene (80 mg, 0.4 mmol, internal standard). The flask was outfitted with a sealed cap, and then evacuated and filled with argon (2×). The solution was made up to 10 mL with n-butanol and loaded into a 10 mL syringe

4.2.2.2 Automated Optimization

The automated system maximized the yield of **6** by varying the residence time and the ratio of alkene:aryl chloride employed. The reaction components were loaded into three syringes. The first contained a solution of **1**, amine base, **LI**, and Pd(OAc)$_2$. The second and third syringes contained neat **5** and n-butanol, respectively. Manipulating the flow rates of these three syringes allowed the number of equivalents of **5** and residence time to be adjusted for each experiment, although the concentration of the aryl chloride was always held constant at 1.0 M. The design of the system used in this case study was a slight variation of that which was previously described, and is shown in Figure 4-7.

The three solution streams were combined and mixed in an interdigital micromixer and then heated to 90 °C in a 140 μL silicon microreactor. At the outlet of the reactor, the concentration of the solution was diluted to one third with acetonitrile in order to prevent precipitation of the ammonium salt and for analysis by HPLC. Steady-state data collection was achieved after equilibrating the system for 3 system volumes before HPLC analysis was initiated. A 2 μL sample of the reaction stream was introduced into the HPLC via an actuated six-port valve. The yield of the reaction was calculated by comparison to an internal standard.
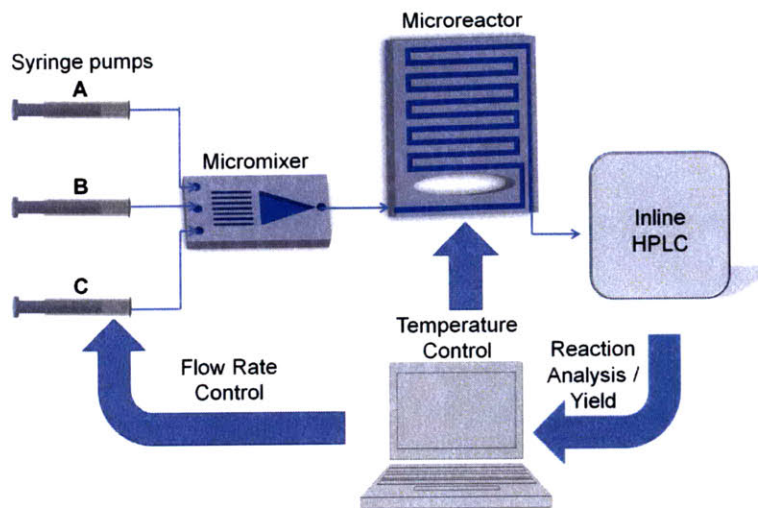
Figure 4-7: Automated microreactor system used for Heck reaction.
For the example Heck reaction, syringe A contained the aryl chloride, amine base, and palladium source, syringe B contained the alkene, and syringe C contained *n*-butanol

An upper boundary of 6.0 was placed on the equivalents of **5** because this is the near the maximum concentration of alkene that can be obtained while maintaining a 1.0 M concentration of aryl choride **4**. Any potential reaction conditions selected by the optimization algorithm that exceeded 6.0 equivalents of **5** were projected onto this upper boundary. Although the yields at this boundary line were performed and analyzed, these points were "penalized" by substituting a yield of 0% into the optimization algorithm. The use of a penalty function improves the efficiency of the algorithm by preventing the simplex from prematurely contracting or collapsing. To allow the system to find optima that are located on the boundary, this penalty function was removed after the simplex had contracted.

Input parameters for the optimization algorithm are given in Table 4.4. The implemented VI for this problem was "Heck.vi" and operational details are located in Appendix F.

Table 4.4: Parameters that were used in Simplex Method for Heck reaction case study.

T^o (°C)	50	Initial temperature
t^o (s)	180	Initial residence time
Δt (s)	45	Residence time step size
5 equiv.^{o}	1.0	Initial alkene equivalence
Δ**5** equiv	1.0	Alkene step size
$[Ar\text{-}Cl]^o$ (M)	1.0	Reactor inlet concentration of **4**
α	2	Simplex step size metric
N	2	Dimensionality

4.2.2.3 **Results and Discussion**

Yields obtained from the optimization are shown in Figure 4-8. The initial simplex (Figure 4-8, Exp. 1-3) indicated that the yield of **6** improves as the residence time and the equivalents of **5** were increased. The Simplex Method therefore reflected the point in the simplex with the shortest residence time and lowest number of equivalents of **5** (Figure 4-8, Exp. 1). This trend continued until the number of equivalents of **5** exceeded the boundary of 6.0 equivalents. This point was projected back onto the boundary, the yield was determined, and then penalized by converting the yield to 0% as previously discussed. The Simplex Method then reflected the second lowest yield and found a higher yield at a longer residence time. At the longest residence times sampled by the simplex, the yield of **6** decreased slightly, and the simplex contracted to refine the search for the optimum. This contracted simplex (Figure 4-8, Exp. 11–19) located the optimal conditions near a residence time of 6 minutes and 5.0 equivalents of **5**; corresponding to yield of 83%. The entire optimization process required ~6 g of the aryl chloride and proceeded at a rate of approximately 1 experiment per 20 minutes including the time required for HPLC analysis.
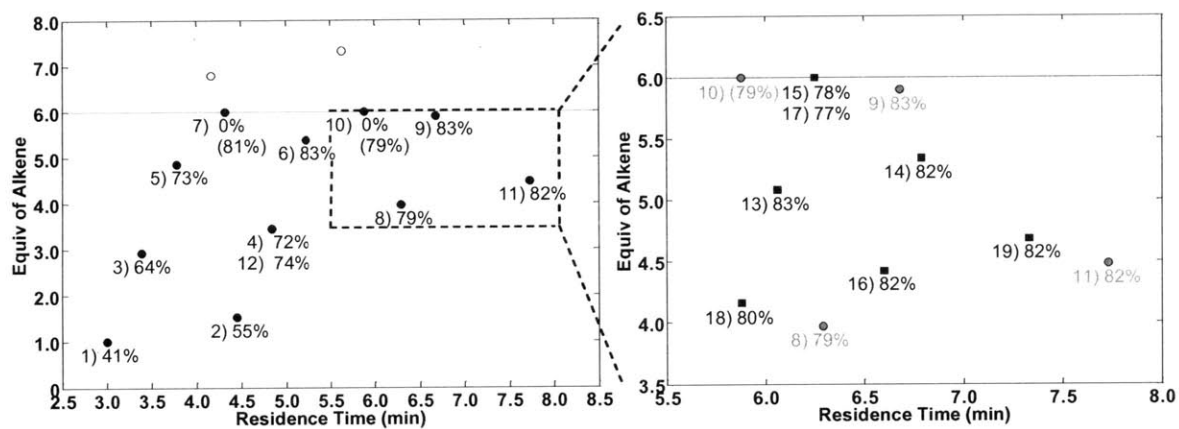
Figure 4-8: Optimization results for the Heck reaction depicted in Scheme 4.2.
Results are indexed by experiment number and corresponding yield of 6. (*Left*) Simplex method moved from initial experiment at 1.0 equiv of alkene and 3.0 minute residence time towards higher equiv of alkene and longer residence times. Experiments above the 6.0 equiv of alkene (○) were projected toward the boundary (6.0 M) and penalized with a 0% yield in the optimization program. Experimental yields at these points are parenthesized. (*Right*) Simplex size contracted and performed experiments (■) to find optimum with experiments from larger simplex (●) included for reference.

The overall picture of the reaction space showed that increasing the equivalents of **5** resulted in an optimum yield in the region of 4.5 to 5.5. Yields gathered at the boundary of 6.0 equivalents were slightly less, which might be explained by the fact that at this concentration the alkene has nearly replaced *n*-butanol as the solvent in the reaction solution. The yield also increased significantly with residence time until reaching a plateau around 5.5 minutes. As is true with any local search optimization routine, it was impossible to identify a single optimum when there are several yields in a region that are equivalent within experimental error. However, the ability to move quickly from an initial non-optimal point to a higher yielding region was demonstrated in this example. Further extensions of this system could be accomplished by incorporating additional components into the objective function to achieve multiple goals (i.e. maximizing yield while trying to minimize the equivalents of **5**), but the weighting of these factors would be highly dependent on the application.

83

4.2.3 Case Study III: Oxidation Reactions in Series

The oxidation of benzyl alcohol **8** to benzaldehyde **9** by chromium trioxide with further oxidation to benzoic acid **10** was selected as the model reaction for multi-parameter optimization (Scheme 4.3).[165, 166] For this reaction, the system varied temperature, residence time, and the inlet concentrations of reagents to maximize the yield of **9**. Although alternative oxidation pathways that produce only the intermediate **9** in excellent yields have been developed[167-172] and implemented in continuous flow microreactors,[21, 173, 174] the challenging features of maximizing the yield of **9**, given the highly oxidative environment created by the acidic solvent,[175] serve to demonstrate convincingly the advantages associated with the automated microreactor continuous flow reaction system.
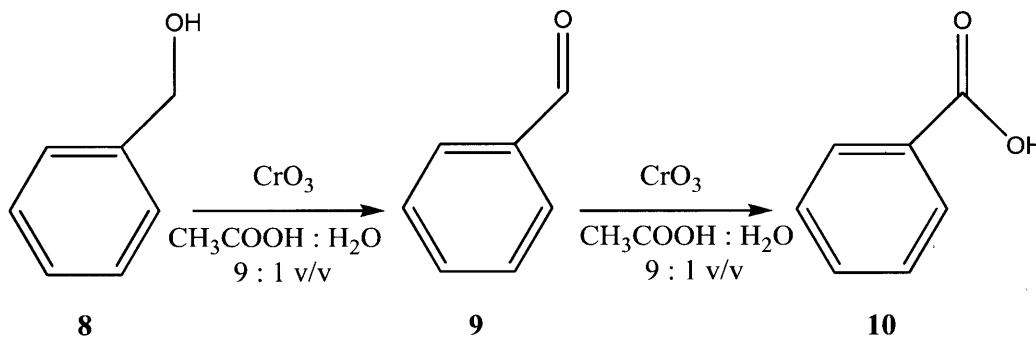
Scheme 4.3: Oxidation of benzyl alcohol **8** and benzaldehyde **9** was used to demonstrate multi-parameter optimization with the automated microreactor system.

4.2.3.1 Experimental Procedure

General Method Benzyl alcohol, benzaldehyde, benzoic acid, glacial acetic acid, and sodium bisulfite were purchased from the Sigma-Aldrich chemical company and used as received.

Chromium trioxide was purchased from Alfa Aesar and used as received. The chromium trioxide was refrigerated when not in use.

Preparation of acetic acid solution To a 500 mL flask was add 450 mL of acetic acid and 50 mL of deionized water.

Preparation of the aromatic solution To a 50 mL flask was added benzyl alcohol (30 mM, 162 mg) and 50 mL of the acetic acid solution. The flask was agitated vigorously by hand to ensure a well-mixed solution.

Preparation of the Cr(VI) solution To a 50 mL flask was added chromium trioxide (30 mM, 150 mg) and 50 mL of the acetic acid solution. The flask was agitated by hand to ensure a well-mixed solution. When not in use, the solution was refrigerated to prevent degradation of the oxidizer.

Preparation of the sodium bisulfite solution To a 500 mL was added sodium bisulfite (200 mM, 10.41 g) and 500 mL of deionized water. This stock solutions would be used for several experiments.

4.2.3.2 Automated Optimization

Each solution was loaded into a 25 mL SGE syringe and mounted on a syringe pump. To operate at different reactant concentrations and residence times independently, a third syringe pump was used to adjust the flow rate of a 90% v:v acetic acid:water solvent solution. A bulk solution of sodium bisulfate (200 mM) in water was prepared, loaded into a 60 mL B.D. plastic

syringe, and mounted on a syringe pump. Sodium bisulfite reduces Cr(VI) to Cr(III) and eliminates oxidation of the aromatic species once the solution exits the reactor.[176] Effective quenching was observed numerically and experimentally with a sodium bisulfite flow rate twice that of the CrO_3 flow rate. Water was loaded into two 60 mL B.D. plastic syringes, mounted on a syringe pump, and added to the reactor outlet stream to dilute the reaction mixture before HPLC detection. A 101-channel interdigitated micromixer was used to ensure fast, thorough mixing of these two streams before sample injection.[147] Referring to Figure 4-1, this arrangement corresponded to the aromatic solution as "Reagent 1," the Cr(VI) solution as "Reagent 2," "Reagent 3" stream was the acetic acid solution, the sodium bisulfite solution was the "Quench," and deionized water was the "Dilution" stream.

A 6-way actuated valve with a 10 µL sample loop was used to inject reaction samples into the HPLC for analysis. Adequate and reproducible analyte separation was observed with an isocratic technique using 1.05 mL/min of water and 0.45 mL/min of acetonitrile. The concentrations of benzaldehyde and benzoic acid were measured using absorbance data at 248.5 nm and 226 nm, respectively.

For the model oxidation system, the reaction parameters that were controlled by the automated system and varied during optimization trials included reaction temperature (T), the residence time (τ), the reactor inlet concentration of benzyl alcohol ($[PhCH_2OH]^o$), and the molar equivalence of chromium trioxide (CrO_3 equivalence). The objective function for this optimization investigation was the maximization of benzaldehyde yield (Eq. 4.15). Sequential experiments were directed by the Nelder-Mead Simplex Method, and the experiments were constrained by several inequalities (Eq. 4.16 - 4.18) on the design variables. Although the multi-dimensional optimization presented in the current work was limited to these four reaction

variables, the same approach can clearly be extended to include other reaction variables, such catalyst loading, ionic strength, pH, and solvent composition. Parameters that were used in the Simplex Method are listed in Table 4.5. The program implemented for this optimization problem was "Simplex.vi."

$$f_3 = \max_{T, \tau, [CrO_3]^o, [PhCHO_2H]^o} Y_{PhCHO} \qquad 4.15$$

$$\tau \geq 5s \qquad 4.16$$

$$CrO_3{}^o \geq 1\ \text{mM} \qquad 4.17$$

$$PhCH_2OH{}^o \geq 1\ \text{mM} \qquad 4.18$$

Table 4.5: Algorithm parameters that were used in Nelder-Mead Simplex Method.

T^o (^{o}C)	50	Initial temperature
ΔT (^{o}C)	10	Temperature step size
t^o (s)	60	Initial residence time
Δt (s)	10	Residence time step size
CrO_3 equivalence^o	1.0	Initial CrO_3 equivalence
ΔCrO_3 equivalence	0.2	CrO_3 step size
$[PhCH_2OH]^o$ x10^{-3} (M)	8	Initial benzyl alcohol inlet concentration
$\Delta [PhCH_2OH]$ x10^{-3} (M)	0.5	Benzyl alcohol inlet concentration step size
α	1	Simplex step size metric
N (4D optimization)	4	Dimensionality

4.2.3.3 Results and Discussion

A four-dimensional optimization using the Simplex Method was performed where values of T, τ. $[PhCH_2OH]^o$, and equivalents of CrO_3 were varied. The condition of 50°C at 1 minute residence time, with $[PhCH_2OH]^o = 8 \times 10^{-3}$ M and 1.0 CrO_3 equivalents was selected as the starting point for the automated optimization studies. The automated microreactor system performed 46 sequential experiments to determine the local optimum of benzaldehyde yield at

80% (Figure 4-9). The range of values that the algorithm investigated are shown in Table 4.6, with the optimal conditions corresponding to $T = 88^{\circ}C$, $\tau = 48s$, $[PhCH_2OH]^{\circ} = 8.2 \times 10^{-3}M$, and 0.65 CrO_3 equivalents.

Table 4.6. Range of values for each reaction parameter varied during 4-dimensional optimization.

Reaction parameter	Min.	Max.
Temperature ($^{\circ}C$)	50	94
Residence time (s)	25	79
$[PhCH_2OH] \times 10^{-3}$ (M)	6.7	9.3
CrO_3 equivalence	0.25	1.37
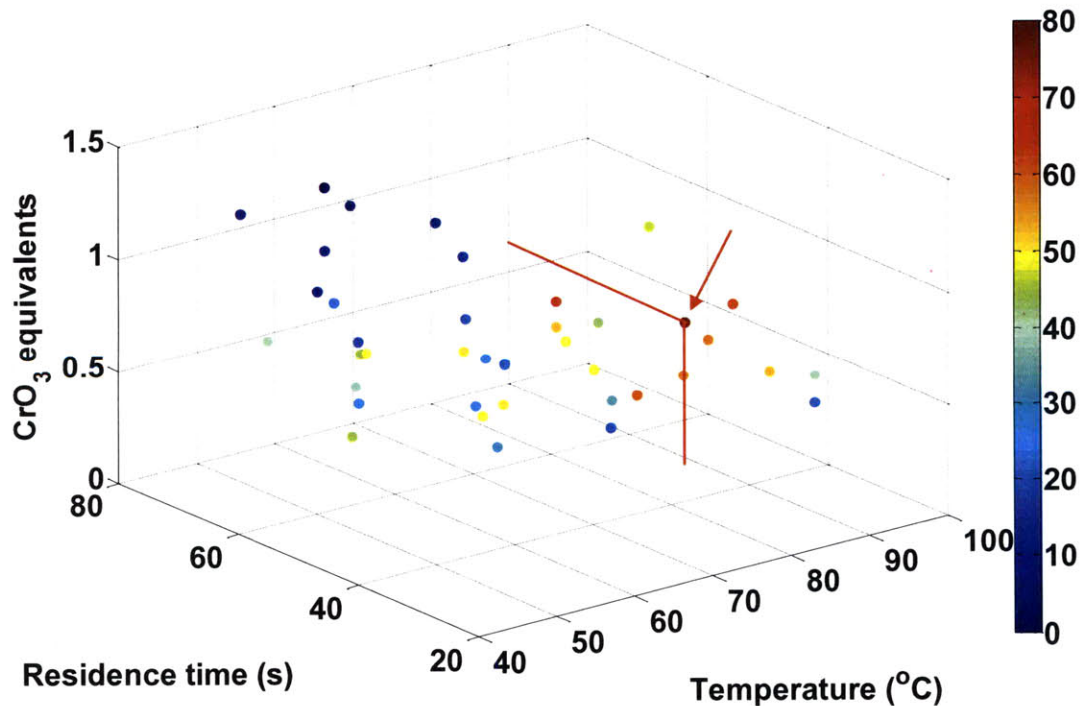
Figure 4-9. Benzaldehyde yield measured during 4-dimensional optimization by Simplex algorithm. Inlet reactor concentrations of benzyl alcohol are not shown in this graph in order to present the benzaldehyde yield data in the clearest possible form, but are located in Appendix G.

With a throughput of approximately 1 experiment per 10 minutes, a rate which includes time for system equilibration and sample analysis, this reaction example also demonstrated the system's potential to quickly determine the optimal conditions while using minimal amounts of reaction material. Results from these optimization trials provided additional insight into the chemistry. The benzaldehyde yield improved at lower residence times and higher temperatures in comparison to conditions typically used in batch. The ability to operate at more aggressive conditions without compromising reaction performance was possible due to the increased reaction control in microreactors. Additionally, for the optimal conditions, the CrO_3 equivalents were less than the yield of benzaldehyde formed, which suggested that more than one state of chromium can oxidize the alcohol. In fact, it has been reported that both Cr(VI) and Cr(V) play a role in the oxidation.[176] This ability to draw conclusions of the reaction behavior from the numerous experiments performed by the automated system provides an additional advantage of this system. Finally, in the 4-dimensional trial, the optimal yield was not associated with the optimal selectivity (see Appendix G), indicating that some benzaldehyde must be sacrificed to form benzoic acid in order to increase conversion of benzyl alcohol to benzaldehyde.

4.3 Conclusions

The concepts and design principles of an automated microreactor system for online reaction optimization were established as part of this thesis research. The developed system was used to optimize various organic reactions. Local and global optimization search techniques can be applied, and the parameters of these algorithms can be adjusted in an effort to reduce the number of required experiments to locate the optimum. Direct search optimization approaches have been explored in this effort to create a microfluidic system suitable for reaction optimization when kinetic information is limited. Moreover, the ability to perform a high

throughput of sequential experiments indicates that automated optimization in integrated microfluidics could be applied to rapidly establish libraries of reaction data by optimizing a specific reaction for several different objection functions, or by optimizing the same class of reactions with different substrates and solvents.

Chapter 5
Rapid Kinetic Modeling Using Automated Microreactor Systems

In addition to using common algorithms to maximize a specific reaction metric, such as yield or selectivity, model-based optimization algorithms were implemented in the automated microreactor system to extract kinetics. Components of process development, such as reaction optimization, scale up, and establishing the appropriate process control schemes, are greatly facilitated with the insight of reaction kinetics. Obtaining accurate reaction rate parameters in conventional laboratory bench-scale equipment can be limited by several factors. In the pharmaceutical and fine chemical industries where availability of reaction material can be limited, insufficient data and improper experimental designs do not provide adequate information for reaction modeling. In-situ analytical techniques, such as infrared spectroscopy and calorimetry,[177, 178] can be incorporated in batch reactors to increase the information content per experiment. However, concentration and temperature gradients that exist in these systems provide misleading reaction results when assuming an ideal batch reactor kinetic model. This error is exacerbated for reactions that involve volatile reagents or reactions performed under reflux because the concentration in the liquid solution and the headspace is unknown.[179]

These limitations, however, are not present for reactions that are performed in microreactor systems. In addition to improving the accuracy of kinetic investigations, the enhanced heat and mass transfer rates in microreactors enables one to explore reactions that are not easily achieved in batch, such as reactions that involve rapid kinetics,[180] unstable intermediates,[181] and highly toxic compounds.[30] The ability to achieve a high throughput rate of

sequential experiments in microreactors renders these devices powerful instruments for precise and efficient kinetic investigations. To evaluate this capability, model-based optimization algorithms were implemented into the framework of the automated microreactor system to model the kinetics of the Diels-Alder reaction of isoprene and maleic anhydride (Scheme 5.1).

(11)   **(12)**   **(13)**
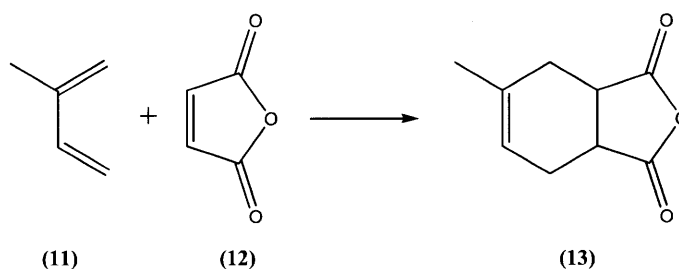
Scheme 5.1: Diels-Alder reaction of isoprene (11) and maleic anhydride (12).
This reaction was used to demonstrate online reaction modeling capabilities of automated microreactor system.

5.1 Algorithms for Kinetic Modeling

Reaction rate modeling includes two aspects – determining the reaction rate order and estimating the parameters of the rate constants (pre-exponential and activation energy). Common procedures to extract this information have been outlined in classical Chemical Engineering texts.[182, 183] First a global rate expression, such as a common power law or complex rate form is assumed. Numerous investigative experiments are performed, and data are collected and analyzed to determine the reaction order and rate constant parameters. Great advances in high throughput technology and parallel experimentation have significantly decreased the amount of time required to acquire these data,[184, 185] but the amount of useful information gained per experiment is low. For example, when considering the experimental variance and the sensitivity of a rate model to the fitted parameters, different rate laws will behave similarly under

certain experimental conditions. Therefore, results from these investigative experiments cannot be used to statistically distinguish the form of the rate law and the reaction order. Even when the rate law is known, these experiments may not be useful for precisely estimating the pre-exponential and the activation energy because the statistical significance of these estimates is highly dependent upon the experimental design. A superior approach to kinetic modeling is to perform an experiment, analyze the results, use the data to discriminate between various rate models and estimate kinetic parameters, and use the appropriate algorithm to select sequential experiments that maximize the reaction information. Although this procedure would be slow and laborious for batch experimentation, this approach is straightforward when using integrated microreactor systems with inline analysis and feedback control to automate experimentation.

To determine the global rate law for the Diels-Alder reaction of Scheme 5.1, a technique developed by Box and Hill that uses Information Theory and Bayesian statistics was implemented to select experiments aimed at reaction model discrimination.[186] After determining the correct rate law, a D-optimal strategy was used to precisely estimate the pre-exponential and activation energy of the rate constant.

5.1.1 Model Discrimination

In the approach by Box and Hill,[186] the ability of a particular rate law to predict experimental observations is related to the Shannon's entropy, H. Mathematically, this relationship is given by Eq. 5.1, where Π_i is the probability that rate law model i best describes the reaction from the M potential rate laws.

$$H = -\sum_{i=1}^{M} \Pi_i \ln \Pi_i \qquad 5.1$$

Initially, before any experimental data is obtained, there is no information to determine which model describes the reaction rate. Therefore, the probability for each rate law model to describe the reaction rate is equal and the Shannon's entropy metric is at a maximum value. Ideally, after obtaining adequate experimental data, one model has a higher probability of describing the reaction rate over the other models, corresponding to a less entropic state. The design by Box and Hill aims at selecting sequential experiments where the change in Shannon's entropy is expected to be maximized.

After performing N-1 experiments, the expected change in Shannon's entropy by performing the Nth experiment is expressed by Eqs. 5.2 and 5.3, where y_N is the Nth experimental observation, such as yield or conversion, and p_i is the probability density function of the Nth observation under rate law model i.

$$\Delta H = -\sum_{i=1}^{m} \Pi_{i,N-1} \ln \Pi_{i,N-1} + \int \left(\sum_{i=1}^{m} \Pi_{i,N} \ln \Pi_{i,N} \right) q\ y_N\ dy_N \qquad 5.2$$

$$q\ y_N = \sum_{i=1}^{m} \Pi_{i,N-1} p_i \qquad 5.3$$

For each model, it is assumed that the observation y_N is normally distributed in each probability density function with known variance σ^2 and that the expected value for each model, $E(y_N)$, is linear with respect to the best-fit parameters, $\mathbf{p}^* = \begin{bmatrix} \theta_1 & \theta_2 & \cdots & \theta_k \end{bmatrix}$. These simplifications lead to a probability density function, p_i, and a maximum change in Shannon's entropy, D, given by Eqs. 5.4 and 5.5, respectively, where $\hat{y}_N^i$ and $\hat{y}_N^j$ are the expected experimental observations predicted by models i and j, respectively, σ_i^2 and σ_j^2 are the variances in model i and j, respectively, σ^2 is the experimental variance, $\Pi_{i,N-1}$ and $\Pi_{j,N-1}$ are the prior probabilities for

models i and j, respectively, and $\mathbf{x}$ is the vector of experimental conditions (i.e. temperature, residence time, concentrations). The variance in model i is defined by Eqs. 5.6 and 5.7, where $\mathbf{W}_i^T\mathbf{W}_i^{-1}\sigma^2$ is the variance-covariance matrix.

$$p_i\left(\mathbf{x}\right) = \frac{1}{\sqrt{2\pi\left(\sigma^2\left(\mathbf{x}\right)+\sigma_i^2\left(\mathbf{x}\right)\right)}}\exp\left\{-\frac{y_N-\hat{y}_N^i\left(\mathbf{x}\right)}{2\left(\sigma^2+\sigma_i^2\left(\mathbf{x}\right)\right)}\right\} \qquad 5.4$$

$$D\left(\mathbf{x}\right) = \frac{1}{2}\sum_{i=1}^{M-1}\sum_{j=i+1}^{M}\Pi_{i,N-1}\Pi_{i,N-1}\left\{\frac{\left(\sigma_i^2\left(\mathbf{x}\right)-\sigma_j^2\left(\mathbf{x}\right)\right)^2}{\left(\sigma^2\left(\mathbf{x}\right)+\sigma_i^2\left(\mathbf{x}\right)\right)\left(\sigma^2\left(\mathbf{x}\right)+\sigma_j^2\left(\mathbf{x}\right)\right)} + \left(\hat{y}_N^i\left(\mathbf{x}\right)-\hat{y}_N^j\left(\mathbf{x}\right)\right)^2\left(\frac{1}{\sigma^2\left(\mathbf{x}\right)+\sigma_i^2\left(\mathbf{x}\right)}+\frac{1}{\sigma^2\left(\mathbf{x}\right)+\sigma_j^2\left(\mathbf{x}\right)}\right)\right\} \qquad 5.5$$

$$\mathbf{w}_i\left(\mathbf{x}\right) = \left[\frac{d\hat{y}_i\left(\mathbf{x}\right)}{d\theta_1} \quad \frac{d\hat{y}_i\left(\mathbf{x}\right)}{d\theta_2} \quad \ldots \quad \frac{d\hat{y}_i\left(\mathbf{x}\right)}{d\theta_k}\right] \qquad 5.6$$

$$\sigma_i^2\left(\mathbf{x}\right) = \mathbf{w}_i\left(\mathbf{W}_i^T\mathbf{W}_i\right)^{-1}\mathbf{w}_i^T\sigma^2 \qquad 5.7$$

After obtaining the observation y_N, the posterior probabilities are computed for each model, as defined by Eq. 5.8.

$$\Pi_{i,N} = \frac{\Pi_{i,N-1}p_i}{\sum_i^M\Pi_{i,N-1}p_i} \qquad 5.8$$

The posterior probability is the metric used to assess a model's capabilities to describe the experimental observations – a model with a posterior probability near unity describes the experimental observations better than any other model. If model discrimination cannot occur after the y_N observation, the process of sequentially performing experiments through the use of Eq. 5.5 is continued and the posterior probabilities are updated. This process is repeated until a

posterior probability for a model surpasses a threshold, such as 0.95, or when further discrimination is not possible. Although these equations may appear daunting, the concept is relatively straightforward – experiments where the most likely models provide statistically different predictions are chosen for discrimination.

The method by Box and Hill was implemented for reaction model discrimination because the Bayesian approach considers previous information and parametric uncertainty to discriminate models in few experiments. The ability to determine the correct rate law with a minimal number of experiments is important for modeling pharmaceutical and fine chemical reactions because availability of reagents or catalysts can be limiting. However, significant advances in the robustness and efficiency in model discrimination algorithms have been established over the years.[187-191] Selection of the most appropriate criterion for model discrimination approaches has been a primary focus,[192, 193] as well as extending these techniques to multi-response models.[194-197] Computer simulations have primarily been performed to demonstrate the improvements to reaction modeling for myriad applications.[198-204] Incorporation of these techniques with experimental data are less reported, but applications include hydrogenation,[205] crystallization,[206] and the fermentive production of L-valine.[207] The experimental designs in these applications were developed beforehand, or updated off-line after data collection. Imbedding a feedback mechanism to perform experiments, collect data, and update the sequential experimental design offers a great improvement to the speed and efficiency for model discrimination applications.

5.1.2 Optimal Design of Experiments for Precise Kinetic Estimates

Optimal experimental design is an iterative process that is used to improve the precision of parameters in a model. In the Diels-Alder investigation, this approach was used to estimate the pre-exponential (A) and the activation energy (E_a) terms of the rate constant. Computing

precise values for pre-exponential and activation energy is a challenging task because of the high degree of correlation. Additionally, the precision of these estimates is highly dependent upon experimental design, indicating that some experimental conditions provide more information content than others. Even if ample experimental information is available, the precision in the kinetic values will be poor if the appropriate experiments were not performed. The relationship between the experimental design and the precision in parameter estimates is apparent in the definition of the linearized joint confidence region, c, around the best fit parameters, $\mathbf{p}^*$,[208] as shown in Eqs. 5.9 and 5.10, where c is a constant given by the F-distribution and Σ^{-1} is the variance estimate.

$$\left(\mathbf{p}-\mathbf{p}^*\right)^T \mathbf{M_f} \left(\mathbf{p}-\mathbf{p}^*\right) = c \qquad\qquad 5.9$$

$$\mathbf{M_f}\left(\mathbf{p},\mathbf{x}\right) = \sum_{i=1}^{N-1}\left(\left[\frac{\partial y\left(\mathbf{p},\mathbf{x}_i\right)}{\partial \mathbf{p}}\right]^T \Sigma^{-1}\left[\frac{\partial y\left(\mathbf{p},\mathbf{x}_i\right)}{\partial \mathbf{p}}\right]\right) \qquad\qquad 5.10$$

As shown in Eq. 5.9, the volume of this joint confidence region is proportional to a matrix, $\mathbf{M_f}$, known as the Fisher Information matrix, which is also the inverse of the parameter variance-covariance matrix.[189] Optimal experimental designs, such as A-, D-, E-, and G-optimal designs, use various properties associated with $\mathbf{M_f}$ to select experiments aimed at maximizing parameter estimate precision.[189] Benefits of these designs have been demonstrated for various process chemical fields, including chemical kinetics,[208] bio-kinetics,[209] crystallization,[210] and heat and mass transfer.[211] Perhaps the most common approach, D-optimal, was used in this thesis research for kinetic parameter estimation. After performing N-1 experiments, the D-optimal criterion selects the Nth experimental conditions that minimizes the volume of the joint

confidence region. Mathematically, these conditions correspond to the experiment that minimizes the determinant of the inverse of $\mathbf{M_f}$ (Eq. 5.11).

$$\mathbf{x}_N = \arg\min \left| \mathbf{M_f}^{-1} \right| \qquad 5.11$$

By continuously updating the Fisher Information matrix for each new experiment, and sequentially selecting experiments according to Eq 5.11, precise kinetic parameters can be calculated in a minimal number of experiments.

5.2 Online Kinetic Modeling of Diels-Alder Reaction

The approaches mentioned above were implemented in the automated microreactor system and experimentally tested with the Diels-Alder reaction of Scheme 5.1. From the list of rate laws given by Eqs. 5.12 - 5.15, where C_{11} and C_{12} denote the concentration of isoprene and maleic anhydride, respectively, this system applied model discrimination techniques to select the correct model, Eq. 5.12, that describes the isoprene consumption. After selecting the most likely reaction model, the automated system performed sequential experiments using a D-optimal design to determine the rate constant parameters.

$$-r_I = -k_I C_{11} C_{12} \qquad 5.12$$

$$-r_{II} = -k_{II} C_{11}^2 C_{12} \qquad 5.13$$

$$-r_{III} = -k_{III} C_{11} C_{12}^2 \qquad 5.14$$

$$-r_{IV} = -k_{IV,f} C_{11} C_{12} + k_{IV,r} C_{13} \qquad 5.15$$

5.2.1 Automated Microreactor System for Online Reaction Modeling

A schematic of the automated system that was used in these investigations is illustrated in Figure 5-1. Standard photolithography and deep reactive ion etching techniques were used to create a 120 µL reactor with 400 x 400 µm channel dimensions. A spiral reactor design was used so that this reactor system could be used for future kinetics studies of reactions that involve solids by-products, such as those formed in palladium-catalyzed coupling reactions. A compression packaging scheme was used to make fluidic connections between the microreactor and macrofluidic instruments. Residence time and reagent concentrations were adjusted by varying the flow rates of the syringe pumps. A halo etch was incorporated into the microreactor design, enabling the device to operate at two different temperature zones. The temperature of the mixing and outlet zones was controlled by pumping $20^{\circ}C$ water through the fluidic chuck using a circulating bath, while the reaction zone was heated using a thermoelectric module. Cooling the reaction to $20^{\circ}C$ effectively quenched the Diels-Alder reaction. The reaction stream was immediately diluted off-chip by a factor of five and an interdigital micromixer was used to ensure rapid mixing before inline HPLC analysis.[181] Reaction model discrimination and parameter estimation was performed by monitoring the reactor outlet concentration of isoprene.

Because the reaction results were not expected to be influenced by the $\pm 1^{\circ}C$ tolerance in the temperature control or slight oscillations in the syringe pump, the experimental variance was assumed to be that of the HPLC measurement variance and constant. The variance was measured from a calibration curve of isoprene with repeat concentration points, which was created in automated manner by using three syringe pumps and the micromixer. By loading a concentrated solution of isoprene in one syringe, biphenyl in the second, and the solvent, DMF, in the third to act as diluent, a calibration curve for isoprene and biphenyl was created over a

range of concentrations. Conducting these calibrations at various flow rates verified that there was no correlation between HPLC measurement and the syringe pump performance.
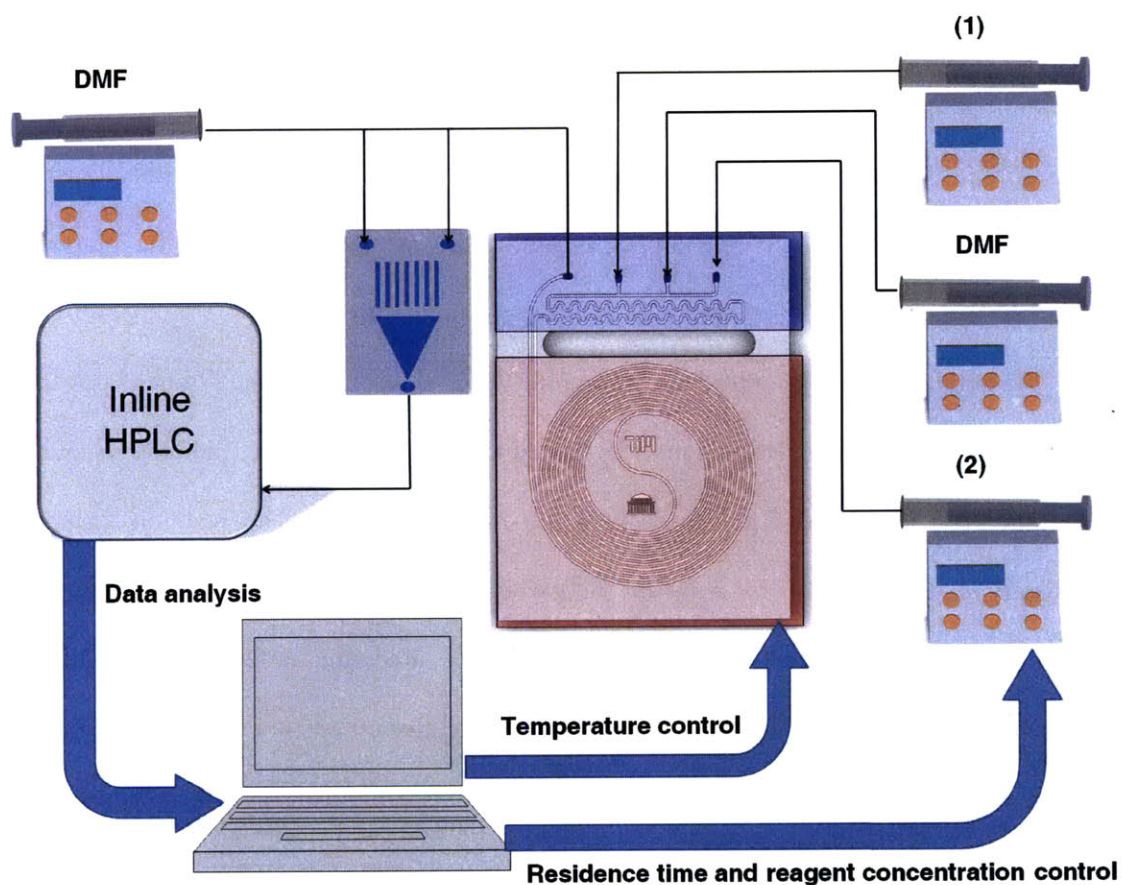
Figure 5-1: Automated microreactor system for online model discrimination and parameter estimation.

5.2.2 Feasible Design Space Consideration[†]

The parameter estimation investigation of this work used a plug flow reactor model for parameter estimation. For a plug flow reactor model and stoichiometric amounts of **11** and **12**,

---

[†]I gratefully acknowledge the help from D. Wayne Blaylock and Michael R. Harper with the Gaussian 3.0 computations that were used in the transition state calculations of this section.

the conversion of **11** ($X_{11,PFR}$) is given by Eq. 5.16, where C_{11}^o is the reactor inlet concentration of isoprene. However, the laminar flow in microfluidics creates a parabolic velocity profile that results in axial dispersion.[212] Dispersion in flow systems has been characterized,[81, 212-214] and can be modeled to assess the deviation between plug flow and laminar flow reactor models. Numerical simulations were performed to determine the effect of axial dispersion on the conversion of isoprene.

$$X_{11,\text{PFR}} = \frac{k(T)C_{11}^o \tau}{1 + k(T)C_{11}^o \tau} \qquad 5.16$$

A dispersion model was used to estimate residence time distribution, *E(t)*, in the microreactor and is given by Eq. 5.17,[183] where U is the average fluid velocity, L is the length of the reactor, t is the time the fluid spends in the reactor, and D^* is the dispersion coefficient defined by Eq. 5.18.[215] The factor f has been estimated for a variety of channel geometries, and is equal to 1.76 for square microchannels.[216] The residence time distribution can be used to estimate expected conversion of **11** in a microreactor ($X_{11,LFR}$), defined by Eq. 5.19.

$$E\left(t\right) = \frac{U}{\sqrt{4\pi D^* t}} \exp\left(-\frac{\left(L - Ut\right)^2}{4D^* t}\right) \qquad 5.17$$

$$\frac{D^*}{\mathcal{D}} = \left(1 + \frac{f}{210}\right)\text{Pe}^2 \qquad 5.18$$

$$\overline{X}_{11,LFR} = \int_{t=0}^{\infty} X_{11,PFR}\left(t\right) E\left(t\right) dt \qquad 5.19$$

An estimation of the pre-exponential factor is required to perform these simulations, and it was made by averaging previously reported values for this Diels-Alder reaction in various

solvents.[217]   In this manner, the pre-exponential for this reaction was estimated to be

$2.4 \times 10^5 \, M^{-1} s^{-1}$. This value was incorporated in the simulations to compare $X_{11,PFR}$ and $X_{11,LFR}$

using activation energy values of 45, 50, 53, 55, 57, and 60 kJ/mol. These activation energy

values were chosen because they span a large range of potential rate constants for this reaction.

The relative error, ε (Eq. 5.20), was plotted as a function of residence time and temperature for

1.0 M reactor inlet concentrations of **11** and **12**, and results as a function of activation energy are

shown in Figure 5-2.

$$\varepsilon = \frac{\left| X_{11,PFR} - \bar{X}_{11,PFR} \right|}{X_{11,PFR}} \qquad\qquad 5.20$$

These simulations indicated that the Diels-Alder reaction could be modeled as a plug-

flow reactor model in the range of $50 - 200^\circ C$ and residence times between 1 and 10 minutes. A

reaction temperature of $150^\circ C$ was selected as the maximum temperature to prevent the solder on

the TE device from melting. As predicted from theory,[218] dispersion plays a critical role at

residence times below 1 minute in this reactor, where values of UL/D^* are less than 40. An

alternative to this predictive approach for determining the appropriate design space would

involve a feedback method to determine if axial dispersion influenced the reaction outcome by

comparing the kinetic parameters to the Bodenstein number.[219, 220]

To determine the appropriate design space when the rate law is known, but no previous

kinetic information is available for the exact or similar reaction, the pre-exponential value can be

estimated from quantum chemistry computations. To demonstrate this principle, transition state

theory calculations in Gaussian 3.0 were performed to estimate the pre-exponential factor for the

Diels-Alder reaction under investigation. The CBS-QB3 (quadratic complete basis system with

B3LYP density functional geometry) method was used to determine the optimal geometry and
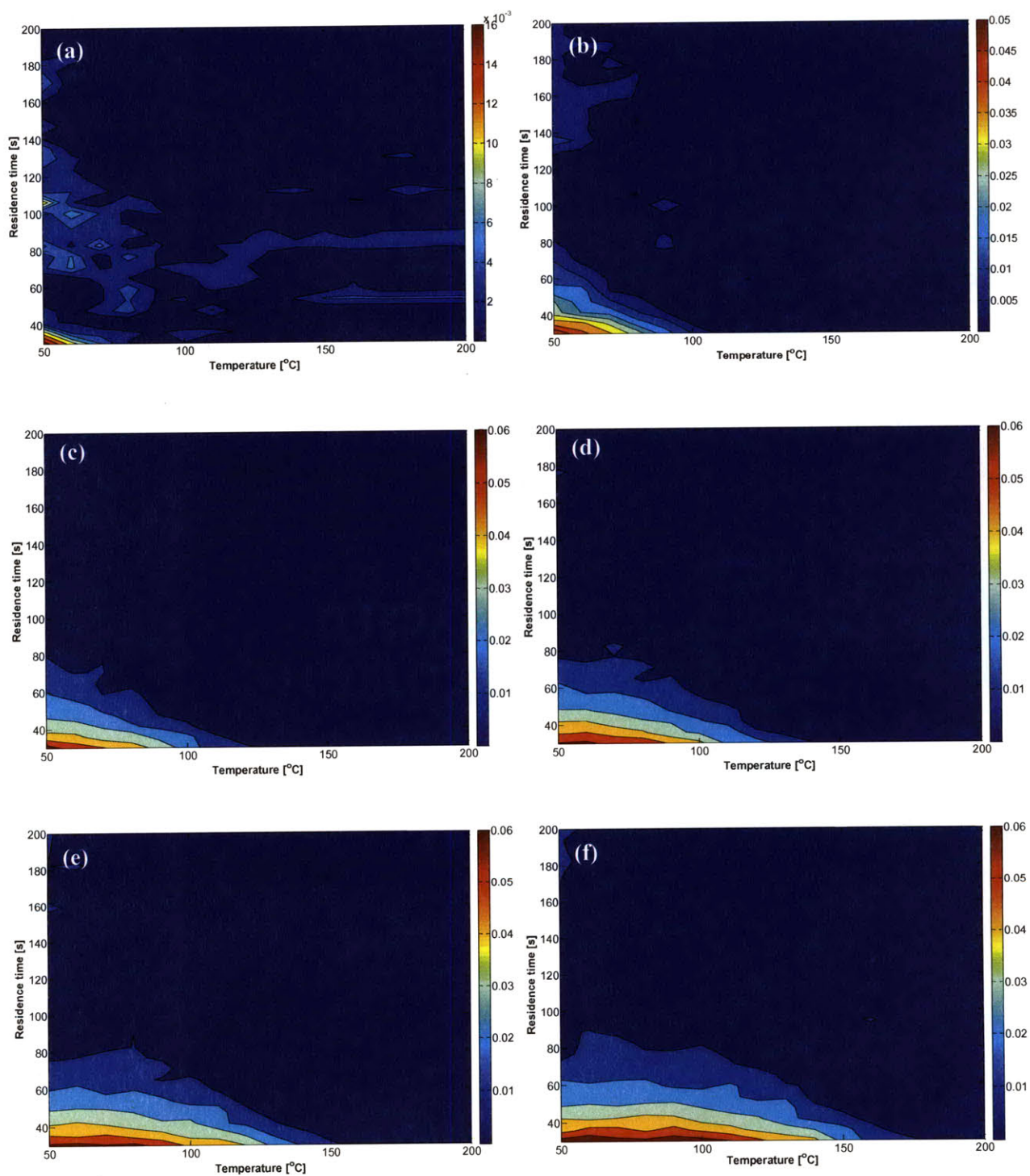
Figure 5-2: Comparison of isoprene conversion in PFR and LFR.
Comparison was made using kinetic parameters of $A = 4.2 \times 10^5 \ M^{-1}s^{-1}$ and E_a values ranging of (a) 45 kJ/mol,
(b) 50 kJ/mol, (c) 53 kJ/mol, (d) 55 kJ/mol, (e) 57 kJ/mol, and (f) 60 kJ/mol.

103

partition function of isoprene and maleic anhydride. Force constants were calculated once in these transition state computations. The resulting atomic coordinates of the transition state are given in Table 5.2.

Partition functions which were used to estimate the pre-exponential reaction are given in Table 5.1. The methyl group stemming from the butadiene backbone in isoprene and the cylohexene of the product is a hindered rotor. CanTherm was used for a more precise calculation of the hindered rotor contributions to the vibrational partition functions for these molecules.

Table 5.1: Transition state results for Diels-Alder reaction.

	Isoprene	Maleic Anhydride	Transition State ($\ddagger$)
$(E_0 + E_{ZPE}) \cdot (GJ/mol)^a$	-0.512749	-0.996189	-1.50887
Partition functions			
$q_{translational}/V_{STD} \cdot 10^7$	2.20708	3.81326	8.41133
$q_{rotational} \cdot 10^4$	8.62057	15.6881	91.3518
$q_{vibrational}$	7.68963	3.93039	778.988
$q_{electronic}$	1	1	1

a: E_0 is the electronic energy and E_{ZPE} is the zero point energy

The activation energy (E_a, Eq. 5.21) for the rate constant was calculated as 67 kJ/mol, and the pre-exponential factor for the rate constant (A, Eq. 5.22) was computed to be 2.4 x 10^4 $M^{-1}s^{-1}$.

$$E_a = E_0 + E_{ZPE}{}^{\ddagger} - \sum_{reactants} E_0 + E_{ZPE} \qquad 5.21$$

$$A = \frac{k_B T}{h} \frac{Q^{\ddagger}}{Q_1 Q_2} \left(\frac{RT}{P} \right) \qquad 5.22$$

$$Q = q_{translational} q_{rotational} q_{vibrational} q_{electronic} \qquad 5.23$$

Table 5.2: Atomic geometry of resulting transition state for Diels-Alder reaction of isoprene and maleic anhydride computed by Gaussian 3.0.

Atomic number	Atomic type	Atomic coordinates (Å)		
		X	Y	Z
6	0	-0.053605	0.011505	0.136821
1	0	0.051768	-0.280804	1.172701
1	0	0.873607	0.115224	-0.413944
6	0	-1.241391	-0.16815	-0.542075
1	0	-1.219153	-0.142897	-1.627559
6	0	-2.502613	-0.113115	0.083049
6	0	-2.570985	0.138502	1.450533
1	0	-1.800497	-0.229829	2.114618
1	0	-3.537195	0.304982	1.914085
6	0	-3.761779	-0.078702	-0.750408
1	0	-4.363874	0.802412	-0.510378
1	0	-3.535424	-0.056035	-1.81745
1	0	-4.380232	-0.959876	-0.553359
6	0	-0.360172	2.106521	1.069867
6	0	-1.624778	2.112126	1.653617
6	0	-2.531839	2.840501	0.72955
6	0	-0.452479	2.822929	-0.215296
8	0	-3.67902	3.151946	0.853127
8	0	0.383526	3.145431	-1.002956
8	0	-1.811636	3.124293	-0.425546
1	0	0.586697	2.028946	1.581097
1	0	-1.833544	2.10774	2.712829

The calculated activation energy for the rate constant is higher than experimentally reported values, while the pre-exponential value is lower than previously published values $(A_f \sim 1 \times 10^5 \text{ M}^{-1}\text{s}^{-1}, \text{ Ea} \sim 55 \text{ kJ/mol})$.[217] Because the quantum calculations are based on gas-phase reactions, the discrepancies between the computational values and solution-phase experimental results are not surprising. However, accurate computational parameters are not necessary for the purpose of evaluating the feasible region for the model-based optimization experiments.

In order to determine the appropriate design space, this pre-exponential factor was used in numerical simulations to compare the isoprene conversion in an ideal plug flow reactor $(X_{11,PFR})$ and in a laminar flow reactor $(X_{11,LFR})$ with a model residence time distribution $(E(t,D^*))$, as was previously discussed. Again, these simulations indicated that we could model the Diel-Alder reaction with a plug-flow reactor model in the range of $50 - 200^\circ\text{C}$ and residence times between 1 and 10 minutes.

5.2.3 Experimental Procedure

<u>General Methods</u> All reagents were purchased from the Sigma-Aldrich chemical company and used as received. Isoprene and N,N-dimethylformamide (DMF) were received in Sure-Seal bottles and were stored under argon. Protocol for automated experiments is similar to that described in Chapter 4.1.5. Online monitoring of the reaction was achieved using an actuated 6-way valve (Rheodyne, MXP7900) to inject 2 μL reaction samples into the HPLC system (Waters, 1525 binary pumps, Nova-Pak C18 4μm, 3.9 x 150 mm column, 2996 PDA detector, Empower software). An isocratic HPLC method using 1:1 water:acetonitrile at 1.5 mL/min was used to measure the concentration of isoprene. This concentration was determined by using a

response factor and the ratio of the isoprene chromatogram at 247 nm and the chromatogram for the internal standard, biphenyl, at 280 nm.

Experimental Procedure for Model Discrimination Investigation

Preparation of maleic anhydride solution To a 5 mL volumetric flask was added maleic anhydride (2.06 g, 21 mmol) and made up to 5 mL with DMF. The contents were transferred to a 25 mL glass vial, agitated vigorously by hand to ensure a uniform mixture, and loaded into a 5 mL plastic Norm-Ject syringe.

Preparation of isoprene solution To a 5 mL volumetric flask was added isoprene (1.43 g, 21 mmol), biphenyl (0.21 g, 1.38 mmol) and made up to 5 mL with DMF. The contents were transferred to a 25 mL glass vial, agitated vigorously by hand to ensure a uniform mixture, and loaded into a 5 mL plastic Norm-Ject syringe.

Experimental set-up The maleic anhydride and isoprene solutions were loaded onto separate syringe pumps. DMF was also charged into a 5 mL plastic Norm-Ject syringe and loaded onto a syringe pump, enabling the automated microreactor system to vary reagent inlet concentrations between 0.5 and 2.0 M independent of residence time. Two 10 mL plastic Norm-Ject syringes containing DMF were loaded onto a fourth syringe pump, and were used to dilute the reaction stream before HPLC detection. One DMF stream was added to the reaction stream through a T-union (IDEX Health and Science) immediately off-chip, and the resulting stream was combined with the second DMF stream in the micromixer. The use of the 101-interdigital micromixer created a uniform mixture for reproducible HPLC detection.

Experimental Procedure for Kinetic Parameter Estimation Investigation

Preparation of maleic anhydride solution To a 5 mL volumetric flask was added maleic anhydride (0.98 g, 10 mmol) and made up to 5 mL with DMF. The contents were transferred to a 25 mL glass vial, agitated vigorously by hand to ensure a uniform mixture, and loaded into a 5 mL plastic Norm-Ject syringe.

Preparation of isoprene solution To a 5 mL volumetric flask was added isoprene (0.68 g, 10 mmol), biphenyl (0.21 g, 1.38 mmol) and made up to 5 mL with DMF. The contents were transferred to a 25 mL glass vial, agitated vigorously by hand to ensure a uniform mixture, and loaded into a 5 mL plastic Norm-Ject syringe.

Kinetic parameter investigation experimental set-up The maleic anhydride and isoprene solutions were loaded onto a single syringe pump. Two 10 mL plastic Norm-Ject syringes containing DMF were loaded onto a fourth syringe pump, and were used to dilute the reaction stream before HPLC detection. One DMF stream was added to the reaction stream through a T-union (IDEX Health and Science) immediately off-chip, and the resulting stream was combined with the second DMF stream in the micromixer.

5.2.4 Implementation of Model Discrimination Algorithms

Using the model discrimination algorithm described above, the automated microreactor system selected and performed experiments aimed at choosing the correct rate law from the potential models given by Eqs. 5.12 - 5.15. The manipulated variables during this investigation were the residence time and the reactor inlet concentrations of **11** and **12**. The LabVIEW

108

program that was used for this investigation was titled "Model_discrimination.vi" and more details of the operations are given Appendix H. The parameter space consisted of the discretized grid points defined by residence times between 1 and 10 min in intervals of 0.5 min and inlet concentrations of **11** and **12** between 0.5 and 2.0 M in increments of 0.25M. Temperature remained constant at 90°C.

To obtain an initial estimate for the rate constants in each model, preliminary experiments were performed corresponding to a half-fractional factorial near the center of the feasible space.[124] This design was created using the *rowexch* function in Matlab. After performing the initial set of experiments, rate constants were estimated for each model (Eqs. 5.12 - 5.15) by minimizing the sum of least squared errors between the experimental data and model predictions. Computationally, best-fit values for the rate constants were achieved with a nonlinear optimization solver (*fmincon*) using the active-set algorithm for models r_I - r_{III} and the interior-point algorithm for model r_{IV} and using the *ode15s* command to evaluate model predictions. The lower and upper bounds that were used for the rate constants in *fmincon* corresponded to 0 and 1 $M^{-1}s^{-1}$, respectively, to cover a wide range of practical rates. The sensitivity matrix for each rate law was also computed in the function handle of *ode15s*, corresponding to the set of equations defined by Eqs. 5.24 and 5.26, where c is an index for concentrations, N_c is the total number of components, j is an index for the rate constants, and f_c is functional form of the differential equation that governs component c.

$$\frac{dZ_{cj}}{dt} = \frac{\partial f_c}{\partial k_j} + \sum_{l=1}^{N_c} \frac{\partial f_c}{\partial C_l} \frac{\partial C_l}{\partial k_j}$$

5.24

$$z_{cj} = \frac{\partial C_c}{\partial k_j}$$

5.25

$$\mathbf{Z} = \begin{bmatrix} z_{11} & \cdots & z_{1K} \\ \vdots & \ddots & \vdots \\ z_{N_c 1} & \cdots & z_{N_c K} \end{bmatrix} \qquad\qquad 5.26$$

Define the vector of elements in $\mathbf{Z}$ that describe the sensitivity on the isoprene concentration in rate law model i as $\mathbf{w}_i$. Because the elements of the sensitivity matrix are functions of the experimental conditions, the variance for model i, σ_i^2, can be calculated for the sequential experimental conditions, $\mathbf{x_N}$, as depicted in Eqs. 5.27 and 5.28.

$$\sigma_i^2 \left(\mathbf{x}_N \right) = \mathbf{w}_i \left(\mathbf{x}_N \right) \left(\mathbf{W}_i^T \mathbf{W}_i \right)^{-1} \mathbf{w}_i \left(\mathbf{x}_N \right)^T \sigma^2 \qquad\qquad 5.27$$

$$\mathbf{W}_i = \begin{bmatrix} \mathbf{w}_i \left(\mathbf{x}_1 \right) \\ \mathbf{w}_i \left(\mathbf{x}_2 \right) \\ \vdots \\ \mathbf{w}_i \left(\mathbf{x}_{N-1} \right) \end{bmatrix} \qquad\qquad 5.28$$

The variance and the prediction for each model were used to determine the sequential experimental conditions that maximize the D metric defined in Eq. 5.5. After performing this sequential experiment, the posterior probability distribution was updated. If a posterior probability for any model surpassed 0.95, experimentation was halted; otherwise the process of selecting a sequential experiment was repeated.

5.2.5 Implementation of D-Optimal Design Algorithm

After determining the correct rate law (Eq. 5.12), the automated microreactor system was used to estimate the pre-exponential and the activation energy parameters of the rate constant. The isoprene reactor outlet concentration was modeled with PFR kinetics and stoichiometric ratios of 11 and 12, as given by Eq. 5.29.

$$C_{11}\left(T,\tau\right) = \frac{C_{11}^o}{1+k(T)C_{11}^o\tau} = \frac{C_{11}^o}{1+A\exp\left(-E_A\Big/RT\right)C_{11}^o\tau}$$ 5.29

The design space was discretized to form a grid of potential experiments, corresponding to temperatures between 50° and 150°C in increments of 10°C and residence times between 1 and 10 min in intervals of 0.5 min. The reactor inlet concentrations of **11** and **12** remained constant during these experiments at 1.0 M. The LabVIEW program developed for this investigation was "Model_estimation" and details of the operations are given in Appendix I. Four preliminary experiments corresponding to a full factorial were performed to arrive at the initial estimates for the pre-exponential (A) and activation energy (E_a). Parameter estimation was performed by minimizing the sum of squared errors between the experimental data and the model predictions using the *fminsearch* function in Matlab. These estimates were used substituted into the Fisher Information matrix, M_f, as defined by Eq. 5.30 and 5.31, and the sequential experiment was selected through Eq. 5.11. Sequential experimentation continued until the values of E_a and the 95% confidence intervals, ΔE_a, converged according to Eq. 5.32 and 5.33.

$$M_f\left(x_N\right) = \sum_{i=1}^{N}\left(\left[\frac{\partial C_{11}\left(p,x_i\right)}{\partial p}\right]^T \sigma^2{}^{-1}\left[\frac{\partial C_{11}\left(p,x_i\right)}{\partial p}\right]\right)$$ 5.30

$$\frac{\partial C_{11}\left(p,x\right)}{\partial p} = \left[\frac{\partial C_{11}}{\partial A} \quad \frac{\partial C_{11}}{\partial E_A}\right] = \left[\frac{-\tau\left[C_{11}^o\right]^2\exp\left(-E_A\Big/RT\right)}{\left(1+A\tau\left[C_{11}^o\right]\exp\left(-E_A\Big/RT\right)\right)^2} \quad \frac{\tau A\left[C_{11}^o\right]^2\exp\left(-E_A\Big/RT\right)}{\left(1+A\tau\left[C_{11}^o\right]\exp\left(-E_A\Big/RT\right)\right)^2 RT}\right]$$ 5.31

$$\frac{\left|E_{a_N}-E_{a_{N-1}}\right|}{E_{a_N}} \leq 5\%$$ 5.32

$$\frac{\left| \Delta E_{a_N} - \Delta E_{a_{N-1}} \right|}{\Delta E_{a_N}} < 10\%$$

5.33

5.3 Results and Discussion

5.3.1 Model Discrimination Results

Results for the model discrimination investigation are listed in Table 5.3. Initially, each reaction model was assumed to be equally as likely to be the correct rate law; therefore the prior probability was 0.25 for each model. Rate constants for each model were estimated from the preliminary experiments (Exp. 1-4), and the results are given in Table 5.4. The rate constant for the correct model, k_I, is similar to a previously reported value for this specific Diels-Alder reaction.[221] Although one would expect the value of $k_{IV,r}$ (Eq. 5.15) to be approximately zero and the value of $k_{IV,f}$ to be similar to that of k_I (Eq. 5.12), instability in the nonlinear solver determined a solution for the estimation of $k_{IV,f}$ and $k_{IV,r}$ that satisfied the search criteria but did not correspond to the minimum value of squared errors.

Table 5.3: Experimental results and posterior probabilities associated with model discrimination experiments.

Exp	Residence Time (min)	11 (M)	12 (M)	Conversion	Posterior Probability Π_I	Π_{II}	Π_{III}	Π_{IV}
1	6.0	1.0	1.0	89	0.250	0.250	0.250	0.250
2	5.0	1.5	1.0	68	-	-	-	-
3	6.0	1.0	1.5	95	-	-	-	-
4	5.0	1.5	1.5	87	-	-	-	-
5	1.0	0.5	0.5	37	0.470	0.356	0.173.	<0.001
6	1.0	2.0	1.25	40	0.999	<0.001	<0.001	<0.001

Table 5.4: Parameter estimates for each rate law considered in model discrimination investigation.

Best-Fit Values

Rate constant[a]	After Exp. #4	After Exp #5	After Exp. #6
$k_I \times 10^2$ (M^{-1}s^{-1})	1.69	1.74	1.34
$k_{II} \times 10^2$ (M^{-2}s^{-1})	6.63	5.95	1.95
$k_{III} \times 10^2$ (M^{-2}s^{-1})	8.88	6.90	3.15
$k_{IV,f} \times 10^2$ (M^{-1}s^{-1})	13.40	2.08	1.34
$k_{IV,r} \times 10^3$ (s^{-1})	2.56	0.21	0.00

a: Rate constants are indexed according to the notation used in Eqs. 5.12 – 5.15.

Rate constant information for each model were used to select Exp. 5 by finding the conditions that maximize the value of D (Eq. 5.5). These conditions corresponded to a residence time of 1 min and 0.5 M reactor inlet concentrations for both **11** and **12**. The weighted probability density functions $(p_i\Pi_i)$ of rate models r_I - r_{III} for the reactor outlet concentration of isoprene for the fifth experiment are shown in Figure 5-3, along with the experimental outcome. These probability functions indicate the most likely experimental outcome for a given set of reaction conditions, as well as the distribution of potential outcomes predicted by each model. Discrimination can be achieved when the experimental outcome falls within a single model probability function. For experimental outcomes that fall within the prediction of several models, such as the results for Exp. 5, additional experiments are required for satisfactory discrimination.
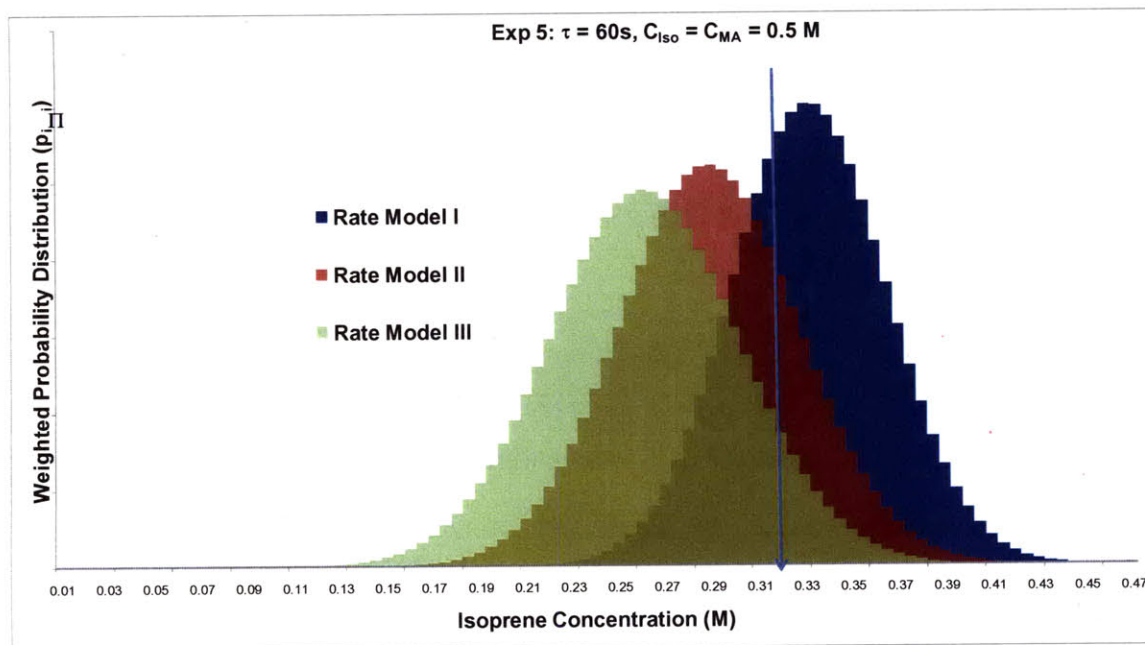
Figure 5-3: Weighted probability distributions of potential rate laws used for model discrimination calculations involved in selecting conditions for experiment 5. Experimental result is denoted by the arrow.

The poor parameter estimates of model r_{IV} resulted in a model that was insensitive to the $k_{IV,f}$ term over the explored experimental conditions; thereby creating a singular variance-covariance matrix, $\mathbf{W}_{IV}^T \mathbf{W}_{IV}^{-1} \sigma^2$. This singularity resulted in a large model variance, and as a consequence, a broad probability distribution function. The probability that model r_{IV} could best describe the experimental outcome of Exp. 5 was significantly smaller than other candidate models, and resulted in a low posterior probability value. Due to the recursive nature of Bayesian statistics, this low posterior probability prevented r_{IV} from being considered a likely reaction model in subsequent experiments regardless of any improvements that that were made in the estimation of $k_{IV,f}$ and $k_{IV,r}$ with additional data.

The outcome for Exp. 5 was used to update the posterior probability of each model according to Eq. 5.8. The posterior probabilities served as the prior probabilities of the next

114

experiment, and used in the calculation of D to determine the conditions of Exp. 6. The result from Exp. 5 was also used to revise the rate constant estimate of each model. As indicated by Table 5.4, the estimates for $k_{IV,f}$ and $k_{IV,r}$ are in better agreement with expectations after five experimental observations. Similar to the selection of Exp. 5, the prior probabilities and the rate constant values were used in the calculation of D to determine the conditions of Exp. 6, corresponding to 1 min residence, 2.0 M and 1.5 M reactor inlet concentrations of **11** and **12**, respectively. The weighted probability density function for the outlet isoprene concentration of Exp. 6 and the observed outcome are shown in Figure 5-4. As this figure indicates, the outcome from Exp. 6 was predicted only by reaction model r_I, implying that this model is the correct rate law. Mathematically, the posterior probabilities denoted that r_1 was the correct rate law, and the experimental procedure was terminated. This prediction is in agreement with the known rate law for this reaction.[221]

Using the experimental data from all six experiments to estimate the rate constants illustrates the expected redundancy of models r_I and r_{IV} for the investigated Diels-Alder reaction. Discrimination between models r_I and r_{IV} was only possible due to the poor estimations of $k_{IV,f}$ and $k_{IV,r}$ after Exp. 4. Therefore, while this approach showed great potential for reaction model discrimination after only a few experiments, it is subject to the stability of the nonlinear solver if used in a completely automated manner without user intervention.
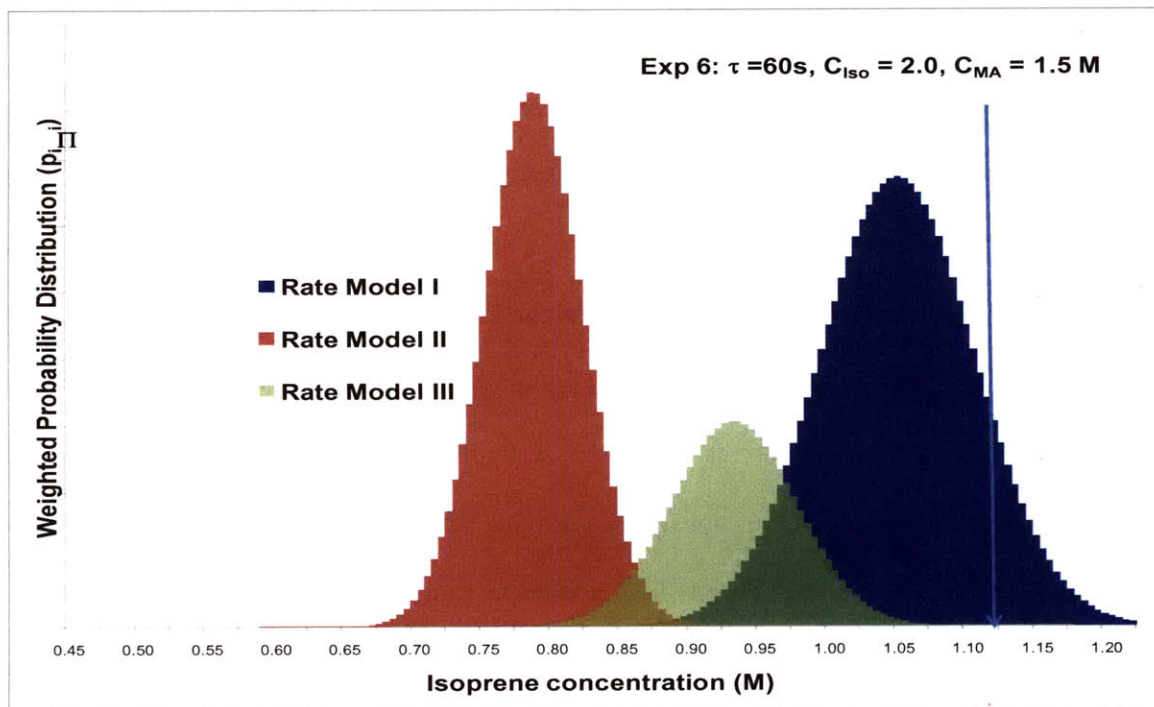
Figure 5-4: Weighted probability distributions of potential rate laws used for model discrimination calculations involved in selecting conditions for experiment 6.
Experimental result is denoted by the arrow.

5.3.2 Kinetic Parameter Estimation Results

Using the correct rate expression r_1 from the model discrimination investigation, the microreactor system selected and performed experiments to estimate the kinetic parameters. Progression of the parameter estimation and the 95% confidence intervals for the sequential experiments are shown in Table II. Using a D-optimal approach and the termination criteria given by Eqs. 5.32 and 5.33, precise estimates were achieved after six experiments. Further experimentation with the D-optimal approach showed that the parameter estimates and the 95% confidence intervals appeared to have converged at the sixth experiment. Observed values in

this work are in good agreement with Hoffmann et al, who previously reported the activation energy for this Diels-Alder reaction as 58.5 ± 2 kJ/mol.[221]

Table II: Parameter estimation and associated 95% confidence intervals for Diels-Alder reaction.

Exp	Residence Time (min)	Temp (^{O}C)	Conversion	Kinetic Parameters	
				$A \cdot 10^6$ $M^{-1}s^{-1}$	E_a kJ/mol
1	5.0	90	82	-	-
2	5.0	110	93	-	-
3	6.0	90	86	-	-
4	6.0	110	94	1.9 ± 10.5	56.1 ± 17.3
5	1.0	50	50	1.4 ± 1.0	55.3 ± 2.0
6	1.0	120	81	$\mathbf{2.1 \pm 1.3}$	$\mathbf{56.3 \pm 1.9}$

5.4 Conclusions

An automated microreactor system combined with model-based optimization feedback has been presented as a technique to quickly model reactions while requiring a minimum number of experiments. Using less than five grams of each starting reagent in a Diels-Alder reaction, the microreactor system selected and performed 12 experiments to determine the appropriate rate law expression and precisely estimate the pre-exponential and activation energy of the rate constant. This information will prove vital in reaction scale up, and can be incorporated with advanced control schemes to ensure product quality during changes in production schedules. Modeling the different reactions rates using the tools and techniques demonstrated in this work will lead to fast and accurate reaction optimization results for complex chemical systems, such as those that involve multiple reactive pathways. Kinetic information for individual reactions will

be extended to the design of optimal multi-step processes. Furthermore, advances in in-situ monitoring in microreactors will enable automated microreactor systems with model-based feedback to complement chemical computational techniques for reaction mechanism generation.

Chapter 6
Reaction Scale Up from Microreactors to Mesoflow Reactors

Successful reaction scale up can be defined as obtaining the same conversion, selectivity, and product distribution as determined in the laboratory.[222] For batch reactors, however, successful scale up is complicated by the disparity of the important process parameters in the laboratory and larger reactors. Lower heat transfer rates in larger batch reactors can create an exotherm, which can lead to product degradation, the appearance of unanticipated side reactions, and reaction runaway.[223] Semi-batch operations are commonly used to control the heat generation in exothermic reactions,[224] but are inherently inefficient and the longer dosage time may have implications on the product selectivity. At conditions where the reaction rate is on the same order of magnitude as the mixing rate, product selectivity can be influenced by changes in micro-, meso-, and macro-mixing during scale up.[225] Like batch reactors, the heat transfer and mixing rates of flow reactors also vary with size, but theoretical and empirical correlations have been established for flow reactors due to their dominant presence in the petroleum and the commodity chemical industry.[226] This higher knowledge baseline motivates the investigation to identify the appropriate reaction scale up method from a single microreactor operation.

Previous methods of increasing product throughput in microreactors have focused on a scale out approach, where microreactors are operated in a parallel arrangement.[33, 79] While this approach would be feasible for small-scale production, problems such as uniform fluid distribution, process control, packaging, and the cost of multiple microreactors are significant concerns when trying to scale up a reaction to the necessary production rates for pre-clinical and

pilot-plant trails. For flow systems made from metal tubing, an alternative approach has been to use microreactors to find the optimal conditions, and then scale up by simply increasing the reactor length proportionally to the desired reaction flow rate.[227] This scale up method can result in undesirable axial dispersion and significant pressure drops; thereby limiting the potential production rate. Additionally, because the diameter of this system has not increased, the potential for clogging the reactor remains. While reactor clogging is a nuisance when studying a reaction in the laboratory, it becomes an unacceptable outcome for manufacturing applications. For microreactor technology to be adopted into pharmaceutical research and development practices, the optimal conditions determined in a microreactor with characteristic length scales of ~100 μm must transfer to larger flow reactors of length scales of ~1 cm.

This thesis research investigated reaction scale up by 1) identifying the relevant microreactor features and mimicking these features in a larger reactor system and by 2) using accurate kinetic information obtained in a microreactor to model the reaction environment in a larger reactor.

6.1 Direct Transfer of Operating Conditions for Reaction Scale Up

For homogeneous liquid reactions, performing the reaction in microreactor can result in a higher product yield and selectivity than that which would be achieved if the reaction were performed in a flask reactor due to enhanced mixing and heat transfer rates. Therefore, one method to successful reaction scale up could involve implanting the necessary "process intensification"[228] component present in the microreactor to larger reactor systems. Scale up of the Heck reaction and Knoevenagel condensations that were discussed in Chapter 4 were attempted using this strategy.

6.1.1 Case Study: Heck Reaction[†]

After determining the optimal conditions for the Heck reaction of Scheme 4.2, the reaction was scaled up by a factor of 50 in an Advanced Flow Reactor (AFR) by Corning. Nine semi-automated experiments were performed in the AFR.

6.1.1.1 Experimental Procedure

General method

General experimental methods for this case study are reported in Chapter 4.2.2.1.

Preparation of solution for reservoir #1: To a 100 mL volumetric flask was added palladium(II) acetate (0.449 g, 2 mmol), 2-di-tert-butylphosphino-2'-methylbiphenyl (1.87mg, 6 mmol), and naphthalene (0.512 g, 4 mmol, internal standard). The flask was outfitted with a sealed cap, and then evacuated and filled with argon (2×). Then 4-chlorobenzotrifluoride (26.7 mL, 36.1 g, 0.20 mol), dioxane (10 mL), and N,N-dicyclohexylmethylamine (51.4 mL, 46.9 g, 0.24 mol) were added via syringe. The solution was made up to 100 mL with n-butanol.

Preparation of solution for reservoir #2: To a 100 mL volumetric flask was added 2-methylnaphthalene (0.569 g, 4 mmol, internal standard). The flask was outfitted with a sealed cap, and then evacuated and filled with argon (2×). Then 2,3-dihydrofuran (3 equiv: 45.5 mL, 42.2 g, 0.60 mol; 4 equiv: 60.5 mL, 56.1 g, 0.80 mol; 5 equiv: 75.6 mL, 70.1 g, 1.0 mol) was added via syringe. The solution was made up to 100 mL with n-butanol.

[†]The work involved in the case study of the Heck reaction was done in close collaboration with Dr. Matthew Stone and Professor Stephen Buchwald.

Isolated Yield from Meso-Scale Reactor: Solutions for reservoirs #1 and #2 were prepared as described above however the internal standards (naphthalene and 2-methylnaphthalene) were omitted. Two reactor volumes of reaction solution were allowed to pass through the reactor at a temperature of 90 °C and then the reaction mixture was collected without dilution for 127 minutes giving 156.5 mL of crude solution. The crude mixture was diluted with diethyl ether (200 mL) and the resulting ammonium chloride salt precipitate was removed by filtration and rinsed with an additional portion of ether (300 mL). The resulting solution was concentrated in vacuo and then run through a large plug of silica gel eluting with 5% ethyl acetate in hexanes. The solution was concentrated in vacuo to an orange colored oil. The oil was distilled under vacuum and fractions were collected at room temperature, 30 °C, 35 °C, and 50 °C. The fraction collected at 35 °C consisted of 23.81 g and was determined to have greater than 98% purity by GC. The other three fractions were purified via the Biotage SP4 (silica-packed 100 g SNAP column; 0%-3%, ether/hexanes) to provide compound 2-(4-trifluoromethylphenyl)-2,3-dihydrofuran151 3 as a clear oil (26.93 g, 0.126 mols, 80% yield). 1H NMR (500 MHz, CDCl3) δ 7.62 (d, J = 8.1 Hz, 2H), 7.47 (d, J = 8.3 Hz, 2H), 6.47 (q, J = 2.5 Hz, 1H), 5.57 (dd, J = 10.8, 8.1 Hz, 1H), 4.97 (q, J = 2.5 Hz, 1H), 3.14 (ddt, J = 15.4, 10.9, 2.4 Hz, 1H), 2.56 (ddt, J = 15.2, 8.0, 2.4 Hz, 1H). 13C NMR (126 MHz, CDCl3) δ 147.16 (s), 145.26 (s), 129.71 (q, J = 32.3 Hz), 125.72 (s), 125.46 (q, J = 3.8 Hz), 124.14 (q, J = 271.9 Hz), 98.97 (s), 81.37 (s), 37.91 (s). 19F NMR (282 MHz, CDCl3) δ -62.89 (s). IR (neat, cm-1): 2937, 2864, 1620, 1419, 1326, 1166, 1126, 1069, 1052, 1018, 938, 843, 708, 603 450.

6.1.1.2 Automated Meso-Scale Reactor System Design

Because the Heck reaction of Scheme 4.2 was not known to be particularly exothermic, successful scale up would require a meso-scale system designed with sufficient mixing of reagents and an isothermal reactor. To evaluate the Heck reaction of **4** and **5** at 50 fold larger scale, an automated meso-scale system was developed using a Corning AFR module was employed. A schematic of this system is provided in Figure 6-1.
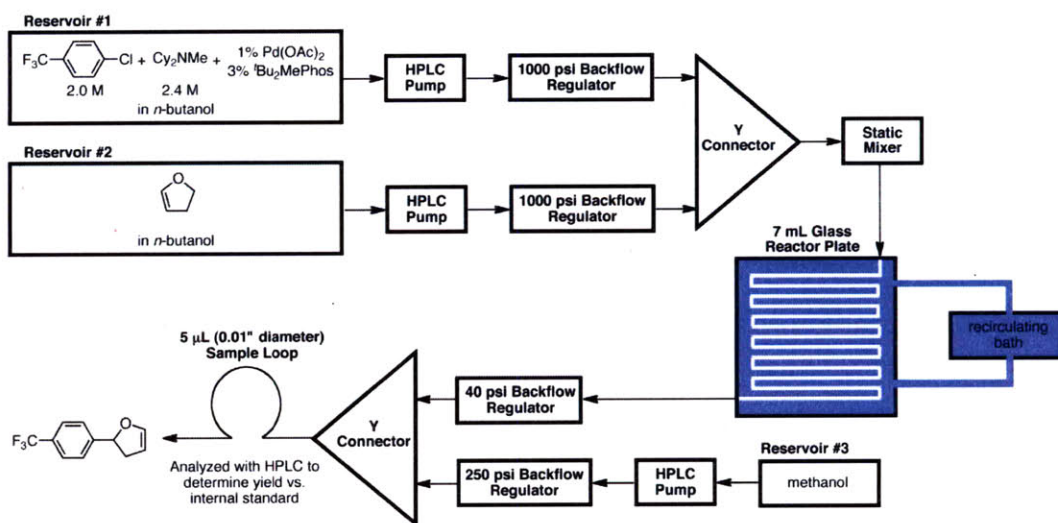
Figure 6-1: Schematic of automated meso-scale reactor system used for Heck reaction.

The dimensions of the reaction channels corresponded to 0.7 mm in depth, 4 mm in width, and the reactor had an internal volume of 7 mL. A circulating temperature bath pumped water at 15 L/min through the integrated heat-exchanger to maintain a reactor temperature of 90 °C. A 1,000 psi back pressure regulator (Idex) was added to the outlet of each dual piston pump (LabAlliance, 1500 series) to provide stable flow rates. Flow rates were controlled remotely through the central computer control and analog output device (National Instruments). A solution of 4-chlorobenzotrifluoride (2.0 M), N,N-dicyclohexylmethylamine (2.4 M),

palladium(II) acetate (0.02 M), and 2-di-tert-butylphosphino-2'-methylbiphenyl (0.06 M) in *n*-butanol with a small amount of dioxane as a cosolvent was loaded for reservoir #1. A solution of 2,3-dihydrofuran in *n*-butanol was loaded into reservoir #2. The solutions were pumped into the flow reactor with dual piston pumps and the residence time was controlled by varying their flow rate. The number of equivalents of alkene was adjusted by changing the concentration of **5** in the reservoir solution. To ensure a high degree of mixing, a commercial static packed bed mixer (HPLC gradient mixer, Waters) that was packed with stainless steel ball bearings was added immediately upstream of the reactor. Upon exiting the reactor the concentration of the solution was diluted to one seventh for detection. Inline analysis of the reaction was again performed by HPLC, as described in Chapter 4.1.3.

Nine reaction conditions were selected that encompassed the region containing the optimum yields that were previously determined in the microreactor. The residence times and initiation of HPLC analysis were directed by an automated centralized control, although there was no feedback involved in the system. Automation was achieved through Matlab scripts and LabVIEW software. It was verified that steady-state data could be recorded after flushing the system with three reactor volumes of material. This observation was incorporated into the central control scheme and used to determine when to sample the reaction mixture by inline HPLC through a 5 μL sample loop.

6.1.1.3 Results and Discussion

Results for the Heck reaction scale up are shown in Figure 6-2, and listed in Table 6.1. The highest yielding conditions were determined to have a residence time of 5.5 or 6.5 minutes at 5.0 equivalents of **5**. These results indicated that the optimal conditions were successfully translated from the microreactor to the meso-scale system. To validate the yields obtained by HPLC

124

analysis, the reaction was allowed to proceed for just over two hours, during which time 168 mL of crude solution was collected. The monoarylated product was isolated by distillation and chromatography to provide 26.9 g of **6** with a yield of 80%. This is in good agreement with the yields determined by HPLC and corresponds to an annual production rate of 114 kg/year.
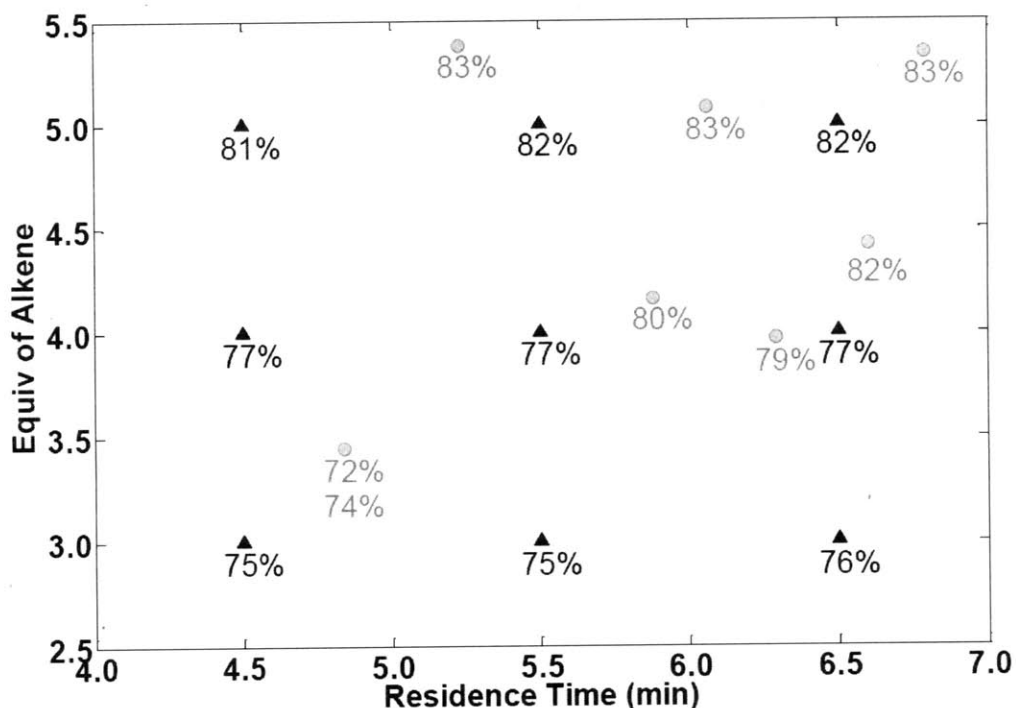
Figure 6-2: Yields of 50-fold reaction scale up in meso-scale flow reactor.
Yields obtained in the meso-scale system (▲) are compared with yields observed in the microreactor (●).

Table 6.1: Experimental yields of 3 obtained in meso-scale reactor system.

Ratio Alkene	Residence Time (min)	1st Run	2nd Run	Average of Runs
3	4.5	75.0%	75.6%	75.3%
3	5.5	74.9%	74.3%	74.6%
3	6.5	75.9%	74.6%	75.3%
4	4.5	77.2%	76.5%	76.9%
4	5.5	76.9%	76.6%	76.8%
4	6.5	76.5%	79.7%	78.1%
5	4.5	81.0%	80.8%	80.9%
5	5.5	82.4%	80.7%	81.6%
5	6.5	81.0%	82.3%	81.7%

125

6.1.2 Case Study: Knoevenagel Condensation

The Knoevenagel condensation of Scheme 4.1 was scaled up by a factor 60 using a simple flow system consisting of stainless steel tubing.

6.1.2.1 Experimental Procedure

General Information   Reagent information for this case study is reported in Chapter 4.2.1.1. Acetonitrile was purchased from Omnisolv and used as received.

Preparation of reservoir #1   To a 500 mL flask was added 4-methoxybenzaldehyde (6.81 g, 200 mmol), malonitrile (3.3 g, 200 mmol), and the internal standard, naphthalene (3.20 g, 100 mmol). The solution was made up to 250 mL with acetonitrile. To pump this fluid, a 1/8" tube fitted with a stainless steel frit was submerged into reservoir. Aluminum foil was wrapped around the top of the flask and the tubing to seal the reservoir.

Preparation of reservoir #2   To a 500 mL flask was added 1,8-diazobicyclo[5.4.0]undec-7-ene (DBU) (3.04g, 80mmol). The solution was made up to 250 mL with acetonitrile. To pump this fluid, a 1/8" tube fitted with a stainless steel frit was submerged into reservoir. Aluminum foil was wrapped around the top of the flask and the tubing to seal the reservoir.

Preparation of reservoir #3   To a 500 mL flask was added trifluoroacetic acid (TFA) (29 mL, ~1000 mmol). The solution was made up to 250 mL with acetonitrile. To pump this fluid, a 1/8" tube fitted with a stainless steel frit was submerged into reservoir. Aluminum foil was wrapped around the top of the flask and the tubing to seal the reservoir.

6.1.2.2 **Design of Meso-Scale Reactor System**

A schematic of the meso-scale system used for this investigation is given in Figure 6-3. The heat generated by this exothermic reaction was not believed to be an issue at the concentrations investigated; therefore, successful scale up was believed to be associated with good mixing of the reaction components and isothermal reaction conditions. Thorough mixing was realized by incorporating a static mixer (HPLC gradient mixer, Waters) that was packed with stainless steel ball bearings immediately upstream of the reactor. The reactor was a 1/4" o.d. stainless steel tube from Swagelok. The wall thickness of this tube was of 0.035" and the length was cut to 12" to give a reactor volume of 5 mL. The remaining tubing in this reaction system was 1/16" o.d. (0.04" i.d.) from Idex. The flow rates for solutions from reservoir #1 and #2 were controlled manually with double piston HPLC pumps (Waters, model 510), and the flow rate of the quench stream in reservoir #3 was controlled manually with a single piston HPLC pump (Dynamax, model SD200). These pumps were calibrated with water using a stopwatch and volumetric flask method. The ratio of the flow rates of reservoir #1, #2, and #3 remained constant at 1:1:1, and the residence time was adjusted by manipulating the combined flow rate of reservoirs #1 and #2.

A heating tape (Omega) was used to heat solutions from reservoirs #1 and #2 before mixing at the T-connector. The tubing in this pre-heating zone was approximately 1 m long for each reagent. A second heating tape (Omega) was used to the heat the static mixer and the reactor. A handheld temperature processor (Omega, HH202A, K-type thermocouples) was used to measure the temperature in these sections. Each heating tape was connected to a variac (variable transformer) and the power output to the heating tape was manually adjusted to provide the desired temperature. A 1,000 psi back pressure regulator (Idex) was added downstream of

the reactor to ensure stable flow from the HPLC pumps and prevent degassing of the solution. The reaction was quenched by mixing the outlet stream with TFA stream in an interdigitated micromixer before collection.
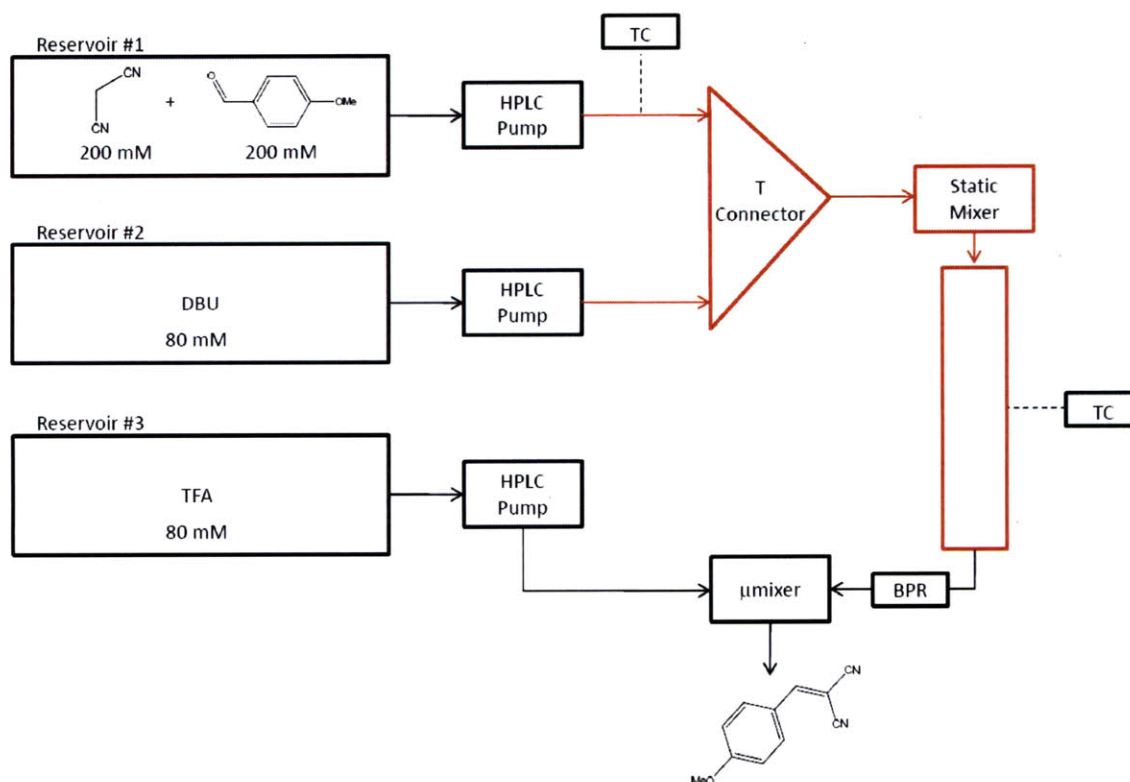
Figure 6-3: Meso-scale system design used for Knoevenagel scale-up.
Components highlighted in red indicate a component that was in contact with heating tape. TC represents thermocouple measurement and the 1,000 psi back pressure regulator is denoted by BPR.

Six experiments were performed at 15, 30, and 60 s at temperatures of 90 and 100 °C. Three samples were collected for each experiment. One milliliter aliquots were taken from the collected material, and 6 μL of this sample were injected into the HPLC via an autosampler (Waters, 717 plus autosampler). Analysis was performed using the same techniques described in Chapter 4.2.1.2.

6.1.2.3 Results and Discussion

Results from the Knoevenagel condensation scale up are shown in Figure 6-4. Although the tight 95% confidence intervals suggest that experiments were repeatable, the resulting yields in this mesoflow system were significantly less than those values that were observed in the microreactor system. There are several potential explanations for these discrepancies. The characteristic time scale for thermal equilibrium in the pre-heating zone is approximately equal to the actual time that the material resided in this zone. Therefore, if there was imperfect contact between the heating tape and the sections of tubing in the pre-heating zone, the reagent streams would not be fully heated to the reaction temperature and the reaction would proceed non-isothermally. This outcome could also exist if perturbations to the temperature in the pre-heating zone occurred, but were unnoticed due to limited temperature measurements. Additionally, if a dispersion coefficient of 5×10^{-3} m^2/s is assumed for the flow conditions of a 30 s residence time, a Bodenstein number of 0.1 is calculated for this reactor. This value indicates that there was a significant level of axial dispersion in this reactor at the flow rates explored. The expanding and contracting connections upstream and downstream of the reactor could have also introduced stagnant mixing zones. Both the axial dispersion and the dead volume broaden the residence time distribution, which can also play a significant role in lowering the yield for second order reactions.
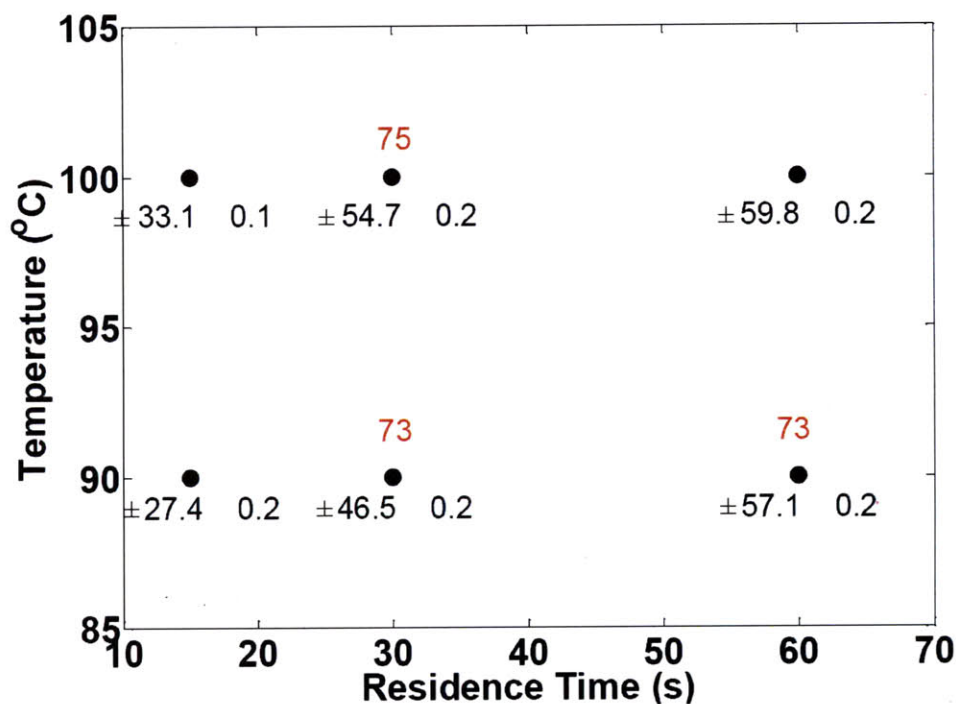
Figure 6-4: Yields of 60-fold reaction scale up in meso-scale flow reactor. Reaction yield obtained in the microreactor are shown in red.

6.1.3 **Analysis of Technique**

Directly transferring the optimum conditions obtained in the automated microreactor system to larger mesoflow reactors appeared to be appropriate for one reaction type, and ill-suited for a different reaction type. For the Knoevenagel case study, several explanations were offered to justify the differences in the reaction yields that were observed in the microreactor and in the mesoflow reactor. These problems were related to the reactor configuration, indicating that direct transfer of reaction conditions from smaller to larger flow systems will result in an unsuccessful scale up when fluid dynamics play a key role in the reaction. However, rather than going through the rigors of modeling the fluid dynamics in mesoflow reactors for each scale up

applications, determining when directly transferring reaction conditions to larger reactors is appropriate can be done through a time scale argument.

The characteristic time scale for a reaction, t_{rxn}, is defined by Eq. 6.1, where k is the rate constant, C^o is the initial concentration of the reagent in excess, and n is the overall reaction order.

$$t_{rxn} \sim \frac{1}{kC^{o^{n-1}}}$$
6.1

The time scale for mixing by diffusion in a static mixer can be estimated through Eq. 6.2, where R_p is the radius of the packing material in the static mixer, and D is the diffusion coefficient.

$$t_{D,SM} \sim \frac{R_p^2}{D}$$
6.2

Again, the time required for heating a reaction stream in the axial position is derived from the Graetz problem with the characteristic time scale defined by Eq. 6.3, where K is a constant, Pe is the Peclet number, R is the channel radius, and U is the average axial velocity.

$$t_{Gz} \sim \frac{K \cdot Pe \cdot R}{U}$$
6.3

Furthermore, moving from a microreactor to a mesoflow reactor can result in a higher degree of axial dispersion. Therefore, the reaction would behave less like a plug flow reactor (PFR) and more like a laminar flow reactor (LFR). The degree of axial dispersion is assessed by a Bodenstein number, Bo, which relates the axial convective forces to the back-mixing from axial dispersion.

$$Bo = \frac{UL}{D^*}$$
6.4

Small Bo values indicate that there is a large deviation from plug flow, but a small value does not necessarily indicate that there is a large deviation from the results that would be obtained in a PFR. To make this assessment, a comparison between the kinetic time scale and residence time distribution is required. For first order reaction kinetics with a conversion of X, the deviation from plug flow has a magnitude of $\ln(1-X)^2/Bo$;[218] therefore reactor dimensions and conditions that satisfy Eq. 6.5 should be selected to ensure that the kinetic data is accurate for reaction optimization and scale up applications.

$$f = \frac{\ln(1-X)^2}{Bo} \ll 1 \quad \text{for negligible dispersion effects} \qquad 6.5$$

Comparison of PFR and dispersion models for reaction rate expressions other than first order have been provided in previous reports.[229] At times this analysis is performed with a similar metric, the Péclet number, Pe, where the molecular diffusion coefficient, D_{AB}, is used to characterize the radial diffusion. Because D^* is typically much larger than D_{AB}, careful attention should be given to the various correlations and formulae used to characterize axial dispersion.[230, 231]

With these definitions, the relative time scales for the Heck reaction and the Knoevenagel condensation are listed in Table 6.2.

Table 6.2: Relative time constants associated with the scale up of reactions.

| Reaction | Res. time (τ) | Time Constants | | | Disp. Metric |
		t_{rxn}	$t_{D,SM}$	t_{Gz}	f [a]
Heck	6 m	1.5 m[b]	1 s	2 s	0.7
Knoevenagel	30 s	15 s[c]	1 s	5 s[d]	15

a: Conversion determined from data of automated optimization investigations.
b: Rate constant estimated as 0.07 M^{-1}min^{-1} by assuming 2nd order irreversible reaction rate using data from automated optimization experiments.
c: Rate constant estimated as 0.6 M^{-1}s^{-1} by assuming 2nd order irreversible reaction rate using data from automated optimization experiments.
d: Characteristic length used in calculation corresponds to radius of tubing in the pre-heating zone, 0.04".

Although both reactors follow the trend $\tau > t_{rxn} > t_{Gz} > t_{D,SM}$, the range of these time constants is much smaller for the Knoevenagel condensation than that of the Heck reaction. Consequently, the reaction outcome of the Knoevenagel is more susceptible to disturbances in mixing and heat transfer. Furthermore, the dispersion metric, f, is significantly higher in the Knoevenagel case study than it is for the Heck reaction. Therefore, the width of the residence time distribution for the tube reactor is broad for the Knoevenagel condensation.

Rather than limit successful reaction scale up to applications where there is a large span in the process time constants, as was the case for the Heck reaction, an alternative approach to scale up would involve modeling the reaction environment in the microreactor and the mesoflow reactor system to determine the appropriate operating conditions.

6.2 Model-Based Approaches for Reaction Scale Up

In addition to predicting optimal reaction conditions, kinetics can be used to facilitate scale up by modeling the reaction environment for a given reactor configuration. Kinetics can also be used in the design of more sophisticated reactors, such as those with sequential addition of a reagent, recycle loops, and non-isothermal reactors. Realization of these goals is dependent on the precision of the kinetic estimates. The concentration and temperature gradients that can exist in flask reactors provide misleading kinetic information. Using microreactors to study reactions furnishes experimenters with the so-called "intrinsic kinetics," the observed kinetics when mass or heat transfer limitations are not present. Therefore, intrinsic kinetics are capable of describing the extent of reaction regardless of reactor size. The Diels-Alder reaction of Scheme 5.1 that was investigated in Chapter 5 was scaled up by a factor of 500 by using the kinetics obtained through the automated microreactor system to model the reaction.

6.2.1 Case Study: Diels-Alder Reaction

6.2.1.1 Experimental Procedure

General method

General experimental information for this reaction was reported in Chapter 5.2.2. DMF from Omnisolv was used as purchased for the scale up experiments.

Preparation of maleic anhydride solution To a 1 L volumetric flask was added maleic anhydride (196 g, 2 mol) and made up to 1 L with DMF. The contents were transferred to a 1 L glass flask, agitated vigorously by hand to ensure a uniform mixture, and charged into the cylinders of an Isco 500D syringe pump.

Preparation of isoprene solution To a 1 L volumetric flask was added isoprene (136 g, 1 mol), biphenyl (42.4 g, 275 mmol) and made up to 1 L with DMF. The contents were transferred to a 1 L glass flask and agitated vigorously by hand to ensure a uniform mixture. The flask was submerged in an ice bath to prevent the isoprene from vaporizing into the head space. A Fuji super metering pump was used to pump the isoprene solution into the AFR system.

6.2.1.2 Advanced Flow Reactor System Design

A schematic of the AFR system for scale-up is shown in Figure 6-5. A high pressure Isco pump and a Fuji Super Metering pump were used to deliver maleic anhydride and isoprene, respectively. Two plates were used to pre-heat the reagents to the reaction temperature before entering the first reaction plate. A static mixer in the first reactor plate was used to create a uniform mixture. Previous reports indicated that mixing in these devices is sufficient for flow

rates above 15 mL/min for each reagent.[232] Reaction temperature was controlled by pumping Kryo 55 oil with a Lauda circulating bath (Integral XT 150) through the two 18-channel heat exchangers that cap the reaction channel. Temperature was monitored by measuring the temperature of the heating oil with thermocouples at the positions marked in Figure 6-5. The glass thickness between the heat exchange fluid and the reaction channel was measured to be 2 mm. An adjustable back pressure regulator was added to the outlet to prevent solvent degassing during reaction.

After reaching thermal equilibrium and setting the flow rates of the Isco and Fuji pumps, the system was flushed for three reactor volumes (180 mL) to ensure steady-state sample collection. Reaction samples were taken by collecting approximately 20 mL of the reaction outlet stream into 80 mL of DMF, which was kept in a 100 mL flask and chilled in an ice bath prior to and during experimentation. These samples were analyzed by HPLC using the isocratic method involved in the microreactor investigations.

6.2.1.3 Reaction Modeling of AFR System

The overall heat transfer coefficient in Corning AFR systems was previously reported by Lavric for a combination of fluids pumped through the heat exchanger and reactor channels.[233] Data from Lavric for the experiments that involved silicone oil as the heat exchanger fluid to heat toluene at various flow rates was used in this investigation. The overall heat transfer coefficient is described as a series of resistances.[234] As depicted in Eq. 6.6, these resistances include the thermal resistance to convective heat transfer of the heating oil ($1/h_{oil}$), the thermal resistance to conductive heat transfer through the Pyrex between the heat exchanger and the reaction channel (δ/k_{pyrex}), and the thermal resistance to convective heat transfer in the reaction stream (h_{rxn}).

135
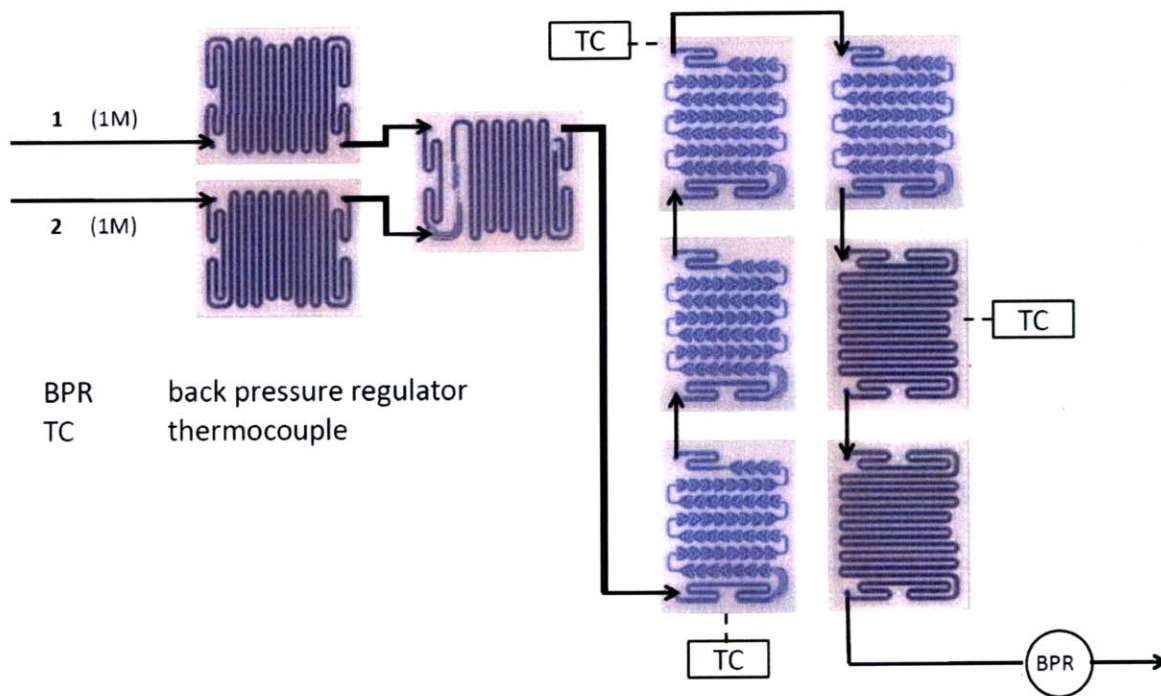
Figure 6-5: Illustration of Corning AFR system used to scale-up reaction by a factor of 500.

$$U_{HX} = \cfrac{1}{\cfrac{1}{h_{oil}} + \cfrac{\delta}{k_{pyrex}} + \cfrac{1}{h_{rxn}}} \qquad 6.6$$

$$h_{oil} \equiv \text{convective heat transfer coefficient of heating oil} \qquad 6.7$$

$$\delta \equiv \text{thickness of Pyrex between heat exchanger and reaction channel} \qquad 6.8$$

$$k_{Pyrex} \equiv \text{thermal conductivity of Pyrex} \qquad 6.9$$

$$h_{rxn} \equiv \text{convective heat transfer coefficient of reaction stream} \qquad 6.10$$

The overall heat transfer coefficients reported by Lavric for toluene flow rates that span the flow rates used in this scale up investigation are listed in Table 6.3.

Table 6.3: Overall heat transfer coefficient in Corning AFR system as a function of toluene flow rate through the reactor channel.

Toluene flow rate (mL/min)	$U_{HX} \times 10^5$ (W/m^{3}K)	U_{HX} (W/m^{2}K)[a]
10	1.7	70
30	4.6	185
60	8.8	350

a: Heat transfer coefficients were converted from units of W/m^{3}K to W/m^{2}K by multiplying second column data by typical surface area/volume ratio of AFR plates, 2500 m^2/m^3.

Over the range of flow rates listed in Table 6.3 the heat transfer coefficient is linear and can be modeled by Eq. 6.11, where F is the toluene flow rate in units of mL/min.

$$U_{HX}\left[\frac{W}{m^2 K}\right] = 6F \qquad\qquad 6.11$$

This linear trend was expected to hold true for this scale up investigation since the fluidic properties of toluene are similar to that of the solvent in the Diels-Alder reaction, DMF. Additionally, it was anticipated that the U_{HX} values determined by Eq. 6.11 underestimated the true heat transfer coefficient value because 1) the flow rates of the heating fluid used in this scale up work were twice that of the one used in Lavric's work and 2) the thermal conductivity of DMF is slightly larger than that of toluene. These features would result in equal or larger values of h_{oil} and larger values of h_{rxn}.

The following thermophysical properties were used in the scale up calculations. Thermophysical properties for the reaction stream were approximated to be that of the solvent, DMF.

Table 6.4: Thermophysical properties of reaction stream.

Thermal conductivity (W/mK)	0.178
Density (kg/m^3)	949
Kinematic viscosity, (m^2/s)	7.3 x 10^{-7}
Heat capacity (J/kgK)	2,106

Assuming PFR behavior, the ode15s function in Matlab was used to model the isoprene mass and energy balances (Eqs. 6.12 and 6.13, respectively) in the AFR. Due to the large flow rate of the heating oil in comparison to the reaction stream flow rate, the temperature of the heating oil (T_{oil}) remained relatively constant. The heat of reaction was assumed to be -142.7 kJ/mol,[221] and the channel dimensions were measured as 4 x 2 mm. Over the range of reaction flow rates investigated in this work, the values of the overall heat transfer coefficient ranged from 170 to 420 W/m^{2}K. A dispersion coefficient of 2.6 x 10^{-3} m^2/s was measured using an UV detectable tracer injection, and was used to calculate the residence time distribution given by Eq. 6.14. Results from the tracer injection experiment are given in Figure 6-6, and the dispersion coefficient was calculated according to Eq. 6.16. The isoprene concentration exiting the AFR system was computed by incorporating the solution from Eqs. 6.12 and 6.13 into the RTD model, as shown in Eq. 6.15.

$$U \frac{dC_1}{dl} = -kC_1^2 \qquad \qquad 6.12$$

$$\rho C_P U \frac{dT}{dl} = \frac{U_{HX} P \left(T - T_{oil} \right)}{A_{CS}} - kC_1^2 \Delta H_{rxn} \qquad \qquad 6.13$$

$$E(t) = \frac{U}{\sqrt{4\pi D^* t}} \exp\left(-\frac{(L - Ut)^2}{4 D^* t} \right) \qquad \qquad 6.14$$

$$\bar{C}_1 = \int_{t=0}^{\infty} C_1 \ t \ E \ t \ dt \qquad\qquad 6.15$$
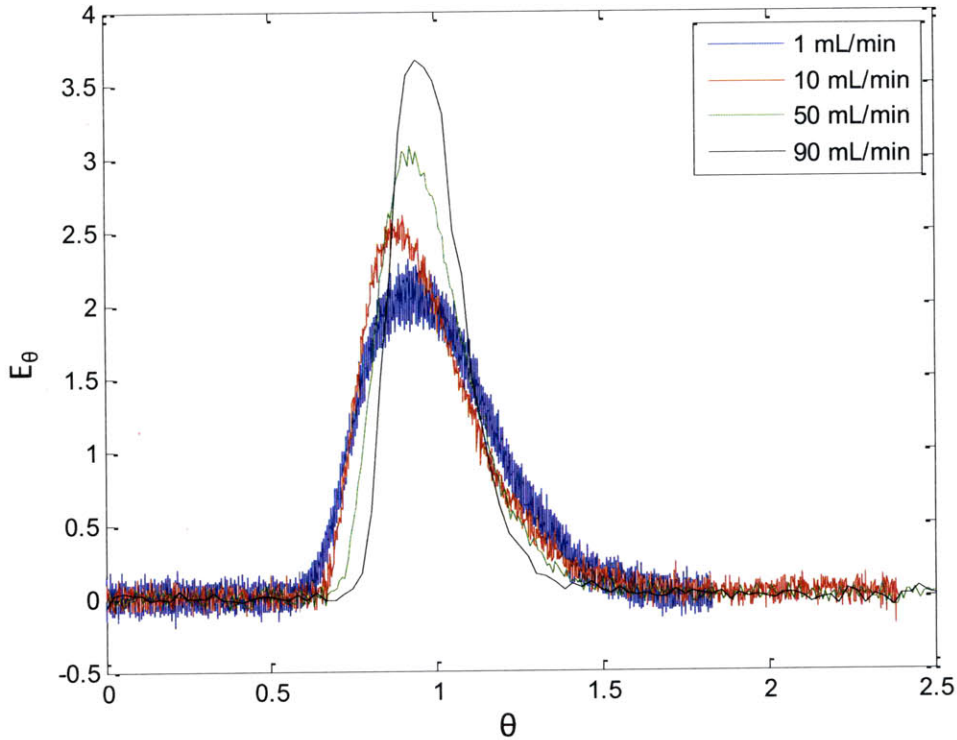
Figure 6-6: Tracer injection curves through a single AFR module.[†]

$$\sigma_{\theta,oo}^2 = 2\frac{\mathbf{D}}{UL} + 8\left(\frac{\mathbf{D}}{UL}\right)^2 \qquad\qquad 6.16$$

6.2.1.4 **Results and Discussion**

Experimental results are compared to the scale up model predictions in Table 6.5, and were found to be in excellent agreement with one another. The predicted isoprene conversion values were consistently higher than the observed experimental conversion. This feature is attributed to the underestimated value of the overall heat transfer coefficient, causing the

[†]I thank Patrick Heider for the tracer injection data.

139

exotherm predicted by the scale up model, which had a maximum value of +5°C, to be larger than what would be observed experimentally.

Table 6.5 Predicted and experimental conversion for scale up investigation for Diels-Alder reaction.

Entry	Samples	Time (min)	Temp. (^{o}C)	Experimental	Predicted
1	2	1.5	110	78.1 ± 0.4	80.5
2	3	2.0	100	82.6 ± 0.1	84.7
3	3	2.5	110	85.2 ± 1.0	87.5
4	2	1.0	126	83.5 ± 3.1	84.8

6.2.2 Analysis of Technique

The Diels-Alder reaction was successfully scaled up by a factor of 500 by using data from 12 automated experiments with a microreactor, a simple RTD experiment to estimate the dispersion coefficient, and solving common material and energy balances. This is the first demonstration of transferring information from a microreactor to a different reactor environment, as well as the largest scale up demonstration from a microreactor. Additionally, this reactor modeling approach could be used to determine how the reaction would perform in different reactor configurations, such as a continuous stirred tank reactor, a sequential addition reactor, or a recycle reactor. The kinetic information could also be used for other components of process development, such as optimal control frameworks. These reasons suggest that the scale up by reactor modeling is the superior approach.

The method of scaling up by reactor modeling, however, also requires more information than the method where the conditions in the microreactor are directly transferred to a larger reactor. At the minimum, the reactor modeling scale up approach also requires heat transfer and RTD studies in the larger reactor, as well as calorimetry studies on the lab scale to determine the heat of reaction. At times this information may be readily available, but at other times it may be

prohibitively difficult to ascertain. Furthermore, as demonstrated in the Heck reaction, the scale up method by directly transferring conditions is appropriate when the reaction time scale is orders of magnitude larger than the transport time scales. In many continuous-flow, multi-step synthesis schemes, a process is bottlenecked by a single operation, such as slow reaction. Therefore, the decision for which reaction scale up approach to apply requires knowledge of the entire process. If the reaction in the overall continuous-flow synthesis is operated such that $\tau >$ $t_{rxn} \gg t_{Gz} \sim t_{D,SM}$, then direct transfer of the microreactor conditions to the mesoflow reactor should be successful; otherwise, the reactor modeling scale up approach should be followed.

6.3 Conclusions

Two reaction scale up methods were explored and critiqued to determine the appropriate application of each technique. In both methods, microreactors were used to extract a wealth of reaction information for scale up while requiring a minimal amount of starting reagents. The ability to use $1 - 10$ g of material in the laboratory, and then scale the reaction up by a factor of 500 is greatly appealing to pharmaceutical research and development. Furthermore, the speed at which this scale up can be performed is impressive. For the Heck reaction, the automated microreactor system optimized the reaction in two days, and the scale up study was one day. Similarly, the kinetics of the Diels-Alder reaction were determined in two days, and then scaled up in a single day. Although these timeframes will vary with the reaction and analytical techniques, it is a significant improvement over current pharmaceutical practices.

Chapter 7
Extensions to Automated Microreactor System for Reaction Development

The synthesis of an active pharmaceutical ingredient involves several reaction and work-up stages. Accordingly, the focus in microchemical research has shifted from investigations that use single unit operations to those that integrate microreactors and microseparators to create a microchemical system.[25, 53] Similarly, future development of the technology established in this thesis research will be used to optimize multi-step syntheses. Towards this end, an automated microreactor system was developed to optimize a two-step reaction - the synthesis of aromatic amines via sequential palladium-catalyzed amination and Suzuki-Miyaura cross-couplings.

In addition to increasing the number of reaction steps explored with an automated microreactor system, the technology must be able to manage the different types of reactions common in pharmaceutical research. Palladium-catalyzed reactions that form carbon-carbon and carbon-nitrogen bonds are standard steps in the synthesis of API's. However, these reactions are difficult to perform in a continuous flow manner because they typically generate an insoluble salt by-product that clogs the microreactor. A method developed in collaboration between the Jensen and Buchwald Research Groups identified the application of acoustic forces as a technique to prolong Pd-catalyzed aminations in continuous-flow reactors.[235] Ultimately, however, the continual salt build-up on the microreactor walls clogs the device and the synthesis must be halted to clean the reactor. This user intervention can be eliminated by using the automation and feedback techniques that were developed in this thesis research to monitor the solid formation

and initiate the removal of solids before the reactor clogs. Advances in this technology will expand the applications of online reaction optimization and kinetic modeling with automated microreactor systems to reactions that produce solids.

7.1 Automated Reaction Profiling for Multi-Step Synthesis[†]

Because reaction systems are coupled, such that the output from one reactor will affect the outcome of the subsequent reaction, future research will investigate finding the reaction conditions that optimize a process rather than an individual reaction. To initiate this research, an automated microreactor system was developed to profile multi-step syntheses. A palladium-catalyzed amination and subsequent Suzuki reaction to afford aromatic amines was selected as the example synthesis (Scheme 7.1). Because homogenous reactions with organic bases have limited success,[12, 236] these reactions were investigated under biphasic flow conditions with inorganic bases. The amination is sensitive to the concentration of the aniline **15**, but an excess of **15** will promote the formation of the undesirable diamine **17**. Additionally, it is important to achieve complete amination of **14** because any unconverted material will couple with the boronic acid **18** during the following Suzuki reaction. The ideal synthesis conditions, therefore, correspond the following outcomes:

- The yield and selectivity of N-(3-chlorophenyl)-3-(trifluoromethyl)aniline **16** is high.

- The reaction is not performed at excessively long residence times.

- The aryl halide **14** is completely converted.

---

†This work was done in close collaboration with Dr. Patrick Bazinet, who at the time, was a post-doctorial associate in the research laboratory of Professor Stephen Buchwald.
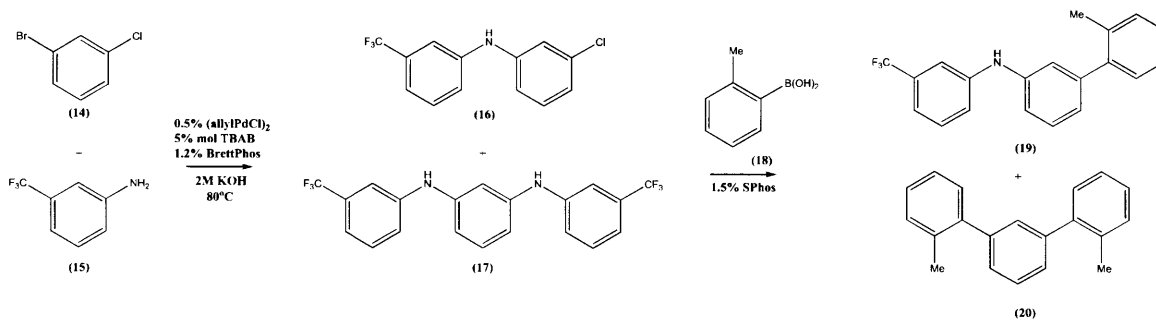
Scheme 7.1: Palladium-catalyzed amination and subsequent Suzuki reaction that were profiled in automated microreactor system.

7.1.1 Experimental Procedure

The biphasic amination reaction was first investigated using an automated system that consisted of syringe pumps, standard fluidic connections and tubing (Idex), and a fraction collector (Gilson FC 204). A schematic of this system is given in Figure 7-1, where syringe pump 'A' contained 3-bromochlorobenzene **14** (2.0 M), allylpalladium chloride dimer (10 mM, 0.5 mol%) and BrettPhos (24 mM, 1.2 mol%), syringe pump 'B' contained 3-(trifluoromethyl)aniline **15** (2.0 M) and tetrabutylammonium bromide (TBAB) (0.1 M, 5 mol%), and syringe pump 'KOH' contained an aqueous solution of 2.0 M KOH. The reaction was quenched with a biphasic stream of 1:1 butyl acetate: water. To promote mass transfer mass transfer throughout the reaction, a packed-bed microreactor was created from 1/4" stainless steel tubing (Swagelok, 0.21" i.d) and packed with 60-125 µm stainless steel spheres (Duke Scientific). The void volume of this reactor was 140 µL. Heating was achieved by submersing the packed-bed reactor in an oil bath equipped with an immersion heater. LabVIEW software was developed to control the syringe pumps, fraction collector, and immersion heater. The program used for these investigations was "profile.vi" and the specific directions to its operations are given in Appendix J.
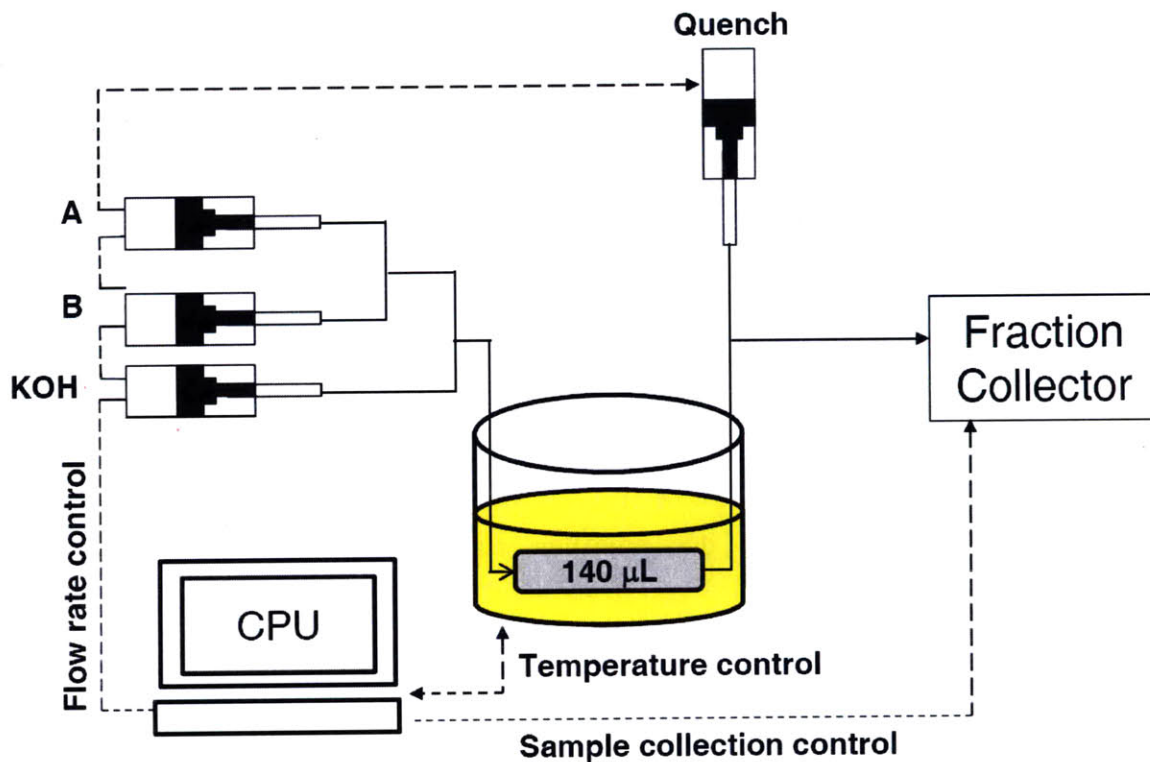
Figure 7-1: Schematic of automated microreactor system for amination investigation.

Experimental conditions were computed based on input parameters associated with each reaction variable. Once an experiment began, the system was equilibrated until the bath temperature was within 1°C of the set point temperature. After thermal equilibrium, the system was flushed with four system volumes of reagent material to ensure steady-state data collection. During this period, the reaction was collected as waste. After purging the system, the program advanced the fraction collector and took two 100 µL samples of reaction material. Once the samples were collected, the program advanced to the next set of experimental conditions and the process was repeated until all experiments were performed. Samples were analyzed off-line by HPLC.

During the amination investigation, the reaction temperature was kept constant at 80°C and the stoichiometric ratio of KOH was maintained at 4 equivalents. The equivalents of **15** was varied from 0.95 to 1.10 in increments of 0.05, and the range of residence times examined spanned 25 to 235 s in increments of 35 s. The combination of these conditions corresponds to a total of 28 experiments. Analysis was performed offline by UPLC.

After analyzing the results from the amination, a second microreactor system was developed where the outlet of the amination reactor was combined with the 2-methylphenylboronic acid **5** in a second packed-bed microreactor. A schematic of this multi-step automated system is given in Figure 7-2. The syringe pumps 'A', 'B', and 'KOH' were loaded in the same manner as previously discussed, and syringe pump 'C' contained **18** (1.5 M) and SPhos (19 mM, 1.5 mol%). The flow rates for the components involved in the amination were constant at 8.48, 8.48, and 33.93 µL/min for syringe pumps 'A', 'B', and 'KOH', respectively. The temperature for both reactors remained constant at 80°C. The automated microreactor system was used to examine the yield of **6** as a function of the residence time in the second reactor and the equivalents of **5**. Due to the limited degrees of freedom, investigating various residence times for the Suzuki reaction required using several packed beds of varying volumes. The void volumes of these reactors were 885, 1284, and 2624 µL.
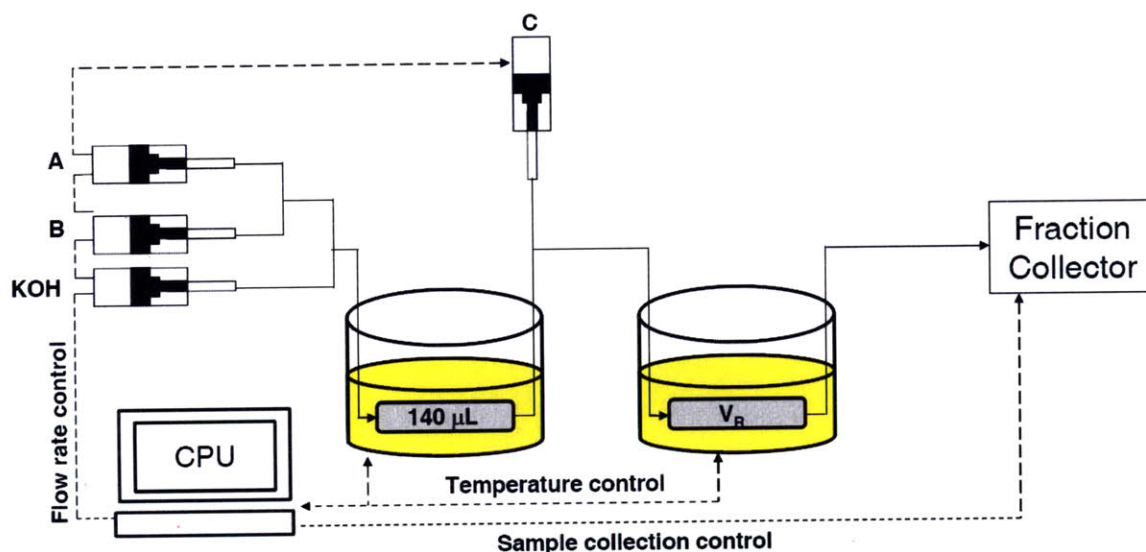
Figure 7-2: Schematic of automated microreactor system used for multi-step synthesis investigation. To vary residence time for the Suzuki reaction, several packed-beds of various void volumes, V_R, were used. These void volumes correspond to 855, 1,284, and 2,264 µL.

7.1.2 Results

The yield of the desired intermediate **16**, the undersirable diamine **17**, and the fractional amount of **14** unconverted in the amination investigation are given in Figure 7-3, Figure 7-4, and Figure 7-5, respectively. The results suggest that amination of **14** was complete after approximately 130 sec. Longer residence times, when complete conversion of **14** was achieved and the excess of analine **15** remained in solution, only resulted in amination of the desired intermediate **16** to form **17**. Diamine **17** was formed in every case with yields ranging from 3% to 11%. Additionally, when less than 1.05 equivalents of **15** were employed, the generation of **17** prevented complete conversion of the aryl chloride **14**. The most desirable reaction outcome corresponded to residence times greater than 95 s and 1.05 equivalents of **15**. These conditions resulted in a 92% yield of the intermediate **16** and only a 6% yield of the diamine **17**.
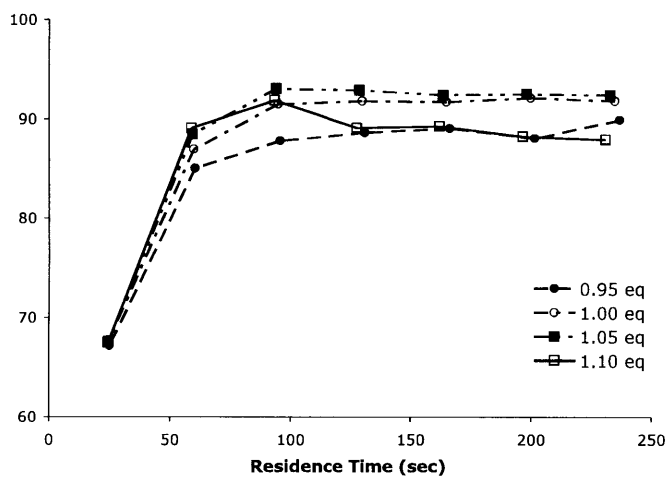
Figure 7-3: **Yield of intermediate 16 as a function of residence time and equivalents of 15.**
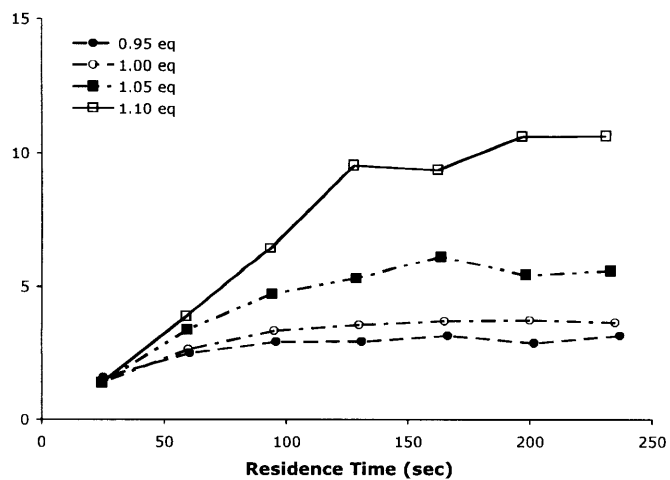
Figure 7-4: **Yield of undesirable diamine 17 as a function of residence time and equivalents of 15.**
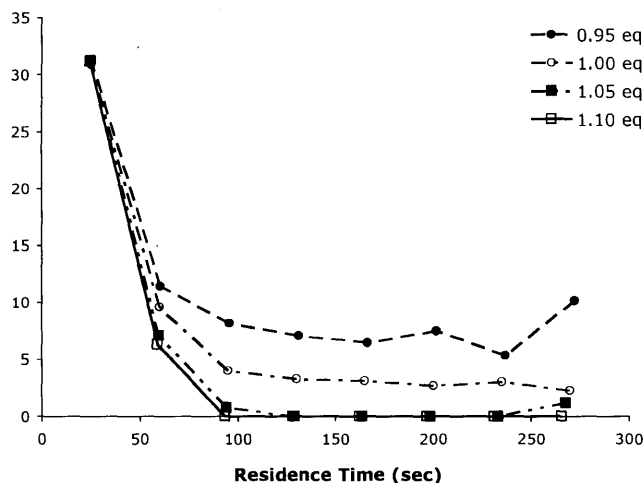
Figure 7-5: Fractional amount of 14 that was uncoverted in amination reaction as a function of residence time and equivalents of 15.

Results for the Suzuki reaction investigation are shown in Table 7.1. The experiments performed with the 855 µL reactor resulted in yields of 77-86% and incomplete conversion of the intermediate **16**. This observation suggested that residence times longer than 13 min. were required. The use of the 1,284 µL reactor allowed a residence time of 20 min. to be examined, and resulted in modest increases to the conversion of the intermediate **16**. Increasing the reactor size to 2,624 µL extended the residence time to 40 min., which resulted in yields of 84-89% of the desired product **19**. Complete conversion of **14** was observed when 1.2 equiv of boronic acid was used, along with the expected amount of diamine **15** (6%).

Table 7.1: Yield of product 19 as a function of residence time and equivalents of 18 for Suzuki reaction investigation.

| ArB(OH)$_2$ (equiv) | 2nd Reactor Volume (Residence Time) | | | | | | | | |
| | 855 µL (13 min) | | | 1284 µL (20 min) | | | 2624 µL (41 min) | | |
	1 (%)	2 (%)	3 (%)	1 (%)	2 (%)	3 (%)	1 (%)	2 (%)	3 (%)
1.0	13	5.5	77	11.3	5.4	78	4.0	6.0	84
1.1	8.7	5.6	81	5.1	6.4	85	1.1	5.7	88
1.2	4.3	5.7	86	4.2	6.8	85	0	6.0	89

7.1.3 Conclusions from Automated Mult-Step Reactor System

Quickly and efficiently exploring a span of reaction conditions provides insight to the reaction behavior that can be used to optimize a multi-step process. This abundant amount of information can be used to examine how the rate limiting step in a reaction pathway or synthesis process changes under different operating conditions. Process engineers can utilize these results to design efficient process with multiple recycle loops, as well as to implement tight process control strategies. Both of these techniques are promising methods for maximizing API yield in a continuous flow process.

7.2 Reaction Development of Chemical Synthesis Involving Solids

A 2005 study by Roberge et al. considered which reactions in the fine chemical and pharmaceutical industry would benefit from the improved mixing and heat transfer in microreactor technology.[1] This survey considered 86 reactions, and concluded that continuous-flow processing would be advantageous for half the reactions. However, only 37% of this reaction subset could physically be performed in a microreactor due to the presence of a solid phase. Several techniques, including gas-liquid segmented flow, ultrasonics and clever pumping mechanisms, have been incorporated with microreactor technology to prevent solids from clogging the channels.[237, 238] For palladium-catalyzed coupling reactions, the integration of these technologies prolong the continuous-flow operations. However, the insoluble salt by-product of these reactions deposits along the reactor wall, inevitably clogging the reactor. By incorporating the feedback and automation methods that were developed in this thesis research, the reaction progress can be monitored and methods can be initiated to remove the accumulated solids from the reactor.

The amination of p-chloromethoxybenzene **21** was selected as the model reaction for this investigation (Scheme 7.2). Investigations by Dr. Ryan Hartman of the Jensen Group and Dr. John Naber of the Buchwald Group demonstrated that this reaction could be operated for an extended amount of time in a 0.04" PFA tubing in a heated ultrasonic bath. The deposition of NaCl along the reactor walls eventually clogged the reactor, and required rinsing the reactor with water. Before this water-wash, however, the reactor was purged with dioxane. This dioxane-flush was required to prevent the t-BuONa from hydrolyzing and forming NaOH, which is also insoluble in dioxane. Therefore, an appropriate wash cycle for continual synthesis involves an initial dioxane purge to remove all reactant material from the reactor, a water-wash to solubilize and remove the accumulated NaCl from the reactor, and a second dixoane purge to return the reactor to anhydrous conditions.

Scheme 7.2: Amination of *p*-chloromethoxybenzene was selected as example reaction to study reactions that generate solid by-products.

7.2.1 Automated Microflow System for Reactions with Solids[†]

The automated microflow system developed to profile reactions that produce solid by-products is shown in Figure 7-6. This system consisted of syringe pumps to control the flow rates of the reagent, dioxane, and water streams, four 3-way solenoid valves (Burkert, 24V

[†] This work was done in close collaboration with Dr. Ryan L. Hartman, who at the time was a post-doctorial associate in the research group of Professor Klavs Jensen, and Dr. John Naber, who at the time was a graduate student in the research group Professor Stephen Buchwald.

actuation, 1/8" NPT fittings, 1/8" NPT to 1/16" bushing to make fluidic connections), and a pressures sensor (Honeywell, model 193C300PG4K). A 240 μL reactor was created using 0.04" PFA tubing, which was coiled and submerged in an ultrasonic bath (Branson). The bath was heated to 80°C with an immersion heater. A K-type thermocouple (Omega) was also submerged in the ultrasonic bath, and a PID controller (Omega, CN9000 series) was used to maintain the reaction temperature of 80°C.
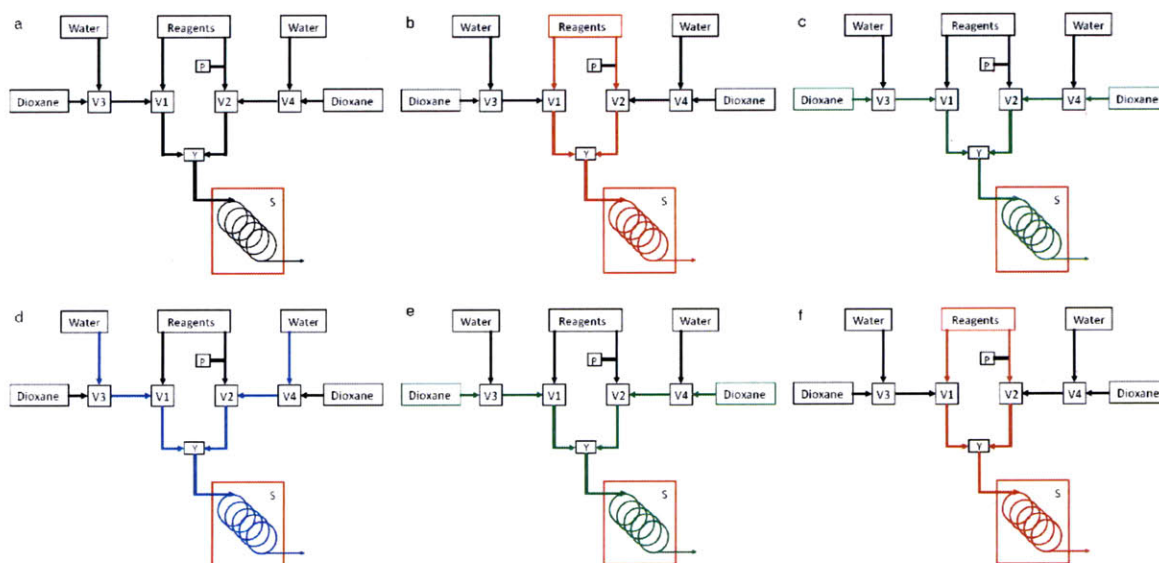
Figure 7-6: Automated system for profiling reactions that produce solid by-products.
(a) Schematic of the components involved in the microfluidic system. The reaction continues until the pressure surpasses a specified threshold (b), above which a the flush cycle begins with a dioxane purge (c), a water-wash (d), a second dioxane purge to return the reactor to anhydrous conditions (e) before starting the reaction (f). Actuated 3-way solenoid valves are denoted by V and are indexed from 1-4, the pressure sensors is denoted by P, and the heated ulatrasonic bath is denoted by S.

7.2.2 Experimental Procedure

The reagent solutions were loaded onto a single syringe pump in 12 mL Norm-Ject syringes. One syringe contained p-chloromethoxybenzene **21** (0.43 M) and aniline **22** (0.36 M) in dioxane. The second syringe contained the base, sodium tert-butoxide (0.5 M), and the

XPhos-precatalyst (1% mol) in dioxane. Anhydrous dioxane was loaded into two 50 mL Norm-Ject syringes and loaded onto a single syringe pump. Deonized water was loaded into two 50 mL Norm-Ject syringes and loaded onto a single syringe pump.

The following discusses the experimental protocol that was developed for reactions that produce solid by-products. The reaction streams flowed at 40 µL/min each to provide a 3 min. residence time (Figure 7-6b). The synthesis would continue until the voltage from the pressure sensor surpassed 100 mV. An excitation voltage of 10 V was provided to the pressure sensor. Once the signal exceeded 100 mV, the reagent syringe pump was stopped, and valves V1 and V2 were activated. One milliliter of dioxane was then pumped through the system at a flow rate of 500 µL/min for one minute (Figure 7-6c). After the dioxane purge, valves V3 and V4 were activated and one milliliter of water was pumped through the system at rate of 500 µL/min (Figure 7-6d). Valves V3 and V4 were then deactivated and eight milliliters of dioxane were pumped through the system at 500 µL/min (Figure 7-6e) to return the system to an anhydrous state and continue with the reaction (Figure 7-6f). The LabVIEW program created for this application was "Solids_reaction.vi" and the details of the operation are provided in Appendix K.

7.2.3 Results and Discussion

After developing the protocol described above, a preliminary investigation was conducted. In this simple experiment, two cycles were performed and two reaction samples were collected. The pressure profiles recorded for these experiments are shown in Figure 7-7. The first experiment, denoted by the blue line, continued until the signal from the pressure sensor exceeded 100 mV at approximately 750 s, at which time the wash cycle began. The pressure spikes noticed before the wash suggested that a bridging mechanism was responsible for reactor clogging.[239, 240] Once the wash cycle was complete, the system returned to the reaction settings.

153

This second experiment, denoted by the red line, indicated that the flushing protocol was effective because the pressure for the second experiment returned to value that was observed in the first experiment. This reaction continued until approximately 2,000 s when the signal from the pressure sensor once again exceeded 100 mV. The yields collected for these experiments were approximately 83%.
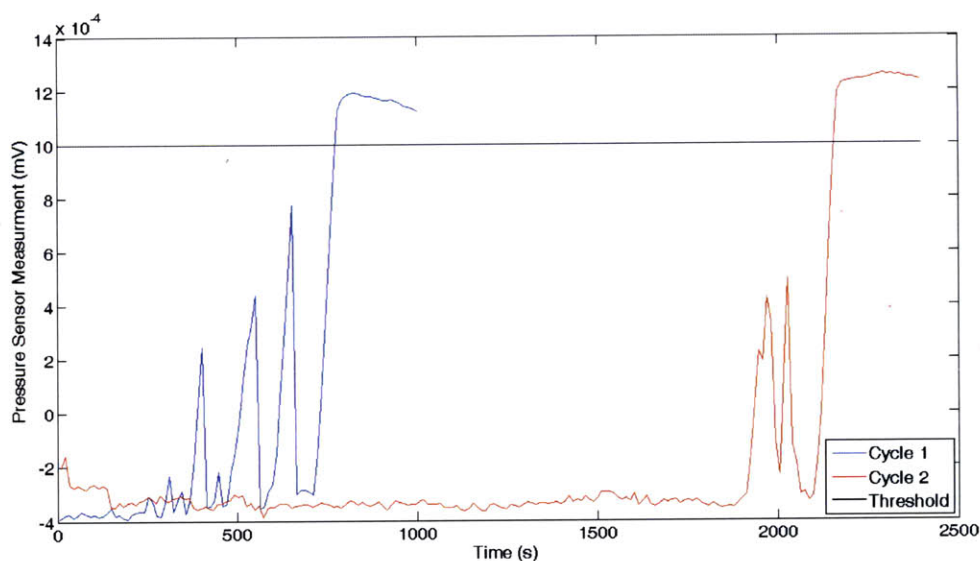
Figure 7-7: Pressure profile for preliminary experiments in automated microflow system for reactions that produce solid by-products.

A second system was proposed and constructed to use two reactors in parallel, so that one reactor could generate product while the other reactor was being flushed. To make the process more efficient, the large dead volume associated with the Burkert valves was avoided by using 3-way micro-solenoid valves (Cole Parmer, 3-way 1/16" 12VDC). Additionally, the lower power, the direct lift mechanism of the valve stem, and the position of the motor in these micro-solenoid valves reduced the heat that reactant material would be exposed to in these valves. An efficient and effective experimental protocol was being developed at the time this thesis was written.

7.2.4 **Conclusions**

An automated microflow system was developed to monitor and profile reactions that generate solid by-products. The initial results are encouraging and suggest that this reaction class, which was once considered impossible to run in a continuous-flow manner, can also be explored in an automated microreactor system to rapidly determine the optimal operating conditions and kinetic parameters. This wash-system can also be used to remove palladium black from microreactor channels, a notorious problem associated with studying palladium-catalyzed reactions at warmer temperatures.[12] Furthermore, developing control strategies for solenoid valves and the starting and stopping of syringe pumps enabled different reagents to be introduced into the reactor system. This feature creates the possibility of using the automated microreactor system for integer optimization so that discrete variables, such as the ligands and the substrates of a reaction, are optimized in addition to the traditional reaction variables.

Chapter 8
Conclusions and Outlook

8.1 Summary of Thesis Contributions

A reoccurring theme throughout this thesis research has been the use of automated microreactors systems to quickly and efficiently gather reaction information. The systems were designed to achieve a high throughput rate of experiments, to use a minimal amount of material for each experiment, and to obtain accurate reaction information that could be applied to various reactor scales. Ingraining these concepts into the various systems will facilitate the adoption of the technology into pharmaceutical research practices.

An automated microreactor system for library development was presented in Chapter 2. Highlights from this system included the ability to perform over 800 automated experiments, and the ability to use less than a milligram of reagent for each experiment. This technology presents a superior alternative to the standard 96-well plate reactor for the investigation of fast reactions or highly exothermic reactions because the transport time scales are enhanced in the microreactor system. Additionally, designing the automation around a silicon microreactor permits the exploration of reactions at unconventional synthesis conditions, such as high temperatures and pressures. Consequently, highly hazardous reactions, such as fluorinations, lithiations, and hydrogenations, can safely be performed at conditions not yet explored.

Incorporating an inline chemical detection method and a feedback algorithm greatly improved the speed and efficiency of reaction optimization, as discussed in Chapter 4. As demonstrated in several case studies, using previous reaction data to select sequential experiments offered a more efficient approach to reaction optimization than the current method

of running parallel experiments in flask reactors. With throughput rates as high as 1 experiment every 10 minutes, optimization of a pharmaceutical reaction can occur in a single day instead of several weeks. This decrease in developmental time and improvement to the precision of reaction optimization is critical to pharmaceutical research, where time and small improvements to yield are highly valued. In addition to being a powerful instrument for chemical research, this technology serves as tool to evaluate the effectiveness and efficiency of new experimental optimization algorithms. The most popular experimental algorithms will be those that find the global solution and require few experiments (iterations).

The ability to incorporate a model-based optimization algorithm to rapidly determine the kinetic parameters was illustrated in Chapter 5. Using a Diels-Alder reaction as an example, a model discrimination method that used Information Theory and Bayesian statistics was applied to find the global rate expression, and a D-optimal framework was used to precisely estimate the kinetic parameters. Although the model-based algorithms employed were established decades ago, the approach was not conducive for batch experimentation. The development of the automated microreactor system provided a setting where these techniques would not be laboriously prohibitive to process chemists and engineers. For the Diels-Alder example, 12 experiments were required to find the global kinetics. Here again, the developed technology offered a more efficient method to extracting reaction information in comparison to the status quo of running parallel experiments in flask reactors.

The information captured by automated microreactor systems can be used to facilitate reactor scale up, as presented in Chapter 6. Two different scale up methods were discussed – 1) the direct transfer of operating conditions from the microreactor to a larger reactor, and 2) the application of accurate kinetics which were determined in the microreactor to predict the reaction

behavior in a larger reactor system. As described in this section, successful application of these two approaches was dependent upon the ratio of the important process time scales, and the availability of information regarding the heat transfer, the fluid dynamics, and the residence time distribution in the larger reactor system. This roadmap for scale up was applied to predict the yield of the Diels-Alder reaction when it was scaled up by a factor of 500. A similar approach could be used to scale up reactions in different reactor configurations, or to design custom reactors with sequential inlets and recycle loops for improved yields.

Several advances to automated microreactor systems for future research were discussed in Chapter 7. One of these applications was in the chemical research area of multi-step synthesis in continuous-flow systems. The selection of operating conditions that maximize the overall yield of a process was simplified by rapidly scanning reaction conditions sequentially in an automated fashion. Understanding chemical outcomes for a variety of conditions is particularly important when investigating highly interrelated reactions, where the outcome of a reaction directly affects the performance of the next reaction. This was demonstrated in the two-step palladium-catlayzed amination and Suzuki reaction example. The second application combined automation and feedback with other process intensification techniques to monitor and profile reactions that produce solid by-products. This capability is vital to pharmaceutical research because many reactions generate a precipitate. Although the technology was specifically designed to remove insoluble salts, the same approach can be used to strip other depositions from microreactors, such as palladium black. The ability to control discrete variables, such as the introduction of different reactant materials, expands the automated microreactor system capabilities to include integer optimization.

The development of automated microreactor systems from this thesis have advanced the field of integrated microreactors from useful tools for the synthetic chemists to intelligent instruments capable of performing, analyzing, and determining sequential experiments to satisfy reaction development goals.

8.2 Outlook for Automated Microreactor Systems

A salient feature of the automated microreactor system for screening applications was the ability to automate over 800 experiments. While this approach can be used to rapidly generate reaction libraries, it does not efficiently determine which combination of reagents result in a reaction and which compounds do not. The integration of inline analysis, clustering algorithms, and chemoinformatics, a computational field of research used in drug discovery to predict system reactivity, can be used to focus on chemical systems that are most likely to react. The most difficult part of this research will be identifying the best "descriptors" for the clustering algorithms. However, the ability to use the automated microreactor to experimentally discriminate and prioritize among the different descriptors will offer a significant improvement over completely *in silico* techniques.

Including a feedback mechanism in the screening system can also be used to perform mixed integer reaction optimization. For example, consider the Heck reaction discussed in Chapter 4. Before the reaction yield was optimized over residence time and alkene equivalence, a suitable base and ligand was selected based on several preliminary experiments. The superior automated microreactor system will incorporate these integer variables in the optimization procedure. This system would be ideal for evaluating the activity and the selectivity of different catalyst sources for synthesis. The development and implementation of efficient algorithms capable of optimizing nonlinear, non-convex problems will be necessary to solve this

superstructure. Because the number of experiments that can be performed may be limited due to availability of material, the convergence metric used in these optimizations should be carefully considered.

The efficiency and capabilities of automated microreactor systems will increase significantly as methods to integrate in-situ analytical methods with microreactors advance. Capturing the concentration profile throughout the reactor provides exceptionally more information than a single steady-state data point collected at the outlet of the reactor. An automated microreactor system that monitors the response of a concentration profile to a change in an input variable is amenable to dynamic optimization approaches. These techniques are ideal for extracting kinetic parameters from just a few experiments, and can be used to find optimal step-sizes for in gradient-based optimization techniques. Furthermore, advanced in-situ methods and model-based algorithms can be combined to validate potential reaction mechanisms if intermediates are detectable.

Complications for automated microfluidic systems compound as the size of the microchemical network grows. Inline pumps, multi-stage counter-current separation systems, and actuated valves with minimal dead volume that are compatible with conditions for typical organic reactions represent a set of unit operations required to realize multi-step chemical synthesis. Control schemes for these microdevices that offer stable operation with fast dynamics are required for the adoption of multi-stage microchemical systems in total synthesis research. As was demonstrated in the multi-step synthesis example in Chapter 7, the design space in downstream reactors shrinks due to constraints in the upstream reactors. This contracting design space is caused by the fixed volume of continuous-flow reactors. Development of an adjustable volume microflow reactor, such as a tubular piston-reactor or a microchip where the flow of the

reaction fluid is manipulated through channels of various volumes, would be ideal for the efficient study of multi-step syntheses. Realization of effective complex systems will require multidisciplinary collaborations among chemists, engineers, microfabricators, and software developers.

Chapter 9
Literature cited

1. Roberge, D. M.; Ducry, L.; Bieler, N.; Cretton, P.; Zimmermann, B., Microreactor Technology: A Revolution for the Fine Chemical and Pharmaceutical Industries? *Chem. Eng. Technol.* **2005,** *28* (3), 318-323.

2. Razzaq, T.; Glasnov, T. N.; Kappe, C. O., Accessing Novel Process Windows in a High-Temperature/Pressure Capillary Flow Reactor. *Chem. Eng. Technol.* **2009,** *32* (11), 1702-1716.

3. Schwalbe, T.; Autze, V.; Hohmann, M.; Stirner, W., Novel Innovation Systems for a Cellular Approach to Continuous Process Chemistry from Discovery to Market. *Org. Process Res. Dev.* **2004,** *8* (3), 440-454.

4. Roberge, D. M.; Zimmermann, B.; Rainone, F.; Gottsponer, M.; Eyholzer, M.; Kockmann, N., Microreactor Technology and Continuous Processes in the Fine Chemical and Pharmaceutical Industry: Is the Revolution Underway? *Org. Process Res. Dev.* **2008,** *12* (5), 905-910.

5. Watts, P.; Haswell, S. J., Microfluidic combinatorial chemistry. *Curr. Opin. Chem. Biol.* **2003,** *7* (3), 380-387.

6. El-Ali, J.; Sorger, P. K.; Jensen, K. F., Cells on chips. *Nature* **2006,** *442* (7101), 403-411.

7. Gerber, D.; Maerkl, S. J.; Quake, S. R., An in vitro microfluidic approach to generating protein-interaction networks. *Nat. Methods* **2009,** *6* (1), 71-74.

8. Srisa-Art, M.; Kang, D. K.; Hong, J.; Park, H.; Leatherbarrow, R. J.; Edel, J. B.; Chang, S. I.; deMello, A. J., Analysis of Protein-Protein Interactions by Using Droplet-Based Microfluidics. *ChemBioChem* **2009,** *10* (10), 1605-1611.

9. Holladay, J. D.; Wang, Y.; Jones, E., Review of Developments in Portable Hydrogen Production Using Microreactor Technology. *Chem. Rev. (Washington, DC, U. S.)* **2004,** *104* (10), 4767-4790.

10. Ajmera, S. K.; Delattre, C.; Schmidt, M. A.; Jensen, K. F., Microfabricated differential reactor for heterogeneous gas phase catalyst testing. *J. Catal.* **2002,** *209* (2), 401-412.

11. Floyd, T. M.; Schmidt, M. A.; Jensen, K. F., Silicon Micromixers with Infrared Detection for Studies of Liquid-Phase Reactions. *Ind. Eng. Chem. Res.* **2004,** *44* (8), 2351-2358.

12. Murphy, E. R.; Martinelli, J. R.; Zaborenko, N.; Buchwald, S. L.; Jensen, K. F., Accelerating reactions with microreactors at elevated temperatures and pressures: Profiling aminocarbonylation reactions. *Angew. Chem. Int. Ed.* **2007,** *46* (10), 1734-1737.

13. Wille, C.; Gabski, H. P.; Haller, T.; Kim, H.; Unverdorben, L.; Winter, R., Synthesis of pigments in a three-stage microreactor pilot plant--an experimental technical report. *Chem. Eng. J. (Lausanne)* **2004,** *101* (1-3), 179-185.

14. Chevalier, B.; Schmidt, F., Corning microreaction technology, a process intensification solution designed for industrial production. *Chimica Oggi - Chemistry Today* **2008,** *26* (5), 6.

15. Pelleter, J.; Renaud, F., Facile, Fast and Safe Process Development of Nitration and Bromination Reactions Using Continuous Flow Reactors. *Org. Process Res. Dev.* **2009,** *13* (4), 698-705.

16.   Li, L.; Mustafi, D.; Fu, Q.; Tereshko, V.; Chen, D. L.; Tice, J. D.; Ismagilov, R. F., Nanoliter microfluidic hybrid method for simultaneous screening and optimization validated with crystallization of membrane proteins. *Proc. Natl. Acad. Sci. U. S. A.* **2006,** *103* (51), 19243-19248.

17.   Kreutz, J. E.; Shukhaev, A.; Du, W.; Druskin, S.; Daugulis, O.; Ismagilov, R. F., Evolution of Catalysts Directed by Genetic Algorithms in a Plug-Based Microfluidic Device Tested with Oxidation of Methane by Oxygen. *J. Am. Chem. Soc.* *132* (9), 3128-3132.

18.   Chambers, R. D.; Holling, D.; Spink, R. C. H.; Sandford, G., Elemental fluorine - Part 13. Gas-liquid thin film microreactors for selective direct fluorination. *Lab Chip* **2001,** *1* (2), 132-137.

19.   Ajmera, S. K.; Losey, M. W.; Jensen, K. F.; Schmidt, M. A., Microfabricated packed-bed reactor for phosgene synthesis. *AIChE J.* **2001,** *47* (7), 1639-1647.

20.   Usutani, H.; Tomida, Y.; Nagaki, A.; Okamoto, H.; Nokami, T.; Yoshida, J.-i., Generation and Reactions of o-Bromophenyllithium without Benzyne Formation Using a Microreactor. *J. Am. Chem. Soc.* **2007,** *129* (11), 3046-3047.

21.   Wiles, C.; Watts, P.; Haswell, S. J., Clean and selective oxidation of aromatic alcohols using silica-supported Jones' reagent in a pressure-driven flow reactor. *Tetrahedron Lett.* **2006,** *47* (30), 5261-5264.

22.   Antes, J.; Boskovic, D.; Krause, H.; Loebbecke, S.; Lutz, N.; Tuercke, T.; Schweikert, W., Analysis and Improvement of Strong Exothermic Nitrations in Microreactors. *Chem. Eng. Res. Des.* **2003,** *81* (7), 760-765.

23.   Baxendale, Ian R.; Ley, Steven V.; Mansfield, Andrew C.; Smith, Christopher D., Multistep Synthesis Using Modular Flow Reactors: Bestmann-Ohira Reagent for the Formation of Alkynes and Triazoles13. *Angew. Chem. Int. Ed.* **2009,** *48* (22), 4017-4021.

24.   Wiles, C.; Watts, P.; Haswell, S. J., The use of solid-supported reagents for the multi-step synthesis of analytically pure alpha,beta-unsaturated compounds in miniaturized flow reactors. *Lab Chip* **2007,** *7* (3), 322-330.

25.   Sahoo, H. R.; Kralj, J. G.; Jensen, K. F., Multistep continuous-flow microchemical synthesis involving multiple reactions and separations. *Angewandte Chemie-International Edition* **2007,** *46* (30), 5704-5708.

26.   Kikutani, Y.; Ueno, M.; Hisamoto, H.; Tokeshi, M.; Kitamori, T., Continuous-flow chemical processing in three-dimensional microchannel network for on-chip integration of multiple reactions in a combinatorial mode. *QSAR Comb. Sci.* **2005,** *24* (6), 742-757.

27.   Madou, M. J., *Fundamentals of Microfabrication: The Science of Miniaturization.* 2nd ed.; CRC Press: Boca Raton, Florida, 2002.

28.   Whitesides, G. M., The origins and the future of microfluidics. *Nature* **2006,** *442* (7101), 368-373.

29.   Nagaki, A.; Takabayashi, N.; Tomida, Y.; Yoshida, J., Selective monolithiation of dibromobiaryls using microflow systems. *Org. Lett.* **2008,** *10* (18), 3937-3940.

30.   Zhang, X. N.; Stefanick, S.; Villani, F. J., Application of microreactor technology in process development. *Org. Process Res. Dev.* **2004,** *8* (3), 455-460.

31.   Liu, S. F.; Fukuyama, T.; Sato, M.; Ryu, I., Continuous microflow synthesis of butyl cinnamate by a Mizoroki-Heck reaction using a low-viscosity ionic liquid as the recycling reaction medium. *Org. Process Res. Dev.* **2004,** *8* (3), 477-481.

32. Ehrfeld, W.; Golbig, K.; Hessel, V.; Lowe, H.; Richter, T., Characterization of mixing in micromixers by a test reaction: Single mixing units and mixer arrays. *Ind. Eng. Chem. Res.* **1999,** *38* (3), 1075-1082.

33. Vankayala, B. K.; Lob, P.; Hessel, V.; Menges, G.; Hoffman, C.; Metzke, D.; Krtschil, U.; Kost, H.-J., Scale-up of Process Intensifying Falling Film Microreactor to Pilot Production Scale. *International Journal of Chemical Reactor Engineering* **2007,** *5* (A91).

34. Jain, K.; Wu, C.; Atre, S. V.; Jovanovic, G.; Narayanan, V.; Kimura, S.; Sprenkle, V.; Canfield, N.; Roy, S., Synthesis of Nanoparticles in High Temperature Ceramic Microreactors: Design, Fabrication and Testing. *Int. J. Appl. Ceram. Technol.* **2009,** *6* (3), 410-419.

35. Knitter, R.; Liauw, M. A., Ceramic microreactors for heterogeneously catalysed gas-phase reactions. *Lab Chip* **2004,** *4* (4), 378-383.

36. Woolley, A. T.; Mathies, R. A., Ultra-High-Speed Dna Fragment Separations Using Microfabricated Capillary Array Electrophoresis Chips. *Proc. Natl. Acad. Sci. U. S. A.* **1994,** *91* (24), 11348-11352.

37. Mellors, J. S.; Gorbounov, V.; Ramsey, R. S.; Ramsey, J. M., Fully Integrated Glass Microfluidic Device for Performing High-Efficiency Capillary Electrophoresis and Electrospray Ionization Mass Spectrometry. *Anal. Chem.* **2008,** *80* (18), 6881-6887.

38. Becker, H.; Gartner, C., Polymer based micro-reactors. *Reviews in Molecular Biotechnology* **2001,** *82* (2), 89-99.

39. Becker, H.; Gärtner, C., Polymer microfabrication methods for microfluidic analytical applications. *Electrophoresis* **2000,** *21* (1), 12-26.

40. Geyer, K.; Seeberger, Peter H., Optimization of Glycosylation Reactions in a Microreactor. *Helv. Chim. Acta* **2007,** *90* (2), 395-403.

41. Yen, B. K.; Günther, A.; Thalmann, M.; Bawendi, M. G.; Jensen, K. F. In *A Microfabricated Segmented-Flow Reactor for the Synthesis of Cdse Quantum Dots*, 8th International Conference on Miniaturized System in Chemistry and Life Sciences (mTAS2004), Malmoe, Sweden, Royal Society of Chemistry.: Malmoe, Sweden, 2004.

42. Hessel, V.; Hardt, S.; Lowe, H., *Chemical Micro Process Engineering : Fundamentals, Modelling and Reactions*. Wiley-VCH: Weinheim, Germany, 2004.

43. Ehrfeld, W.; Hessel, V.; Lowe, H., *Microreactors: New Technology for Modern Chemistry*. Wiley-VCH.: Weinheim, Germany, 2000.

44. Pennemann, H.; Forster, S.; Kinkel, J.; Hessel, V.; Lowe, H.; Wu, L., Improvement of dye properties of the azo pigment yellow 12 using a micromixer-based process. *Org. Process Res. Dev.* **2005,** *9* (2), 188-192.

45. Hessel, V.; Hardt, S.; Lowe, H.; Schonfeld, F., Laminar mixing in different interdigital micromixers: I. Experimental characterization. *AIChE J.* **2003,** *49* (3), 566-577.

46. Song, H.; Bringer, M. R.; Tice, J. D.; Gerdts, C. J.; Ismagilov, R. F., Experimental test of scaling of mixing by chaotic advection in droplets moving through microfluidic channels. *Appl. Phys. Lett.* **2003,** *83* (22), 4664-4666.

47. Song, H.; Tice, J. D.; Ismagilov, R. F., A microfluidic system for controlling reaction networks in time. *Angew. Chem. Int. Ed.* **2003,** *42* (7), 768-772.

48. Khan, S. A.; Gunther, A.; Schmidt, M. A.; Jensen, K. F., Microfluidic synthesis of colloidal silica. *Langmuir* **2004,** *20* (20), 8604-8611.

49. Khan, S. A.; Jensen, K. F., Microfluidic synthesis of titania shells on colloidal silica. *Adv. Mater. (Weinheim, Ger.)* **2007,** *19*, 2556-+.

50. Hessel, V.; Lowe, H.; Schonfeld, F., Micromixers - a review on passive and active mixing principles. *Chem. Eng. Sci.* **2005,** *60* (8-9), 2479-2501.

51. Nguyen, N.-T.; Wu, Z., Micromixers - a review. *Journal of Micromechanics and Microengineering* **2005,** *15*, R1-R16.

52. Wootton, R. C. R.; deMello, A. J., Continuous laminar evaporation: micron-scale distillation. *Chem. Commun. (Cambridge, U. K.)* **2004,** (3), 266-267.

53. Hartman, R. L.; Sahoo, H. R.; Yen, B. C.; Jensen, K. F., Distillation in microchemical systems using capillary forces and segmented flow. *Lab Chip* **2009,** *9* (13), 1843-1849.

54. Zheng, B.; Gerdts, C. J.; Ismagilov, R. F., Using nanoliter plugs in microfluidics to facilitate and understand protein crystallization. *Curr. Opin. Struct. Biol.* **2005,** *15* (5), 548-555.

55. Gunther, A.; Jhunjhunwala, M.; Thalmann, M.; Schmidt, M. A.; Jensen, K. F., Micromixing of miscible liquids in segmented gas-liquid flow. *Langmuir* **2005,** *21* (4), 1547-1555.

56. Kralj, J. G.; Sahoo, H. R.; Jensen, K. F., Integrated continuous microfluidic liquid-liquid extraction. *Lab Chip* **2007,** *7* (2), 256-263.

57. Gunther, A.; Jensen, K. F., Multiphase microfluidics: from flow characteristics to chemical and materials synthesis. *Lab Chip* **2006,** *6*, 1487 - 1503.

58. Murphy, E. R.; Inoue, T.; Sahoo, H. R.; Zaborenko, N.; Jensen, K. F., Solder-based chip-to-tube and chip-to-chip packaging for microfluidic devices. *Lab Chip* **2007,** *7*, 1309-1314.

59. Jensen, K. F., Silicon-based microchemical systems: Characteristics and applications. *Mrs Bulletin* **2006,** *31* (2), 101-107.

60. Marre, S.; Park, J.; Rempel, J.; Guan, J.; Bawendi, M. G.; Jensen, K. F., Supercritical Continuous-Microflow Synthesis of Narrow Size Distribution Quantum Dots. *Adv. Mater. (Weinheim, Ger.)* **2008,** *20* (24), 4830-+.

61. Losey, M. W.; Jackman, R. J.; Firebaugh, S. L.; Schmidt, M. A.; Jensen, K. F., Design and fabrication of microfluidic devices for multiphase mixing and reaction. *Journal of Microelectromechanical Systems* **2002,** *11* (6), 709-717.

62. Wilms, D.; Klos, J.; Kilbinger, A. F. M.; Löwe, H.; Frey, H., Ionic Liquids on Demand in Continuous Flow. *Org. Process Res. Dev.* **2009.**

63. Löbbecke, S.; Ferstl, W.; Pani, S.; Türcke, T., Concepts for Modularization and Automation of Microreaction Technology. *Chem. Eng. Technol.* **2005,** *28* (4), 484-493.

64. Kuntaegowdanahalli, S. S.; Bhagat, A. A. S.; Kumar, G.; Papautsky, I., Inertial microfluidics for continuous particle separation in spiral microchannels. *Lab Chip* **2009,** *9* (20), 2973-2980.

65. deMello, A. J., Control and detection of chemical reactions in microfluidic systems. *Nature* **2006,** *442* (7101), 394-402.

66. Jensen, K. F., Microreaction engineering - is small better? *Chem. Eng. Sci.* **2001,** *56* (2), 293-303.

67. Quiram, D. J.; Jensen, K. F.; Schmidt, M. A.; Mills, P. L.; Ryley, J. F.; Wetzel, M. D.; Kraus, D. J., Integrated microreactor system for gas-phase catalytic reactions. 1. Scale-up microreactor design and fabrication. *Ind. Eng. Chem. Res.* **2007,** *46*, 8292-8305.

68. Lopeandia, A. F.; Cerdo, L. l.; Clavaguera-Mora, M. T.; Arana, L. R.; Jensen, K. F.; Munoz, F. J.; Rodriguez-Viejo, J., Sensitive power compensated scanning calorimeter for

analysis of phase transformations in small samples. *Rev. Sci. Instrum.* **2005,** *76* (6), 065104-5.

69. Zhang, X.; Coupland, P.; Fletcher, P. D. I.; Haswell, S. J., Monitoring of liquid flow through microtubes using a micropressure sensor. *Chem. Eng. Res. Des.* **2009,** *87* (1), 19-24.

70. Garbe, C.; Roetmann, K.; Beushausen, V.; Jähne, B., An optical flow MTV based technique for measuring microfluidic flow in the presence of diffusion and Taylor dispersion. *Experiments in Fluids* **2008,** *44* (3), 439-450.

71. Lien, V.; Vollmer, F., Microfluidic flow rate detection based on integrated optical fiber cantilever. *Lab Chip* **2007,** *7* (10), 1352-1356.

72. Fletcher, P. D. I.; Haswell, S. J.; Pombo-Villar, E.; Warrington, B. H.; Watts, P.; Wong, S. Y. F.; Zhang, X. L., Micro reactors: principles and applications in organic synthesis. *Tetrahedron* **2002,** *58* (24), 4735-4757.

73. Christensen, P. D.; Johnson, S. W. P.; McCreedy, T.; Skelton, V.; Wilson, N. G., The fabrication of micro-porous silica structure for micro-reactor technology. *Analytical Communications* **1998,** *35* (10), 341 - 343.

74. Futterer, C.; Minc, N.; Bormuth, V.; Codarbox, J. H.; Laval, P.; Rossier, J.; Viovy, J. L., Injection and flow control system for microchannels. *Lab Chip* **2004,** *4* (4), 351-356.

75. Braschler, T.; Metref, L.; Zvitov-Marabi, R.; van Lintel, H.; Demierre, N.; Theytaz, J.; Renaud, P., A simple pneumatic setup for driving microfluidics. *Lab Chip* **2007,** *7* (4), 420-422.

76. Jang, L.; Yu, Y., Peristaltic micropump system with piezoelectric actuators. *Microsystems Technologies* **2008,** *14* (2), 241-248.

77. Walker, G. M.; Beebe, D. J., A passive pumping method for microfluidic devices. *Lab Chip* **2002,** *2* (3), 131-134.

78. de Mas, N.; Guenther, A.; Schmidt, M. A.; Jensen, K. F. In *Scalable microfabricated reactors for direct fluorination reactions*, Transducers - 12th International Conference on Solid-State Sensors, Actuators and Microsystems, Boston MA, June 2003; Transducers Research Foundation: Boston MA, 2003; pp 655 - 658.

79. de Mas, N.; Günther, A.; Kraus, T.; Schmidt, M. A.; Jensen, K. F., Scaled-out multilayer gas-liquid microreactor with integrated velocimetry sensors. *Ind. Eng. Chem. Res.* **2005,** *44* (24), 8997-9013.

80. Yang, Z.; Matsumoto, S.; Goto, H.; Matsumoto, M.; Maeda, R., Ultrasonic micromixer for microfluidic systems. *Sensors and Actuators A-Physical* **2001,** *93* (3), 266-272.

81. Lohse, S.; Kohnen, B. T.; Janasek, D.; Dittrich, P. S.; Franzke, J.; Agar, D. W., A novel method for determining residence time distribution in intricately structured microreactors. *Lab Chip* **2008,** *8* (3), 431-438.

82. Chan, K. L. A.; Gulati, S.; Edel, J. B.; de Mello, A. J.; Kazarian, S. G., Chemical imaging of microfluidic flows using ATR-FTIR spectroscopy. *Lab Chip* **2009,** -.

83. Ferstl, W.; Klahn, T.; Schweikert, W.; Billeb, G.; Schwarzer, M.; Loebbecke, S., Inline Analysis in Microreaction Technology: A Suitable Tool for Process Screening and Optimization. *Chem. Eng. Technol.* **2007,** *30* (3), 370-380.

84. Leung, S.-A.; Winkle, R. F.; Wootton, R. C. R.; deMello, A. J., A method for rapid reaction optimisation in continuous-flow microfluidic reactors using online Raman spectroscopic detection. *The Analyst* **2005,** *130* (1), 46-51.

85. Hubner, S.; Bentrup, U.; Budde, U.; Lovis, K.; Dietrich, T.; Freitag, A.; Kuľpper, L.; Jaľhnisch, K., An Ozonolysis - Reduction Sequence for the Synthesis of Pharmaceutical Intermediates in Microstructured Devices. *Org. Process Res. Dev.* **2009**.

86. Maguire, Y.; Chuang, I. L.; Zhang, S.; Gershenfeld, N., Ultra-small-sample molecular structure detection using microslot waveguide nuclear spin resonance. *Proc. Natl. Acad. Sci. U. S. A.* **2007**, *104* (22), 9198-9203.

87. Damean, N.; Sia, S. K.; Linder, V.; Narovlyansky, M.; Whitesides, G. M., Space- and time-resolved spectrophotometry in microsystems. *Proc. Natl. Acad. Sci. U. S. A.* **2005**, *102* (29), 10035-10039.

88. Albrecht, J. W.; El-Ali, J.; Jensen, K. F., Cascaded free-flow isoelectric focusing for improved focusing speed and resolution. *Anal. Chem.* **2007**, *79*, 9364-9371.

89. Ohno, K.-i.; Tachikawa, K.; Manz, A., Microfluidics: Applications for analytical purposes in chemistry and biochemistry. *Electrophoresis* **2008**, *29* (22), 4443-4453.

90. Shih, C.-Y.; Chen, Y.; Xie, J.; He, Q.; Tai, Y.-C., On-chip temperature gradient interaction chromatography. *Journal of Chromatography A* **2006**, *1111* (2), 272-278.

91. Benvenuto, A.; Guarnieri, V.; Lorenzelli, L.; Collini, C.; Decarli, M.; Adami, A.; Potrich, C.; Lunelli, L.; Canteri, R.; Pederzolli, C., Fabrication of a MEMS-based separation module for liquid chromatography. *Sensors and Actuators B: Chemical* **2008**, *130* (1), 181-186.

92. Chan, K. L. A.; Gulati, S.; Edel, J. B.; Mello, A. J. d.; Kazarian, S. G., Chemical imaging of microfluidic flows using ATR-FTIR spectroscopy. *Lab Chip* **2009**, *9* (20), 2909-2913.

93. Wu, R.; Hu, L. G.; Wang, F. J.; Ye, M. L.; Zou, H., Recent development of monolithic stationary phases with emphasis on microscale chromatographic separation. *Journal of Chromatography A* **2008**, *1184* (1-2), 369-392.

94. Piehl, N.; Ludwig, M.; Belder, D., Subsecond chiral separations on a microchip. *Electrophoresis* **2004**, *25* (21-22), 3848-3852.

95. Fernandez-Suarez, M.; Wong, S. Y. F.; Warrington, B. H., Synthesis of a three-member array of cycloadducts in a glass microchip under pressure driven flow. *Lab Chip* **2002**, *2* (3), 170-174.

96. Garcia-Egido, E.; Spikmans, V.; Wong, S. Y. F.; Warrington, B. H., Synthesis and analysis of combinatorial libraries performed in an automated micro reactor system. *Lab Chip* **2003**, *3* (2), 73-76.

97. Schwalbe, T.; Kadzimirsz, D.; Jas, G., Synthesis of a Library of Ciprofloxacin Analogues By Means of Sequential Organic Synthesis in Microreactors. *QSAR Comb. Sci.* **2005**, *24* (6), 758-768.

98. Griffiths-Jones, C. M.; Hopkin, M. D.; Jonsson, D.; Ley, S. V.; Tapolczay, D. J.; Vickerstaffe, E.; Ladlow, M., Fully Automated Flow-Through Synthesis of Secondary Sulfonamides in a Binary Reactor System. *J. Comb. Chem.* **2007**, *9* (3), 422-430.

99. Yu, L., Pharmaceutical Quality by Design: Product and Process Development, Understanding, and Control. *Pharm. Res.* **2008**, *25* (4), 781-791.

100. Sugimoto, A.; Fukuyama, T.; Rahman, M. T.; Ryu, I., An Automated-Flow Microreactor System for Quick Optimization and Production: Application to 10- and 100-gram Order Productions of a Matrix Metalloproteinase Inhibitor Using a Sonogashira Coupling Reaction. *Tetrahedron Letters In Press, Accepted Manuscript*.

101. Koch, K.; van Weerdenburg, B. J. A.; Verkade, J. M. M.; Nieuwland, P. J.; Rutjes, F. P. J. T.; van Hest, J. C. M., Optimizing the Deprotection of the Amine Protecting p-

Methoxyphenyl Group in an Automated Microreactor Platform. *Org. Process Res. Dev.* **2009,** *13* (5), 1003-1006.

102. Krishnadasan, S.; Brown, R. J. C.; deMello, A. J.; deMello, J. C., Intelligent routes to the controlled synthesis of nanoparticles. *Lab Chip* **2007,** *7* (11), 1434-1441.

103. Song, H.; Chen, D. L.; Ismagilov, R. F., Reactions in Droplets in Microfluidic Channels. *Angew. Chem. Int. Ed.* **2006,** *45* (44), 7336-7356.

104. Hatakeyama, T.; Chen, D. L.; Ismagilov, R. F., Microgram-Scale Testing of Reaction Conditions in Solution Using Nanoliter Plugs in Microfluidics with Detection by MALDI-MS. *J. Am. Chem. Soc.* **2006,** *128* (8), 2518-2519.

105. Goodell, J. R.; McMullen, J. P.; Zaborenko, N.; Maloney, J. R.; Ho, C.-X.; Jensen, K. F.; Porco, J. A.; Beeler, A. B., Development of an Automated Microfluidic Reaction Platform for Multidimensional Screening: Reaction Discovery Employing Bicyclo[3.2.1]octanoid Scaffolds. *J. Org. Chem.* **2009,** *74* (16), 6169-6180.

106. Arve, L.; Voigt, T.; Waldmann, H., Charting Biological and Chemical Space: PSSC and SCONP as Guiding Principles for the Development of Compound Collections Based on Natural Product Scaffolds. *QSAR Comb. Sci.* **2006,** *25* (5-6), 449-456.

107. Schreiber, S. L., Target-Oriented and Diversity-Oriented Organic Synthesis in Drug Discovery. *Science* **2000,** *287* (5460), 1964-1969.

108. Tan, D. S., Diversity-oriented synthesis: exploring the intersections between chemistry and biology. *Nat. Chem. Biol.* **2005,** *1* (2), 74-84.

109. Wipf, P.; Werner, S.; Woo, G. H. C.; Stephenson, C. R. J.; Walczak, M. A. A.; Coleman, C. M.; Twining, L. A., Application of divergent multi-component reactions in the synthesis of a library of peptidomimetics based on [gamma]-amino-[alpha],[beta]-cyclopropyl acids. *Tetrahedron* **2005,** *61* (48), 11488-11500.

110. Beeler, A. B.; Su, S.; Singleton, C. A.; Porco, J. A., Discovery of Chemical Reactions through Multidimensional Screening. *J. Am. Chem. Soc.* **2007,** *129* (5), 1413-1419.

111. Weber, L.; Illgen, K.; Almstetter, M., Discovery of New Multi Component Reactions with Combinatorial Methods. *Synlett* **1999,** *1999* (03), 366-374.

112. Bailing, L.; Songjun, L.; Jie, H., Technological Advances in High-Throughput Screening. *American Journal of PharmacoGenomics* **2004,** *4*, 263-276.

113. Harre, M.; Neh, H.; Schulz, C.; Tilstam, U.; Wessa, T.; Weinmann, H., Breaking the New Bottleneck: Our Way into Robotics. *Org. Process Res. Dev.* **2001,** *5* (3), 335-339.

114. Wangelin, A. J. v.; Neumann, H.; Gördes, D.; Klaus, S.; Jiao, H.; Spannenberg, A.; Krüger, T.; Wendler, C.; Thurow, K.; Stoll, N.; Beller, M., Unusual Coupling Reactions of Aldehydes and Alkynes: A Novel Preparation of Substituted Phthalic Acid Derivatives by Automated Synthesis. *Chemistry - A European Journal* **2003,** *9* (10), 2273-2281.

115. Di, L.; McConnell, O. J.; Kerns, E. H.; Sutherland, A. G., Rapid, automated screening method for enzymatic transformations using a robotic system and supercritical fluid chromatography. *Journal of Chromatography B* **2004,** *809* (2), 231-235.

116. Buechi, G.; Mak, C.-P., Biomimetic syntheses of the neolignans guianin, burchellin, 2-epi,3a-epiburchellin and futoenone. *J. Am. Chem. Soc.* **1977,** *99* (24), 8073-8075.

117. Comer, E.; Rohan, E.; Deng, L.; Porco, J. A., An Approach to Skeletal Diversity Using Functional Group Pairing of Multifunctional Scaffolds. *Org. Lett.* **2007,** *9* (11), 2123-2126.

118. Couladouros, E. A.; Strongilos, A. T., Generation of Libraries of Pharmacophoric Structures with Increased Complexity and Diversity by Employing Polymorphic Scaffolds. *Angew. Chem. Int. Ed.* **2002,** *41* (19), 3677-3680.

119. Kumagai, N.; Muncipinto, G.; Schreiber, S. L., Short Synthesis of Skeletally and Stereochemically Diverse Small Molecules by Coupling Petasis Condensation Reactions to Cyclization Reactions13. *Angew. Chem. Int. Ed.* **2006,** *45* (22), 3635-3638.

120. Günther, A.; Khan, S. A.; Thalmann, M.; Trachsel, F.; Jensen, K. F., Transport and reaction in microscale segmented gas-liquid flow. *Lab Chip* **2004,** *4* (4), 278-286.

121. Ratner, D. M.; Murphy, E. R.; Jhunjhunwala, M.; Snyder, D. A.; Jensen, K. F.; Seeberger, P. H., Microreactor-based reaction optimization in organic chemistry-glycosylation as a challenge. *Chem. Commun. (Cambridge, U. K.)* **2005,** (5), 578-580.

122. Aggarwal, V. K.; Staubitz, A. C.; Owen, M., Optimization of the Mizoroki - Heck Reaction Using Design of Experiment (DoE). *Org. Process Res. Dev.* **2005,** *10* (1), 64-69.

123. Box, G. E. P.; Hunter, W. G.; Hunter, J. S., *Statistics for Experimenters An Introduction to Design, Data Analysis, and Model Building.* John Wiley & Sons: New York 1978.

124. Montgomery, D. C., *Design and analysis of experiments.* John Wiley: New York, 2001.

125. VanAntwerp, J. G.; Braatz, R. D., A tutorial on linear and bilinear matrix inequalities. *J. Process Control* **2000,** *10* (4), 363-385.

126. Chachuat, B.; Singer, A. B.; Barton, P. I., Global Methods for Dynamic Optimization and Mixed-Integer Dynamic Optimization. *Ind. Eng. Chem. Res.* **2006,** *45* (25), 8373-8392.

127. Grossmann, I. E.; Biegler, L. T., Part II. Future perspective on optimization. *Comput. Chem. Eng.* **2004,** *28* (8), 1193-1218.

128. Michalik, C.; Chachuat, B. t.; Marquardt, W., Incremental Global Parameter Estimation in Dynamical Systems. *Ind. Eng. Chem. Res.* **2009,** *48* (11), 5489-5497.

129. Nelder, J. A.; Mead, R., A Simplex Method for Function Minimization. *Computer J.* **1964,** *7,* 308-313.

130. Himmelblau, D. M., *Applied Nonlinear Programming* McGraw-Hill Book Company: New York, 1972.

131. Reklaitis, G. V.; Ravindran, A.; Ragsdell, K. M., *Engineering Optimization Methods and Applications.* Wiley-Interscience: New York, 1983.

132. Huyer, W.; Neumaier, A., SNOBFIT -- Stable Noisy Optimization by Branch and Fit. *ACM Trans. Math. Softw.* **2008,** *35* (2), 1-25.

133. Myers, R. H.; Montgomery, D. C., *Response Surface Methodology.* John Wiley & Sons: New York, 1995.

134. Devore, J., L., *Probability and Statistics for Engineering and the Sciences.* 5th ed.; Duxbury Press: 2000.

135. Bazaraa, M. S.; Sherali, H. D., On the choice of step size in subgradient optimization. *European Journal of Operational Research* **1981,** *7* (4), 380-388.

136. Poljak, B. T., A General Method for Solving Extremal Problems. *Soviet Mathematics Doklady* **1967,** *8,* 593-597.

137. Press, W. H. T., S. A.; Vetterling, W. T.; Flannery, B. P., *Numerical Recipes in C, The Art of Scientific Computation.* 2 ed.; Cambridge Univ. Press: Cambridge, 1992.

138. Beers, K. J., *Numerical Methods for Chemical Engineering Applications in Matlab.* Cambridge University Press: New York, 2007.

139. Deen, W., *Analysis of Transport Phenomena.* Oxford: 1998.

140. Murphy, E. R. Microchemical Systems for Rapid Optimization of Organic Synthesis. Ph.D. Thesis, Massachusetts Institute of Technology, Cambridge, 2006.

141. Yen, B. K. H.; Gunther, A.; Schmidt, M. A.; Jensen, K. F.; Bawendi, M. G., A microfabricated gas-liquid segmented flow reactor for high-temperature synthesis: The case of CdSe quantum dots. *Angewandte Chemie-International Edition* **2005**, *44* (34), 5447-5451.

142. Baumann, M.; Baxendale, I. R.; Ley, S. V.; Smith, C. D.; Tranmer, G. K., Fully Automated Continuous Flow Synthesis of 4,5-Disubstituted Oxazoles. *Org. Lett.* **2006**, *8* (23), 5231-5234.

143. Herzig-Marx, R.; Queeney, K. T.; Jackman, R. J.; Schmidt, M. A.; Jensen, K. F., Infrared Spectroscopy for Chemically Specific Sensing in Silicon-based Microreactors. *Anal. Chem.* **2004**, *76*, 6476-6483.

144. Geyer, K.; Codee, J. D. C.; Seeberger, P. H., Microreactors as Tools for Synthetic Chemists - The Chemists' Round-Bottomed Flask of the 21st Century? *Chemistry - A European Journal* **2006**, *12* (33), 8434-8442.

145. Kim, D.; Chesler, N. C.; Beebe, D. J., A method for dynamic system characterization using hydraulic series resistance. *Lab Chip* **2006**, *6* (5), 639-644.

146. Burriel, P.; Claret, J.; Ignés-Mullol, J.; Sagués, F., "Bottleneck Effect" in Two-Dimensional Microfluidics. *Phys. Rev. Lett.* **2008**, *100* (13), 134503.

147. Zaborenko, N.; Murphy, E. R.; Kralj, J. G.; Jensen, K. F., Synthesis and Kinetics of Highly Energetic Intermediates by Micromixers: Direct Multistep Synthesis of Sodium Nitrotetrazolate. *Ind. Eng. Chem. Res.* *49* (9), 4132-4139.

148. Bula, W. P.; Verboom, W.; Reinhoudt, D. N.; Gardeniers, H. J. G. E., Multichannel quench-flow microreactor chip for parallel reaction monitoring. *Lab Chip* **2007**, *7* (12), 1717-1722.

149. Hirata, K.; Shinoda, M.; Nohmi, M.; Goto, A.; Takeda, K. Microchannel chip reaction control system, micro total reaction system including the control system, and micro total analysis system. US Patent Application Publication 2008/0153169 A1, June 26, 2008.

150. Nelder, J. A.; Mead, R., A Simplex Method for Function Minimization. *The Computer Journal* **1965**, *7* (4), 308-313.

151. Littke, A. F.; Fu, G. C., A Versatile Catalyst for Heck Reactions of Aryl Chlorides and Aryl Bromides under Mild Conditions. *Journal of the American Chemical Society* **2001**, *123* (29), 6989-7000.

152. Beletskaya, I. P.; Cheprakov, A. V., The heck reaction as a sharpening stone of palladium catalysis. *Chemical Reviews* **2000**, *100* (8), 3009-3066.

153. Oestreich, M., *The Mizoroki-Heck Reaction*. John Wiley & Sons: Chichester, 2009.

154. Prashad, M., *Palladium-Catalyzed Heck Arylations in the Synthesis of Active Pharmaceutical Ingredients*. Springer: Berlin, 2004; Vol. 6.

155. de Vries, J. G., The Heck reaction in the production of fine chemicals. *Can J Chem* **2001**, *79* (5), 1086-1092.

156. Nicolaou, K. C.; Bulger, P. G.; Sarlah, D., Palladium-catalyzed cross-coupling reactions in total synthesis. *Angewandte Chemie-International Edition* **2005**, *44* (29), 4442-4489.

157. Dounay, A. B.; Overman, L. E., The asymmetric intramolecular Heck reaction in natural product total synthesis. *Chemical Reviews* **2003**, *103* (8), 2945-2963.

158. Nikbin, N.; Ladlow, M.; Ley, S. V., Continuous flow ligand-free Heck reactions using monolithic Pd [0] nanoparticles. *Organic Process Research & Development* **2007,** *11* (3), 458-462.

159. Glasnov, T. N.; Findenig, S.; Kappe, C. O., Heterogeneous Versus Homogeneous Palladium Catalysts for Ligandless Mizoroki-Heck Reactions: A Comparison of Batch/Microwave and Continuous-Flow Processing. *Chemistry-a European Journal* **2009,** *15* (4), 1001-1010.

160. Altava, B.; Burguete, M. I.; Garcia-Verdugo, E.; Karbass, N.; Luis, S. V.; Puzary, A.; Sans, V., Palladium N-methylimidazolium supported complexes as efficient catalysts for the Heck reaction. *Tetrahedron Letters* **2006,** *47* (14), 2311-2314.

161. Shore, G.; Morin, S.; Organ, M. G., Catalysis in capillaries by Pd thin films using microwave-assisted continuous-flow organic synthesis (MACOS). *Angewandte Chemie-International Edition* **2006,** *45* (17), 2761-2766.

162. Karbass, N.; Sans, V.; Garcia-Verdugo, E.; Burguete, M. I.; Luis, S. V., Pd(0) supported onto monolithic polymers containing IL-like moieties. Continuous flow catalysis for the Heck reaction in near-critical EtOH. *Chemical Communications* **2006,** (29), 3095-3097.

163. Kunz, U.; Kirschning, A.; Wen, H. L.; Solodenko, W.; Cecilia, R.; Kappe, C. O.; Turek, T., Monolithic polymer/carrier materials: Versatile composites for fine chemical synthesis. *Catalysis Today* **2005,** *105* (3-4), 318-324.

164. Fox, J. M.; Huang, X. H.; Chieffi, A.; Buchwald, S. L., Highly active and selective catalysts for the formation of alpha-aryl ketones. *J. Am. Chem. Soc.* **2000,** *122* (7), 1360-1370.

165. Bakore, G. V.; Banerjee, K. K.; Shanker, R., Kinetic Investigation of the Oxidation of Benzyl Alcohol by Chromic Acid. *Z Phys Chem Neue Fol* **1965,** *45,* 129-135.

166. Wiberg, K. B.; Mill, T., The Kinetics of the Chromic Acid Oxidation of Benzaldehyde. *J. Am. Chem. Soc.* **2002,** *80* (12), 3022-3029.

167. Kockritz, A.; Sebek, M.; Dittmar, A.; Radnik, J.; Bruckner, A.; Bentrup, U.; Pohl, M. M.; Hugl, H.; Magerlein, W., Ru-catalyzed oxidation of primary alcohols. *Journal of Molecular Catalysis a-Chemical* **2006,** *246* (1-2), 85-99.

168. Trend, R. M.; Ramtohul, Y. K.; Stoltz, B. M., Oxidative cyclizations in a nonpolar solvent using molecular oxygen and studies on the stereochemistry of oxypalladation. *J. Am. Chem. Soc.* **2005,** *127* (50), 17778-17788.

169. Fritz-Langhals, E., Technical Production of Aldehydes by Continuous Bleach Oxidation of Alcohols Catalyzed by 4-Hydroxy-TEMPO. *Org. Process Res. Dev.* **2005,** *9* (5), 577-582.

170. Graves, C. R.; Zeng, B.-S.; Nguyen, S. T., Efficient and Selective Al-Catalyzed Alcohol Oxidation via Oppenauer Chemistry. *J. Am. Chem. Soc.* **2006,** *128* (39), 12596-12597.

171. Jiang, N.; Ragauskas, A. J., Selective Aerobic Oxidation of Activated Alcohols into Acids or Aldehydes in Ionic Liquids. *The Journal of Organic Chemistry* **2007,** *72* (18), 7030-7033.

172. Uozumi, Y.; Nakao, R., Catalytic oxidation of alcohols in water under atmospheric oxygen by use of an amphiphilic resin-dispersion of a nanopalladium catalyst. *Angewandte Chemie-International Edition* **2003,** *42* (2), 194-+.

173. Linden, J. J. M. v. d.; Hilberink, P. W.; Kronenburg, C. M. P.; Kemperman, G. J., Investigation of the Moffatt - Swern Oxidation in a Continuous Flow Microreactor System. *Org. Process Res. Dev.* **2008,** *12* (5), 911-920.

174. Kawaguchi, T.; Miyata, H.; Ataka, K.; Mae, K.; Yoshida, J.-i., Room-Temperature Swern Oxidations by Using a Microscale Flow System13. *Angew. Chem.* **2005**, *117* (16), 2465-2468.

175. Lee, D. G.; Spitzer, U. A., Kinetics and Mechanism of the Oxidation of Benzyl Alcohol and Benzaldehyde by Aqueous Sodium Dichromate. *Can. J. Chem.* **1975**, *53* (24), 3709-3713.

176. Clayden, J.; Greeves, N.; Warren, S.; Wothers, P., *Organic Chemistry*. Oxford University Press: New York, 2001.

177. Blackmond, D. G.; Rosner, T.; Pfaltz, A., Comprehensive Kinetic Screening of Catalysts Using Reaction Calorimetry. *Org. Process Res. Dev.* **1999**, *3* (4), 275-280.

178. am Ende, D. J.; Clifford, P. J.; DeAntonis, D. M.; SantaMaria, C.; Brenek, S. J., Preparation of Grignard Reagents: FTIR and Calorimetric Investigation for Safe Scale-Up. *Org. Process Res. Dev.* **1999**, *3* (5), 319-329.

179. Bedore, M. W.; Zaborenko, N.; Jensen, K. F.; Jamison, T. F., Aminolysis of Epoxides in a Microreactor System: A Continuous Flow Approach to Î²-Amino Alcohols. *Org. Process Res. Dev.* 14 (2), 432-440.

180. Yoshida, J.-i.; Nagaki, A.; Yamada, T., Flash Chemistry: Fast Chemical Synthesis by Using Microreactors. *Chem.--Eur. J.* **2008**, *14* (25), 7450-7459.

181. Zaborenko, N.; Murphy, E. R.; Kralj, J. G.; Jensen, K. F., Synthesis and Kinetics of Highly Energetic Intermediates by Micromixers: Direct Multistep Synthesis of Sodium Nitrotetrazolate. *Ind. Eng. Chem. Res.*

182. Fogler, H. S., *Elements of Chemical Reaction Engineering*. 4th ed.; Prentice Hall: Upper Saddle River, NJ, 2006.

183. Levenspiel, O., *Chemical Reaction Engineering*. 3 ed.; Wiley: New York, 1999.

184. Shultz, C. S.; Krska, S. W., Unlocking the Potential of Asymmetric Hydrogenation at Merck. *Acc. Chem. Res.* **2007**, *40* (12), 1320-1326.

185. Rubin, A. E.; Tummala, S.; Both, D. A.; Wang, C.; Delaney, E. J., Emerging Technologies Supporting Chemical Process R&D and Their Increasing Impact on Productivity in the Pharmaceutical Industry. *Chem. Rev. (Washington, DC, U. S.)* **2006**, *106* (7), 2794-2810.

186. Box, G. E. P.; Hill, W. J., Discrimination Among Mechanistic Models. *Technometrics* **1967**, *9* (1), 57-71.

187. Blau, G.; Lasinski, M.; Orcun, S.; Hsu, S.-H.; Caruthers, J.; Delgass, N.; Venkatasubramanian, V., High fidelity mathematical model building with experimental data: A Bayesian approach. *Comput. Chem. Eng.* **2008**, *32* (4-5), 971-989.

188. Hill, P. D. H., A Review of Experimental Design Procedures for Regression Model Discrimination. *Technometrics* **1978**, *20* (1), 15-21.

189. Franceschini, G.; Macchietto, S., Model-based design of experiments for parameter precision: State of the art. *Chem. Eng. Sci.* **2008**, *63* (19), 4846-4872.

190. Asprey, S. P.; Macchietto, S., Statistical tools for optimal dynamic model building. *Comput. Chem. Eng.* **2000**, *24* (2-7), 1261-1267.

191. Ucinski, D.; Bogacka, B., T-Optimum designs for multiresponse dynamic heteroscedastic models. In *Moda 7 - Advances in Model-Oriented Design and Analysis, Proceedings*, DiBucchianico, A.; Lauter, H.; Wynn, H. P., Eds. Physica-Verlag Gmbh & Co: Heidelberg, 2004; pp 191-199.

192. Buzzi-Ferraris, G.; Forzatti, P., A new sequential experimental design procedure for discriminating among rival models. *Chem. Eng. Sci.* **1983,** *38* (2), 225-232.

193. Schwaab, M.; Silva, F. M.; Queipo, C. A.; Barreto, J. A. G.; Nele, M.; Pinto, J. C., A new approach for sequential experimental design for model discrimination. *Chem. Eng. Sci.* **2006,** *61* (17), 5791-5806.

194. Buzzi Ferraris, G.; Forzatti, P.; Emig, G.; Hofmann, H., Sequential experimental design for model discrimination in the case of multiple responses. *Chem. Eng. Sci.* **1984,** *39* (1), 81-85.

195. Buzzi-Ferraris, G.; Forzatti, P.; Paolo, C., An improved version of a sequential design criterion for discriminating among rival multiresponse models. *Chem. Eng. Sci.* **1990,** *45* (2), 477-481.

196. Stewart, W. E.; Shon, Y.; Box, G. E. P., Discrimination and goodness of fit of multiresponse mechanistic models. *AIChE J.* **1998,** *44* (6), 1404-1412.

197. Espie, D.; Macchietto, S., The Optimal-Design of Dynamic Experiments. *AIChE J.* **1989,** *35* (2), 223-229.

198. Lacey, L.; Dunne, A., The design of pharmacokinetic experiments for model discrimination. *J. Pharmacokinet. Phar.* **1984,** *12* (3), 351-365.

199. Hsu, S. H.; Stamatis, S. D.; Caruthers, J. M.; Delgass, W. N.; Venkatasubramanian, V.; Blau, G. E.; Lasinski, M.; Orcun, S., Bayesian Framework for Building Kinetic Models of Catalytic Systems. *Ind. Eng. Chem. Res.* **2009,** *48* (10), 4768-4790.

200. Wiechert, W., Modeling and simulation: tools for metabolic engineering. *J. Biotechnol.* **2002,** *94* (1), 37-63.

201. Burke, A. L.; Duever, T. A.; Penlidis, A., Choosing the right model: Case studies on the use of statistical model discrimination experiments. *Can. J. Chem. Eng.* **1997,** *75* (2), 422-436.

202. Kamenski, D. I.; Dimitrov, S. D.; Silchenko, L. A.; Shestakov, G. K.; Odinzov, K. U.; Temkin, O. N., Modeling the Catalytic Hydrochlorination of Ethyne. *Appl. Catal.* **1990,** *67* (1), 159-168.

203. Farrell, R. J.; Tsai, Y. C., Modelling, Simulation and Kinetic Parameter-Estimation in Batch Crystallization Processes. *AIChE J.* **1994,** *40* (4), 586-593.

204. Froment, G. F., Model Discrimination and Parameter Estimation in Heterogeneous Catalysis. *AIChE J.* **1975,** *21* (6), 1041-1057.

205. Greiner, L.; Ternbach, M. B., Kinetic study of homogeneous alkene hydrogenation by model discrimination. *Adv. Synth. Catal.* **2004,** *346* (11), 1392-1396.

206. Chen, B. H.; Bermingham, S.; Neumann, A. H.; Kramer, H. J. M.; Asprey, S. P., On the Design of Optimally Informative Experiments for Dynamic Crystallization Process Modeling. *Ind. Eng. Chem. Res.* **2004,** *43* (16), 4889-4902.

207. Ternbach, M. B.; Bollman, C.; Wandrey, C.; Takors, R., Application of model discriminating experimental design for modeling and development of a fermentative fed-batch L-valine production process. *Biotechnol. Bioeng.* **2005,** *91* (3), 356-368.

208. Issanchou, S.; Cognet, P.; Cabassud, M., Sequential experimental design strategy for rapid kinetic modeling of chemical synthesis. *AIChE Journal* **2005,** *51* (6), 1773-1781.

209. Felix Oliver Lindner, P.; Hitzmann, B., Experimental design for optimal parameter estimation of an enzyme kinetic process based on the analysis of the Fisher information matrix. *J. Theor. Biol.* **2006,** *238* (1), 111-123.

210. Fujiwara, M.; Nagy, Z. K.; Chew, J. W.; Braatz, R. D., First-principles and direct design approaches for the control of pharmaceutical crystallization. *J. Process Control* **2005,** *15* (5), 493-504.

211. Dantas, L. B.; Orlande, H. R. B.; Cotta, R. M., Estimation of dimensionless parameters of Luikov's system for heat and mass transfer in capillary porous media. *Int. J. Therm. Sci.* **2002,** *41* (3), 217-227.

212. Trachsel, F.; Gunther, A.; Khan, S.; Jensen, K. F., Measurement of residence time distribution in microfluidic systems. *Chem. Eng. Sci.* **2005,** *60* (21), 5729-5737.

213. Ajdari, A.; Bontoux, N.; Stone, H. A., Hydrodynamic Dispersion in Shallow Microchannels: the Effect of Cross-Sectional Shape. *Anal. Chem.* **2005,** *78* (2), 387-392.

214. Hornung, C. H.; Mackley, M. R., The measurement and characterisation of residence time distributions for laminar liquid flow in plastic microcapillary arrays. *Chem. Eng. Sci.* **2009,** *64* (17), 3889-3902.

215. Dutta, D.; Leighton, D. T., Dispersion Reduction in Pressure-Driven Flow Through Microetched Channels. *Anal. Chem.* **2000,** *73* (3), 504-513.

216. Dutta, D.; Ramachandran, A.; Leighton, D., Effect of channel geometry on solute dispersion in pressure-driven microfluidic systems. *Microfluid. Nanofluid.* **2006,** *2* (4), 275-290.

217. Dewar, M. J. S.; Pyron, R. S., Nature of the transition state in some Diels-Alder reactions. *J. Am. Chem. Soc.* **1970,** *92* (10), 3098-3103.

218. Butt, J. B., *Reaction Kinetics and Reactor Design*. 2nd ed.; Marcel Dekker, Inc.: New York, 1999.

219. Fan, L.-t.; Bailie, R. C., Axial diffusion in isothermal tubular flow reactors. *Chem. Eng. Sci.* **1960,** *13* (2), 63-68.

220. Fan, L.-t.; Ahn, Y.-K., Critical Evaluation of Boundary Conditions for Tubular Flow Reactors. *Industrial & Engineering Chemistry Process Design and Development* **1962,** *1* (3), 190-195.

221. Hoffmann, W.; Kang, Y.; Mitchell, J. C.; Snowden, M. J., Kinetic Data by Nonisothermal Reaction Calorimetry: A Model-Assisted Calorimetric Evaluation. *Org. Process Res. Dev.* **2006,** *11* (1), 25-29.

222. Paul, E. L., Design of reaction systems for specialty organic chemicals. *Chem. Eng. Sci.* **1988,** *43* (8), 1773-1782.

223. Caygill, G.; Zanfir, M.; Gavriilidis, A., Scalable Reactor Design for Pharmaceuticals and Fine Chemicals Production. 1: Potential Scale-up Obstacles. *Org. Process Res. Dev.* **2006,** *10* (3), 539-552.

224. Girgis, M. J.; Kiss, K.; Ziltener, C. A.; Prashad, M.; Har, D.; Yoskowitz, R. S.; Basso, B.; Repic, O.; Blacklock, T. J.; Landau, R. N., Kinetic and Calorimetric Considerations in the Scale-Up of the Catalytic Reduction of a Substituted Nitrobenzene. *Org. Process Res. Dev.* **1997,** *1* (5), 339-349.

225. Bourne, J. R., Mixing and the Selectivity of Chemical Reactions. *Org. Process Res. Dev.* **2003,** *7* (4), 471-508.

226. Perry, R. H.; Green, D. W., *Perry's Chemical Engineers' Handbook* McGraw-Hill: New York, 1997.

227. Sugimoto, A.; Fukuyama, T.; Rahman, M. T.; Ryu, I., An automated-flow microreactor system for quick optimization and production: application of 10- and 100-gram order

productions of a matrix metalloproteinase inhibitor using a Sonogashira coupling reaction. *Tetrahedron Lett.* **2009,** *50* (46), 6364-6367.

228. Jachuck, R., Process intensification for responsive processing. *Chem. Eng. Res. Des.* **2002,** *80* (A3), 233-238.

229. Fan, L.-t.; Bailie, R. C., Axial diffusion in isothermal tubular flow reactors. *Chem. Eng. Sci.* **1960,** *13* (2), 63-68.

230. Fogler, H. S., *Elements of Chemical Reaction Engineering.* 4th ed.; Prentice Hall: Upper Saddle River, NJ, 2005.

231. Levenspiel, O., *Chemical Reaction Engineering.* 3rd ed.; Wiley: 1999; p 578.

232. Barthe, P.; Guermeur, C.; Lobet, O.; Moreno, M.; Woehl, P.; Roberge, D. M.; Bieler, N.; Zimmermann, B., Continuous multi-injection reactor for multipurpose production - Part I. *Chem. Eng. Technol.* **2008,** *31* (8), 1146-1154.

233. Lavric, E. D., Thermal Performance of Corning Glass Microstructures. In *ECI International Conference on Heat Transfer and Fluid Flow in Microscale*, Whistler, Canada, 2008.

234. Incropera, F. P.; DeWitt, D. P., *Fundamentals of Heat and Mass Transfer.* 5th ed.; John Wiley & Sons: New York, 2002.

235. Hartman, R. L.; Naber, J. R.; Zaborenko, N.; McMullen, J. P.; Jensen, K. F. Systems and Methods for Handling Solids in Microfluidic Systems. 2009.

236. Tundel, R. E.; Anderson, K. W.; Buchwald, S. L., Expedited Palladium-Catalyzed Amination of Aryl Nonaflates through the Use of Microwave-Irradiation and Soluble Organic Amine Bases. *J. Org. Chem.* **2005,** *71* (1), 430-433.

237. Horie, T.; Sumino, M.; Tanaka, T.; Matsushita, Y.; Ichimura, T.; Yoshida, J.-i., Photodimerization of Maleic Anhydride in a Microreactor Without Clogging. *Org. Process Res. Dev.* *14* (2), 405-410.

238. Braden, T. M.; Gonzalez, M. A.; Jines, A. R.; Johnson, M. D.; Sun, W. Reactors and Methods for Processing Reactants Therein. 2009.

239. Wyss, H. M.; Blair, D. L.; Morris, J. F.; Stone, H. A.; Weitz, D. A., Mechanism for clogging of microchannels. *Physical Review E* **2006,** *74* (6), 061402.

240. Ramachandran, V.; Venkatesan, R.; Tryggvason, G.; Scott Fogler, H., Low Reynolds Number Interactions between Colloidal Particles near the Entrance to a Cylindrical Pore. *J. Colloid Interface Sci.* **2000,** *229* (2), 311-322.

175

Appendix A: Fabrication Details of 5-Port Microreactors

The run-sheet of the 5-port microreactors that were used in the reaction screening example of Chapter 2 is shown below. With exception to the diesawing which was performed in the Integrated Circuits Laboratory (ICL), all wafer processing occurred in the Technology Research Laboratory (TRL) of the MTL at MIT. The machines that were used are abbreviated and correspond to equipment identification tags used in CORAL software of the MTL. The "code" column represents the cleanliness at any particular time during processing – brown represents CMOS compatible, green denotes general silicon processing, and red indicates gold and III-V metals general processing.

General process: First grow a protective oxide on the wafers for sts etching. Then pattern and etch the backside of the silicon wafer using nested masks to create the through-holes and capillary stands for the inlet and outlet ports. Then, etch the frontside of the silicon wafer to create flow channels. Next, anodically bond the pyrex wafer to seal the flow channels. Finally deposit copper around the flow ports and diesaw the devices.

material: 6-inch Double Side Polished Silicon Wafer
6-inch Pyrex Wafer

STEP	DATE	FAC	# WAFS	MACHINE	ACTION	NOTES	CODE
1					**OXIDIZE WAFER**		
1.1		TRL	1	RCA	RCA clean wafer		
1.2		TRL	1	tube-a2	grow wet oxide ~0.4 um (1000 C ~ 45 min)	Used recipe 4 on the tube at 1000C to grow ~4760A (target 5000A)	
2					**PATTERN FLOW PORTS AND STEPS (BACKSIDE)**		
2.1					*Photolithography of Capillary Steps*		
2.1.1		TRL	1	HMDS	Coat wafer with HMDS		
2.1.2		TRL	1	coater	Spincoat OCG 825 to define frontside channels		
2.1.3		TRL	1	prebake	Bake at 95°C for 30 minutes		
2.1.2b		TRL	1	coater	Spincoat OCG 825 to protect backside		
2.1.3b		TRL	1	prebake	Bake at 95°C for 30 minutes		
2.1.4		TRL	1	EV1	Expose resist for 1.5 seconds (4-hole step mask)		
2.1.5		TRL	1	photowet-1	Develop OCG 934:1:1, 1-3min		
2.1.6		TRL	1	postbake	Postbake at 95°C for 30 minutes		
2.1.7		TRL	1	acidhood	BOE patterned SiO2		
2.1.8		TRL	1	acidhood	piranha clean wafer		

2.2				*Photolithography of Through Holes*
2.2.1	TRL	1	HMDS	Coat wafer with HMDS
2.1.2b	TRL	1	coater	coat wafer with OCG825 to protect backside
2.1.2b	TRL	1	prebake	Bake at 95°C for 30+ minutes
2.2.2	TRL	1	coater	Double spincoat thick photoresist AZP4620 on frontside to ~20μm
2.2.3	TRL	1	prebake	Bake at 95°C for 30+ minutes
2.2.4	TRL	1	EV1	Expose resist for 40 seconds to UV (5-hole port mask)
2.2.5	TRL	1	photowet-1	Development, 5min
2.2.6	TRL	1	prebake	Postbake at 95°C for 30 minutes
3				**ETCH FLOW PORTS AND STEPS (BACKSIDE)**
3.1				*Attach Handle Wafer*
3.1.1	TRL	1	coater	spincoat thick resist on handle wafer, attach wafer 1 use "target" pattern to attach wafers
3.1.2	TRL	1	prebake	Postbake at 95°C 30 min
3.2				*STS Etch Thru Holes*
3.2.1	TRL	1	STS2	STS etch, recipe OLE2, 150 um
3.2.2	TRL	1	acidhood	piranha clean wafer
3.3				*Attach Handle Wafer*
3.3.1	TRL	1	coater	spincoat thick resist on handle wafer, attach wafer 1 "target" pattern
3.3.2	TRL	1	prebake	Postbake at 95°C 30 min
3.4				*STS Etch Thru Holes And Capillary Steps*
3.4.1	TRL	1	STS2	STS etch, recipe OLE2, 150 um
3.4.2	TRL	1	acidhood	piranha clean wafer
4				**PATTERN FLOW CHANNELS**
4.1				*Photolithography for BOE Etch*
4.1.1	TRL		HMDS	Coat wafer with HMDS program 3 (if humidity is >41% postbake for 30 mins before HMDS)
4.1.2	TRL		coater	Spin Coat photoresist AZ9260 to 10μm
4.1.3	TRL		prebake	Bake at 90°C for 60 minutes
4.1.4	TRL		EV1	Expose resist for 45 seconds to UV in 3 intervals of 15sec
4.1.5	TRL		photowet-1	Development, 3min AZ440
4.1.6	TRL		coater	Coat photoresist OCG825 to 1μm on backside
4.1.7	TRL		prebake	Bake at 90°C for 30 minutes
4.2				*Pattern Oxide with BOE Etch*
4.2.1	TRL		acidhood2	BOE Etch 7min

5				**ETCH FLOW CHANNELS**		
5.1				*Attach Handle Wafer*		
				spincoat thick resist on handle wafer,		
5.1.1	TRL	1	coater	attach wafer 1	"target" pattern	
5.1.2	TRL	1	prebake	Postbake at 95°C 30 min		
5.2				*STS Etch Thru Holes And Capillary Steps*		
5.2.1	TRL	1	STS2	STS etch, recipe OLE2, 400 um		
5.2.2	TRL	1	acidhood	piranha clean wafer		
5.2.3	TRL		acidhood	HF dip	15-20 minutes	
6				**OXIDIZE CHANNELS**		
6.1	TRL		rcaTRL	RCA clean		
6.2	TRL		A2-WetOxBond	Grow 5000Å wet oxide		
7				**BOND PYREX WAFER**		
7.1				*Wafer Cleaning*		
7.1.1	TRL		acidhood	piranha Pyrex and silicon wafers		
7.2				*Wafer Bonding*		
7.2.1	TRL		EV501-620	Bond Pyrex and silicon wafers		
8				**DEPOSIT COPPER**		
8.1	TRL		photoroom	Align shadow mask		
				Deposit 100nm Ti and 500nm of		
8.2	TRL		ebeamAu	Copper		
9	ICL		diesaw	**DIESAW DEVICES**		

Appendix B: Operational Details of the Standard Temperature Controller

The "temperature_controller.vi" uses a PID control strategy to adjust the duty cycle of PWM power to the TE device. The duty cycle ranged from 0 to 100%. On the front panel, users specify the temperature set point and the PID gains. Fast temperature response was observed with $K_c = 1$, $\tau_I = 0.046$ min, $\tau_D = 0.388$ min. The active cooling parameters are located in the Matlab script located on the block diagram. Typically, cooling the microreactor occurred if the $T_{SP} < (T_{PV} - 5)$ or if T_{SP} was less than ambient temperature, which was set at 25°C. If these conditions were true, a response was set to the case structure containing the PID.vi. If cooling was not necessary, the duty cycle signal was supplied to the solid-state relay module; otherwise, a (100% - PID response) was sent to the relay module and a separate switch was thrown to activate the DPDT switch.

Appendix C: Nelder-Mead Simplex Program for Online Reaction Optimization

From the front panel, the user specifies the number of variables (N), the minimum and maximum range of each reaction variable, the initial simplex size (α), initial conditions, and reaction variable step sizes. Initial simplex coordinates are computed in the Matlab script outside of the while loop, while all sequential experiments and algorithmic computations are performed in the "main" Matlab script. Within this main script is the function "get_exp()" which is used to determine the appropriate flow rates of the different syringe pumps. These flow rates should correspond to the reagent and pump addresses established by the user before experimentation.

Injection time(s) are controlled in "injection time" Matlab script. The first injection is controlled by a user specified flush volume, typically 3-5 system volumes. After this volume has been flushed, a relay is activated and the Rheodyne valve is adjusted to the inject position. The valve returns to the load position after 1 minute. A subsequent injection occurs after the specified HPLC analysis time passes; otherwise, the program sets the termination time for the experiment and analyzes the chromatogram. Two analog output signals from the PDA, corresponding to the absorbance at the specified wavelengths in the HPLC method created with the Empower software, are recorded. This data is filtered to create a smooth chromatogram and numerically integrated using the Matlab trapz function within the mv_area subVI. The "analysis Matlab" script computes the concentrations from these chromatograms and updates the objective

function. Results are written in a file, and are used to determine sequential experiments according to the Simplex Method.

Appendix D: SNOBFIT Program for Online Reaction Optimization

From the front panel, the user specifies the minimum and maximum range of each reaction variable, the reactor volume, the syringe concentrations of the various compounds, the maximum number of SNOBFIT iterations to call, the number of experiments to perform after each call to the SNOBFIT function, and the percentage of class 4 points to be called after each call to the SNOBFIT function. All experiments are selected in the main Matlab script, using the "snobdriver_labview()" function. Within this main script is the function "get_exp()" which is used to determine the appropriate flow rates of the different syringe pumps. These flow rates should correspond to the reagent and pump addresses established by the user before experimentation.

Injection time(s) are controlled in "injection time" Matlab script. The first injection is controlled by a user specified flush volume, typically 3-5 system volumes. After this volume has been flushed, a relay is activated and the Rheodyne valve is adjusted to the inject position. The valve returns to the load position after 1 minute. A subsequent injection occurs after the specified HPLC analysis time passes; otherwise, the program sets the termination time for the experiment and analyzes the chromatogram. Two analog output signals from the PDA, corresponding to the absorbance at the specified wavelengths in the HPLC method created with the Empower software, are recorded. This data is filtered to create a smooth chromatogram and numerically integrated using the Matlab trapz function within the mv_area subVI. The "analysis Matlab" script computes the concentrations from these chromatograms and updates the objective

function. Results are written in a file, and are used to determine sequential experiments according to the SNOBFIT algorithm.

Appendix E: Steepest Descent Method for Online Reaction Optimization

From the front panel, the minimum and maximum range of each reaction variable, the step-size for each reaction variable, the center point for the initial full-factorial DoE, the number of center point repeats, and the tolerance on the gradient size for termination. All experiments are determined in the "main" Matlab script. After performing the initial DoE and center point repeats, an F-test is performed to evaluate the presence of the quadratic curvature. This test is performed in the "Model_run_LOF()" function. If quadratic curvature is present, the experimental design is automatically augmented with CCD points in the "coded_exp_pts()" function; otherwise the gradient is calculated using the "calc_grad()" function. Within this main script is the function "get_exp()" which is used to determine the appropriate flow rates of the different syringe pumps. These flow rates should correspond to the reagent and pump addresses established by the user before experimentation.

Injection time(s) are controlled in "injection time" Matlab script. The first injection is controlled by a user specified flush volume, typically 3-5 system volumes. After this volume has been flushed, a relay is activated and the Rheodyne valve is adjusted to the inject position. The valve returns to the load position after 1 minute. A subsequent injection occurs after the specified HPLC analysis time passes; otherwise, the program sets the termination time for the experiment and analyzes the chromatogram. Two analog output signals from the PDA, corresponding to the absorbance at the specified wavelengths in the HPLC method created with the Empower software, are recorded. This data is filtered to create a smooth chromatogram and numerically integrated using the Matlab trapz function within the mv_area subVI. The "analysis

Matlab" script computes the concentrations from these chromatograms and updates the objective function. Results are written in a file, and are used to determine sequential experiments according to the Steepest Descent Method.

Appendix F: Nelder-Mead Simplex Method Used in Heck Reaction

This method is identical to that given in Appendix C, with the exception that a trigger is sent to an Agilent 2600 series to begin the HPLC method. The results from the HPLC analysis are recorded in a text file, which is imported by the program. By specifying the retention time, the program selects the peak area corresponding to the desired component. This information is used to update the objective function, and sequential experiments are determined by the Nelder-Mead Simplex Method.

Appendix G: Results from Multi-Parameter Optimization in Oxidation Case Study

Experiment	Residence Time (s)	Temperature (^oC)	CrO_3 Equivalence	[PhCH$_2$OH] x 10^3 (M)	Yield (mol/mol %)	Selectivity (mol/mol %)
1	60.0	50	1.00	8.00	21.0	66.4
2	64.4	68.5	1.09	8.22	20.0	46.2
3	78.5	54.3	1.09	8.22	19.0	41.3
4	64.4	54.3	1.37	8.22	14.0	40.9
5	64.4	54.3	1.09	8.93	20.0	49.8
6	69.3	59.2	0.76	8.46	34.0	66.5
7	78.3	68.2	1.01	8.91	17.0	41.2
8	50.5	61.6	0.88	8.59	31.0	64.7
9	64.2	71.9	0.91	9.10	24.0	52.6
10	59.8	55.1	0.73	9.32	29.0	67.6
11	57.5	69.6	0.55	8.80	36.9	79.5
12	54.3	50.9	0.55	8.49	37.0	85.2
13	56.0	65.6	0.64	7.85	56.5	81.8
14	68.0	61.0	0.38	8.22	46.3	90.8
15	48.7	64.3	0.30	8.22	39.9	90.8

16	56.0	51.3	0.38	7.59	51.9	95.0
17	60.0	70.3	0.30	7.45	36.9	86.9
18	68.5	50.1	0.68	7.85	48.7	94.8
19	69.9	63.1	0.49	7.27	51.3	87.8
20	57.1	54.1	0.72	7.06	54.4	83.2
21	51.0	67.0	0.44	7.03	54.8	90.4
22	40.1	56.0	0.61	7.50	56.3	88.0
23	46.2	70.0	0.82	7.14	59.3	76.8
24	39.5	75.2	0.54	7.70	65.7	87.5
25	39.9	66.3	0.86	8.06	55.6	75.7
26	51.0	67.0	0.44	7.03	56.9	88.7
27	56.2	83.0	0.61	7.36	60.2	84.5
28	40.5	82.0	0.56	6.76	63.1	86.5
29	40.2	88.0	0.83	7.45	59.2	77.9
30	42.0	94.1	0.45	7.50	65.6	88.0
31	49.0	79.0	0.25	7.21	31.3	92.6
32	24.9	86.6	0.57	7.34	31.9	84.1
33	48.5	88.2	0.65	8.24	80.1	85.4
34	53.0	82.2	0.30	7.95	42.4	90.8
35	28.9	89.7	0.62	8.08	47.5	81.4
36	50.2	73.1	0.86	7.88	71.6	80.2
37	57.0	71.7	0.51	8.14	63.0	87.0
38	41.4	71.1	0.67	8.62	56.0	79.4

39	40.2	88.0	0.83	7.45	66.8	78.9
40	32.9	79.3	0.83	8.27	60.6	78.3
41	32.9	79.3	0.83	8.27	67.5	86.7
42	56.2	83.0	0.61	7.36	50.8	73.7
43	58.0	91.0	0.94	7.77	54.1	87.0
44	57.0	71.7	0.51	8.14	32.3	80.1
45	32.9	79.3	0.83	8.27	63.5	91.2
46	42.0	94.1	0.45	7.50	58.9	78.1

Appendix H: Model Discrimination Program

From the front panel, users enter the grid of feasible design points by specifying the minimum, maximum, and step-size values of each reaction variable. A partial factorial is performed in the interior of the design space to create an initial estimate for the rate constants. Rate constants are computed through the modelxxx_parameters() function in the main Matlab script, where xxx corresponds to the order on reactant 1, reactant 2, and product, respectively. Additional rate models can be incorporated into this program by including the appropriate parameter estimation and ode15s functions. After estimating the rate constants, discrimination calculations and sequential experiment selection is performed in the "divergence_calc()" function. Sequential experimentation is terminated after the posterior probability of a single model surpasses 0.95.

Appendix I: Parameter Estimation Program

From the front panel, users enter the grid of feasible design points by specifying the minimum, maximum, and step-size values of each reaction variable. A full factorial is performed in the interior of the design space to create an initial estimate of the pre-exponential and activation energy. Parameter estimation and sequential experiment selection according to a D-optimal framework is performed in the "model_estimation()" function. Sequential experimentation continued until the user specified criteria was achieved.

Appendix J: Reaction Profiling Program

In a text file, the user enters the experiment number and the experimental conditions, in order of temperature, time, and equivalents. The user is prompted for the location of this text file when the LabVIEW program is started. The user also enters the reactor volume and the flush volume to determine the appropriate flow rates and the equilibration times for steady-state data collection. Once the system is equilibrated, a relay closes and the fraction collector advances. After collecting the specified reactant volume, the fraction collector advances and collects subsequent reaction samples. If subsequent samples are not required, the program begins the next experiment and the fraction collector begins colleting waste for this new experiment. This procedure is repeated until all experiments have been performed.

Appendix K: Automated Flush Program for Solid-Producing Reactions

From the front panel, the user specifies the pressure sensor measurement threshold (in mV). Typically, this threshold was set at 100 mV. The system operates in the "reaction" stage until the pressure sensor measurement surpasses this specified value. Once this value is exceeded, the program manipulates the appropriate syringe pump flow rates and valve settings according to the wash cycle described in Chapter 7.2. The timing for the flush cycle can be adjusted in the "solids_info()" Matlab function.